QUANTITATIVE SPECTROSCOPIC STUDIES ON THE INFRARED ABSORPTION BY WATER VAPOR AND LIQUID WATER

Thesis by

Robert Goldstein

In Partial Fulfillment of the Requirements
For the Degree of
Doctor of Philosophy

California Institute of Technology
Pasadena, California

1964

(Accepted December 16, 1963)

ACKNOWLEDGMENTS

The author wishes to express his sincere appreciation for the guidance and supervision of Dr. S. S. Penner.

Grateful acknowledgment is also made for the financial assistance provided by the Daniel and Florence Guggenheim Jet Propulsion Fellowships for the academic years 1959-60 and 1960-61 and by a National Science Foundation Fellowship for the 1961-62 academic year; portions of the work described in this thesis were supported by the U. S. Navy (Office of Naval Research) under Contract Nonr-220(45), NR 015-401.

The author also wishes to express his thanks to M. Thomas for writing the computer program, to T. Rose and K. Neel for helping to design and build the absorption cell, to P. Trapane for aid in building the experimental facilities, and to Mrs. R. Toy for her invaluable secretarial assistance.

Finally, sincere and heartfelt thanks are conveyed to the author's parents, Mr. and Mrs. Sam Goldstein, for their love, guidance and encouragement.

ABSTRACT

Measurements have been made of the integrated intensities and spectral absorption coefficients of water vapor in the 1.38μ, 1.87μ, 2.7μ, and 6.3μ regions at temperatures up to 1000°K, using sufficient self-broadening to remove the rotational fine structure. The experiments were performed in a specially designed, isothermal high-pressure absorption cell supplied with vapor from a liquid water reservoir submerged in a constant temperature oil bath.

In addition, theoretical calculations of the spectral absorption coefficients of water vapor at elevated temperatures have been performed using a just-overlapping line model and the results have been compared with the experimental data.

The spectral absorption coefficients of liquid water have been measured in the wave number regions from 2200 to 3000 cm^{-1} and from 3700 to 7600 cm^{-1} at temperatures of 27, 89, 159, and 209°C. From these data, the integrated intensities of the absorption bands at 1.45μ and 1.93μ have been determined. The experimental data have also been used, in a highly simplified analysis, for the determination of hydrogen bonding in liquid water on the assumption of clusters containing only zero, one or two hydrogen bonds per molecule.

The change in the infrared absorption of gaseous and liquid water has been further investigated by measuring the transmission of infrared radiation through equal optical depths of liquid water and of water vapor near the limits of saturation.

TABLE OF CONTENTS

CHAPTER I

INTRODUCTION AND APPARATUS

A. INTRODUCTION

Quantitative knowledge of the infrared absorption of gaseous and liquid water is of importance in the fields of meteorology and astrophysics, as well as in certain military and aeronautical problems. It has also proved to be useful in the attempts to elucidate the structure of the water molecule.

There have been many investigations of the infrared absorption of water vapor. However, only a small number have dealt with quantitative measurements of band strengths and very few reliable values exist. For example, estimates (ranging from 100 to 200 cm^{-2}-atm^{-1} at 300°K) have been given for the ν_3-fundamental band (centered at 3655.8 cm^{-1}) based on a comparison of measured data with total emissivity calculations for water vapor (see Tables 11-13 and 11-14 of Ref. 1), on partially resolved absorption spectra,[2, 3] on rocket burner exhaust measurements,[4] and on the strength of the resolved line at 3806.9 cm^{-1}.[5] Reliable quantitative data are necessary in order to do a priori emissivity calculations from theoretical band models at elevated temperatures. A fairly complete bibliography of the experimental and theoretical work on the infrared absorption

by water vapor has been given by Gray.[6]

In this study, measurements have been made of the integrated intensities and spectral absorption coefficients of water vapor in the 1.38μ, 1.87μ, 2.7μ, and 6.3μ regions at temperatures up to 1000°K, using sufficient self-broadening to remove the rotational fine structure. The experiments were performed in a specially designed, isothermal high-pressure absorption cell supplied with vapor from a liquid water reservoir submerged in a constant temperature oil bath.

In addition, theoretical calculations of the spectral absorption coefficients of water vapor at elevated temperatures have been performed using a just-overlapping line model and the results have been compared with the experimental data.

The near infrared absorption spectrum of liquid water has been studied by a number of investigators. Infrared transmission measurements on ice were reported by Bode[7] as early as 1909 and, more quantitative studies, by Plyler[8] in 1924. Collins[9] studied the change of absorption in the spectral region from 0.70 to 2.1μ for the temperature range from 0 to 100°C; Ganz[10] confirmed Collins' observations on the bands at 0.77μ and 0.84μ; Curcio and Petty[11] investigated the spectral absorption coefficient from 0.70 to 2.1μ at 20°C; and Plyler and Acquista[12] performed

transmission studies on liquid water from 2 to 42μ. A complete bibliography and summary of the experimental work on liquid water up to 1940 is given by Dorsey.[13]

In recent years, spectroscopic measurements on liquid water, ice, and on a variety of water solutions have been performed by a number of investigators in order to elucidate the structure of water and to describe quantitatively the extent of hydrogen bonding and the structure of clusters in the liquid phase.[14-18] A good account of modern ideas on hydrogen bonding and the structure of liquid water is given in a paper by Nemethy and Scheraga[19] and by the authors referred to in this article.

In the present study, the spectral absorption coefficients of liquid water have been measured in the wave number regions, from 2200 to 3000 cm^{-1} and from 3700 to 7600 cm^{-1}, at temperatures of 27, 89, 159, and 209°C. From these data, the integrated intensities of the absorption bands at 1.45μ and 1.93μ have been determined and used to compare the infrared absorption of gaseous and liquid water. The data are then used, according to the method of Buijs and Choppin,[18] to draw some quantitative conclusions on hydrogen bonding if water can be adequately described by clusters containing non-bonded, singly-bonded, and doubly-bonded hydrogens. A more complete program for the utilization of spectroscopic data in structure determination is also indicated briefly.

In addition, the difference between the infrared absorption of gaseous and liquid water has been investigated by measuring the transmission of infrared radiation through equal optical depths of liquid water and of water vapor near the limits of saturation.

B. THE WATER MOLECULE

1. Normal Coordinates- In order to analyze the energy levels of a molecule, the electronic motion and the nuclear motion are separated by using the Born-Oppenheimer (adiabatic) approximation.[20] The electronic energy levels are calculated for stationary nuclei and the nuclear motion is then added as a perturbation. Since the resulting Schrodinger equation is usually too complex to solve exactly, it is customary to assume that the force law between the nuclei is known and to fit the calculated energy levels to experimental data.

In order to study the vibrational and rotational motion of the nuclei of a molecule in a semi-classical way, it is convenient to set up expressions for the kinetic and potential energy, and to transform these expressions by using a suitably chosen coordinate system, and then to study the resultant motion.

It has been found that useful sets of coordinates for studying the motion of a system of nuclei are the following: the translational motion is described by using the three cartesian coordinates of the center of mass of the molecule; the rotational motion is described by using the three eulerian angles of a rotating system of cartesian coordinates, the axes of which coincide with the principal axes of

inertia of the undistorted molecule; the vibrational motion is described by using a system of coordinates coinciding with the equilibrium position of the atoms and fixed with respect to the rotating coordinates. This last coordinate system is a convenient choice because it allows the vibrational motion to be studied without consideration of the rotation and translation of the molecule.

Normal coordinates are generally used to describe the vibrational motion; the normal modes of vibration of the system of particles are immediately apparent in a set of normal coordinates. Normal coordinates form a complete set; that is, the configuration of the system of particles can be described at any time as a sum of displacements of the normal coordinates. The potential and kinetic energies of the system can be expressed in terms of sums of the normal coordinates squared $\left[p^2\right]$ and of the time derivatives of the coordinates squared $\left[(dp/dt)^2\right]$, respectively; the matrices describing the potential and kinetic energies are diagonalized by a transformation to the normal coordinates. The resulting equation of motion for a vibrating system reduces to that of a single harmonic oscillator in each of the normal coordinates.

In studying the vibration of a polyatomic molecule, we shall use the theory of small oscillations;* that is, the amplitude of vibration of a nucleus from a point of equilibrium will be assumed to be small compared to the internuclear distance.

---

* A more detailed discussion of this analysis may be found in Refs. 21 and 22.

For a molecule with n nuclei, there are 3n degrees of freedom. Of these, three correspond to a translation of the molecule as a whole and two (for linear molecules) or three (for nonlinear molecules) correspond to rotational degrees of freedom. Consequently, there are 3n-5 (for linear molecules) or 3n-6 (for non-linear molecules) vibrational degrees of freedom.

In the following discussion, small letters q, c, and p are used as vectors (n x 1 column matrices) and their elements are designated as q_i, c_i, and p_i, respectively. Square matrices are represented by capital letters A, B, C, etc., and their elements by a_{ij}, b_{ij}, etc. The transpose of a matrix is identified by a superscript tilde ($\tilde{q}_{ij}=q_{ji}$, $\tilde{a}_{ij}=a_{ji}$, etc.). The unit matrix is denoted as E($E_{ij}=\delta_{ij}$) and Λ is a diagonal matrix ($\Lambda_{ij}=\lambda_i\delta_{ij}$). The letters U and T represent the potential and kinetic energies, respectively, in coordinate and in matrix notation.

In a cartesian coordinate system, the coordinates of each nucleus of a molecule in the equilibrium position are denoted as x_{ie} (where i=1, 2, . . . , 3n for n nuclei with i=1, 2 and 3 corresponding to the first nucleus, etc.); the deviation from the equilibrium position is q_i for the coordinate x_{ie}. Thus the ith coordinate is

$$x_i = x_{ie} + q_i \quad (i=1, 2, \ldots, 3n). \tag{1}$$

The potential energy may be expanded in a Taylor series about the equilibrium position, viz.,

$$U(x) = U(x_e) + \sum_{i=1}^{3n} \left(\frac{\partial U}{\partial x_i}\right)_e q_i + \frac{1}{2} \sum_{i=1}^{3n} \left(\frac{\partial^2 U}{\partial x_i \partial x_j}\right)_e q_i q_j + \ldots \quad . \tag{2}$$

Close to the equilibrium positions, the higher terms are negligibly small because the quantities q_i are small. Since the choice of the zero of potential energy is arbitrary, we set $U(x_e) = 0$. Furthermore, $(\partial U/\partial x_i)_e = 0$ in view of the definition of the equilibrium point as a minimum of potential energy. Therefore, the potential energy reduces to

$$U(x) = \frac{1}{2} \sum_{i,j=1}^{3n} \left(\frac{\partial^2 U}{\partial x_i \partial x_j} \right)_e q_i q_j \equiv \frac{1}{2} \sum_{i,j=1}^{3n} b_{ij} q_i q_j$$

or, in matrix notation,

$$U = \frac{1}{2} \tilde{q} B q, \qquad B = (b_{ij}) . \tag{3}$$

In first approximation, the kinetic energy is

$$T(\dot{x}) = \frac{1}{2} \sum_{i,j=1}^{3n} a_{ij} \dot{q}_i \dot{q}_j$$

or, in matrix notation,

$$T = \frac{1}{2} \tilde{\dot{q}} A \dot{q} , \qquad A = (a_{ij}) . \tag{4}$$

Because U and T may be expressed in quadratic form, they may be diagonalized simultaneously by the linear transformation*

$$q = Cp . \tag{5}$$

In addition, C may be normalized so that

$$\tilde{C} A C = E . \tag{6}$$

---

* See Ref. 21, Section 10-2 for details.

The congruent transformation of the potential energy is

$$\tilde{C}BC = \Lambda = (\lambda_i); \tag{7}$$

also

$$\tilde{C}\tilde{p} = \tilde{p}\tilde{C} \quad .^{*} \tag{8}$$

From Eqs. (4), (6) and (8) it now follows that

$$T = \frac{1}{2}\tilde{\dot{p}}(\tilde{C}AC)\dot{p} = \frac{1}{2}\tilde{\dot{p}}E\dot{p} = \frac{1}{2}\sum_{j=1}^{3n}\dot{p}_j^2. \tag{9}$$

From Eqs. (3), (7) and (8) we find that

$$U = \frac{1}{2}\tilde{p}(\tilde{C}BC)p = \frac{1}{2}\tilde{p}\Lambda p = \frac{1}{2}\sum_{j=1}^{3n}\lambda_j p_j^2 . \tag{10}$$

In view of Lagrange's equations of motion, Eqs. (9) and (10) yield the differential equations

$$\ddot{p}_j + \lambda_j p_j = 0 \tag{11}$$

which correspond to simple harmonic motion in each of the new coordinates, viz.,

$$p_j = c_j \exp(i\sqrt{\lambda_j}\,t) \tag{12}$$

The eigenvalues λ_i may be found by using Lagrange's equations of motion and Eqs. (9) and (10) to derive the expressions

$$(\tilde{C}AC)\ddot{p} + (\tilde{C}BC)p = 0 \tag{13}$$

---

* See Ref. 21, p. 141.

where $p^{(i)}$ is the eigenvector corresponding to the ith eigenvalue λ_i. From Eqs. (11) and (13) it is evident that

$$(\tilde{C}BC)p = \lambda (\tilde{C} AC)p . \tag{14}$$

or

$$BC = \lambda AC . \tag{15}$$

Hence the 3n eigenvalues are the solutions to the secular equation

$$|B-\lambda A| = 0 . \tag{16}$$

There are 3n-5 (for linear molecules) or 3n-6 (for non-linear molecules) non-zero eigenvalues λ_i, each corresponding to a different frequency of vibration. The zero eigenvalues correspond to the translational and rotational degrees of freedom. The zero eigenvalues could have been eliminated if the constraints of no translation or rotation had been imposed on the original set of 3n equations.

Equation (15) may also be written* as

$$Bc = \lambda Ac \tag{15a}$$

where the 3n eigenvectors ($c^{(i)}$) correspond to the columns of the congruent transformation matrix C. There is one eigenvector $c^{(i)}$ for each value of $\lambda = \lambda_i$. The normalization condition given in Eq. (6) becomes

$$\tilde{c}^{(i)} Ac^{(i)} = 1. \tag{17}$$

Because the motion is simple-harmonic in each of the new coordinates, the molecular motions may be written as the sum of simple harmonic oscillations. The amplitudes and phases of the

---

* See Ref. 14, pp. 322-3.

oscillations are contained in the eigenvectors.

If any of the roots of the secular equation are repeated, then the modes are said to be degenerate; that is, there are two independent normal coordinates which have the same frequency of oscillation. Any linear combination of degenerate normal coordinates is, of course, also a normal coordinate.

2. Normal Coordinate Analysis of the Water Molecule - Water is a non-linear triatomic molecule and therefore has nine degrees of freedom (three translational, three rotational and three vibrational degrees of freedom). The equilibrium position of the water molecule is shown in Fig. 1.

Let q_1 and q_2 be the displacements from equilibrium of the bond distances AB and AC respectively and $\delta\alpha$ be the change from the equilibrium bond angle 2α. The first order expression for the potential energy is assumed to be

$$U = \frac{f}{2}(q_1^2 + q_2^2) + \frac{f_\alpha}{2}(\delta\alpha)^2 , \tag{18}$$

where f is the stretching-force constant and f_α is the bending force constant.

It is convenient to introduce the symmetry coordinates

$$\begin{aligned} s_1 &= \frac{1}{\sqrt{2}}(q_1 + q_2), \\ s_2 &= L\,\delta\alpha, \\ s_3 &= \frac{1}{\sqrt{2}}(q_1 - q_2) . \end{aligned} \tag{19}$$

and

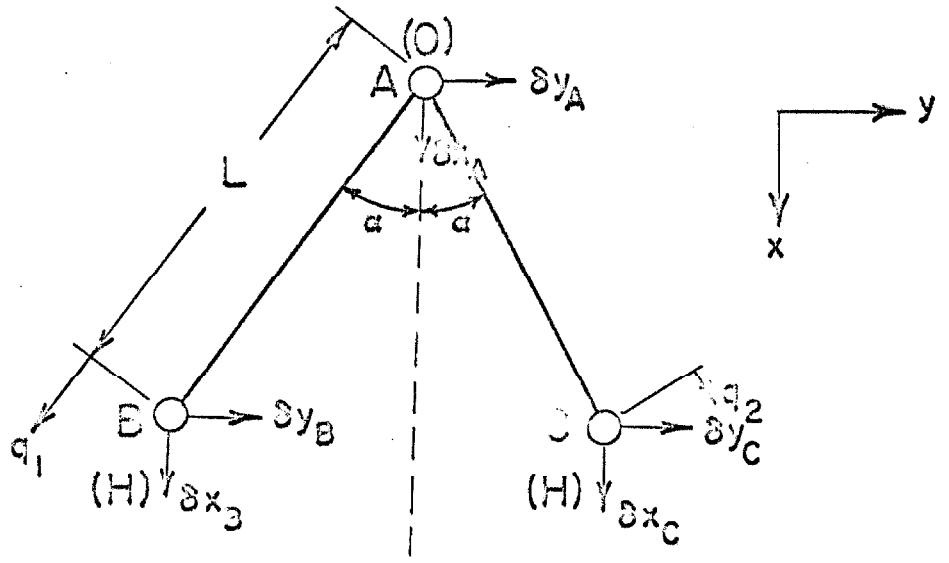

Fig. 1. Equilibrium position of water nuclei and small displacements from equilibrium.

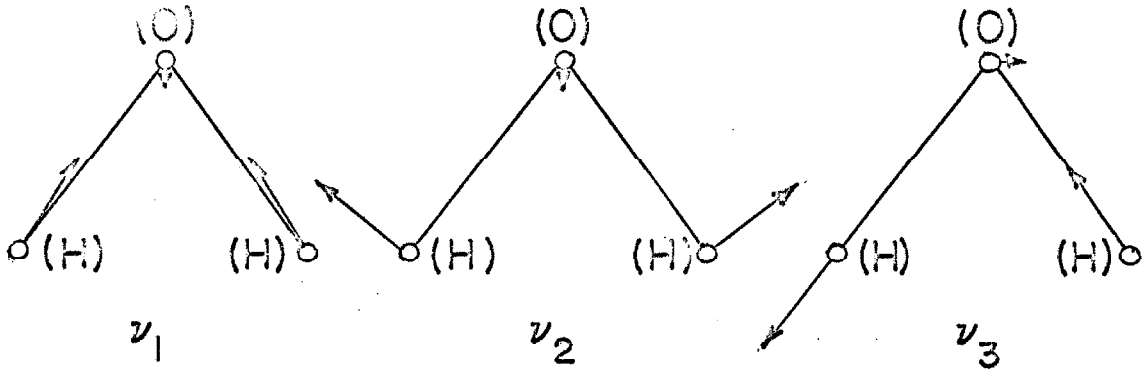

Fig. 2. The normal vibrations of the water molecule.

In terms of these coordinates, the potential energy becomes

$$2U = f(s_1^2 + s_3^2) + \frac{f_\alpha}{L^2} s_2^2 = b_{11} s_1^2 + b_{22} s_2^2 + b_{33} s_3^2 . \tag{20}$$

The problem now is to express the kinetic energy in terms of these coordinates. The kinetic energy is

$$2T = M(\delta\dot{x}_A^2 + \delta\dot{y}_A^2) + m(\delta\dot{x}_B^2 + \delta\dot{y}_B^2 + \delta\dot{x}_C^2 + \delta\dot{y}_C^2), \tag{21}$$

where M and m denote the mass of an oxygen and hydrogen nucleus, respectively, and $\delta\dot{x}_A$ represents the velocity of the displacement from the equilibrium position of the oxygen atom in the x-direction, etc.

From the geometry of Fig. 1, it is readily observable that small displacements from equilibrium can be expressed as

$$\begin{aligned} \delta_\alpha &= \frac{1}{L}\Big[-(\delta x_B - \delta x_A)\sin\alpha - (\delta x_C - \delta x_A)\sin\alpha \\ &\qquad -(\delta y_B - \delta y_A)\cos\alpha - (\delta y_C - \delta y_A)\cos\alpha\Big], \\ q_1 &= (\delta x_B - \delta x_A)\cos\alpha - (\delta y_B - \delta y_A)\sin\alpha, \end{aligned} \tag{22}$$

and

$$q_2 = (\delta x_C - \delta x_A)\cos\alpha + (\delta y_C - \delta y_A)\sin\alpha .$$

From Eqs. (19) and (22), the symmetry coordinates equal

$$\begin{aligned} s_1 &= \frac{1}{\sqrt{2}}\Big[(\delta x_B + \delta x_C - 2\delta x_A)\cos\alpha - (\delta y_B - \delta y_C)\sin\alpha\Big], \\ s_3 &= \frac{1}{\sqrt{2}}\Big[(\delta x_B - \delta x_C)\cos\alpha - (\delta y_B + \delta y_C - 2\delta y_A)\sin\alpha\Big], \end{aligned} \tag{23}$$

and

$$s_2 = -(\delta x_B + \delta x_C - 2\delta x_A)\sin\alpha - (\delta y_B - \delta y_C)\cos\alpha .$$

In order to solve for the six unknowns δx_i and δy_i (i=A, B, C) in terms of the three symmetry coordinates, the conditions of no translation of the center of gravity and no rotation are introduced, viz.,

$$M\delta x_A + m(\delta x_B + \delta x_C) = 0,$$

$$M\delta y_A + m(\delta y_B + \delta y_C) = 0, \tag{24}$$

and

$$(\delta x_B - \delta x_C)\sin\alpha + (\delta y_B + \delta y_C)\cos\alpha = 0.$$

The last equation is easily obtained by equating the moment of the center of gravity before and after the displacement.

By combining Eqs. (21), (23) and (24), the kinetic energy is found in terms of the symmetry coordinates to equal

$$2T = (m)\frac{M+2m\sin^2\alpha}{M+2m}\dot{s}_1^2 + \frac{Mm}{M+2m\sin^2\alpha}\dot{s}_3^2$$

$$+ \frac{m}{2}\frac{M+2m\cos^2\alpha}{M+2m}\dot{s}_2^2 + 2^{3/2}\frac{m^2\sin\alpha\cos\alpha}{M+2m}\dot{s}_1\dot{s}_2$$

$$= a_{11}\dot{s}_1^2 + a_{22}\dot{s}_2^2 + a_{33}\dot{s}_3^2 + 2a_{12}\dot{s}_1\dot{s}_2 . \tag{25}$$

Applying Eqs. (20) and (25) to Eq. (16), the secular equation becomes

$$\begin{vmatrix} b_{11}-\lambda a_{11} & -\lambda a_{12} & 0 \\ -\lambda a_{12} & b_{22}-\lambda a_{22} & 0 \\ 0 & 0 & b_{33}-\lambda a_{33} \end{vmatrix} = 0 . \tag{26}$$

The eigenvalues are

$$\lambda_3 = \frac{b_{33}}{a_{33}} \tag{27}$$

and

$$\lambda_{1,2} = \frac{a_{11}\, b_{22} + (a_{22} b_{11}) \pm \sqrt{(a_{11} b_{22} + a_{22} b_{11})^2 - 4 b_{11} b_{22} (a_{11} a_{22} - a_{12}^2)}}{2(a_{11} a_{22} - a_{12}^2)} ,$$

where a_{ij} and b_{ij} are defined by Eqs. (20) and (25).

The three vibrational frequencies correspond to the square roots of the eigenvalues. From the factoring of the secular equation, it is seen that s_1 and s_2 have the same type symmetry while s_3 has a different type. The normal modes are found by applying Eq. (27) to Eq. (15a), yielding

$$\begin{aligned} &(b_{11} - \lambda_i a_{11})\, c_1^{(i)} - \lambda_i a_{12}\, c_2^{(i)} = 0 , \\ &(b_{33} - \lambda_i a_{33})\, c_3^{(i)} = 0 , \\ &-\lambda_i a_{12}\, c_1^{(i)} + (b_{22} - \lambda_i a_{22})\, c_2^{(i)} = 0, \end{aligned} \tag{28}$$

where $c_j^{(i)}$ is the j^{th} component of the eigenvector belonging to the i^{th} eigenvalue λ_i.

For $i = 3$, $\lambda_3 = b_{33}/a_{33}$ and the only way that Eqs. (28) can be satisfied is for $c_1^{(3)} = c_2^{(3)} = 0$. The unnormalized eigenvector is therefore

$$c^{(3)} = \begin{pmatrix} 0 \\ 0 \\ c_3^{(3)} \end{pmatrix}$$

and the normalized eigenvector is

$$c^{(3)} = \frac{1}{\sqrt{a_{33}}} \begin{pmatrix} 0 \\ 0 \\ 1 \end{pmatrix} . \tag{29}$$

Likewise, it is found that

$$c^{(1,2)} = \frac{1}{\left[a_{11} + \frac{2(b_{11} - \lambda_{1,2} a_{11})}{\lambda_{1,2}} + \left(\frac{b_{11} - \lambda_{1,2} a_{11}}{\lambda_{1,2} a_{12}} \right)^2 a_{22} \right]^{\frac{1}{2}}} \begin{pmatrix} 1 \\ \frac{b_{11} - \lambda_{1,2} a_{11}}{\lambda_{1,2} a_{12}} \\ 0 \end{pmatrix}$$

From the form of the normal modes expressed in terms of the symmetry coordinates in Eqs. (29) and (30), it is evident that the third vibration is due only to bond stretching while the first and second modes are combinations of bond stretching and bending. The three normal vibrations of the water molecule are shown in Fig. 2.

3. Vibrational Energy Levels- From the classical expressions for the potential and kinetic energy of vibration in terms of the normal coordinates, the harmonic oscillator approximation[1,23-25] can be used to give expressions for the vibrational energy levels,

$$E^{(v)} = \sum_{k=1}^{3n} E_k^{(v)} = \sum_{k=1}^{3n} (v_k + \tfrac{1}{2}) \, h \nu_k , \tag{31}$$

where v_k is the vibrational quantum number ($v_k = 0, 1, 2, \ldots$) associated with the k^{th} classical normal mode of vibration ν_k.

Because of symmetry, there may be several of the normal coordinates for which the frequencies will necessarily be identical

and degeneracies will exist. If f_a is the multiplicity of the frequency ν_a, then the vibrational energy levels become

$$E^{(v)} = \sum_a \left[v_a + (\tfrac{1}{2}) f_a \right] h\nu_a \ , \tag{32}$$

where $v_a = \sum_{k=1}^{f_a} v_{ka}$. These degeneracies are usually removed when the anharmonicity of a molecule, which introduces terms of higher order than quadratic into the Hamiltonian, is taken into account. It is then no longer possible to resolve the vibrational motion into a number of normal modes with the vibrational energy being the sum of independent terms, corresponding to the different normal modes. The vibrational energy expression must now include terms containing the vibrational quantum numbers of two or more normal vibrations. For a nonlinear triatomic molecule, such as water, the vibrational energy is given by[26-28]

$$\begin{aligned} \frac{E(v_1, v_2, v_3)}{hc} &= \omega_1(v_1 + \tfrac{1}{2}) + \omega_2(v_2 + \tfrac{1}{2}) + \omega_3(v_3 + \tfrac{1}{2}) \\ &\quad + x_{11}(v_1 + \tfrac{1}{2})^2 + x_{22}(v_2 + \tfrac{1}{2})^2 + x_{33}(v_3 + \tfrac{1}{2})^2 \\ &\quad + x_{12}(v_1 + \tfrac{1}{2})(v_2 + \tfrac{1}{2}) + x_{23}(v_2 + \tfrac{1}{2})(v_3 + \tfrac{1}{2}) + x_{13}(v_1 + \tfrac{1}{2})(v_3 + \tfrac{1}{2}) \ , \end{aligned} \tag{33}$$

where x_{ij} are vibrational constants.

From Eq. (33) and values for the vibrational constants found from spectroscopic data,[27] the wave numbers of the vibration-rotation band centers were computed.[29] The results, along with the relative intensities for the bands in each spectral region, are presented in Table 1.

Table 1. Vibrational Transitions of HHO^{16} at T = 300°K [29]

Region	Transition	ω^* (cm^{-1})	Relative Intensity	ΔK
6.3μ	000→010	1595.0	1.00	± 1
	010→020	1556.4	9.6×10^{-4}	± 1
	010→100	2056.7	1.9×10^{-5}	± 1
	010→001	2160.6	9.6×10^{-5}	0
3.2μ	000→020	3151.4	1.00	± 1
	010→030	3073.4	4.8×10^{-4}	± 1
2.7μ	000→001	3755.8	1.00	0
	000→100	3651.7	.10	± 1
	010→011	3737.0	4.8×10^{-4}	0
	010→110	3630.0	4.8×10^{-5}	± 1
1.87μ	000→011	5332.0	1.00	0
	000→110	5225	2.0×10^{-2}	± 1
	000→030	4668.4	6.7×10^{-3}	± 1
	010→021	5279.0	4.8×10^{-4}	0
	010→120	5166.0	9.6×10^{-6}	± 1
	010→040	4551.0	3.2×10^{-6}	± 1
	010→101	5656.6	4.8×10^{-4}	0
	010→200	5593.1	3.8×10^{-5}	± 1
	010→002	5847.2	5.8×10^{-5}	± 1
1.38μ	000→101	7251.6	1.00	0
	000→021	6874	1.0×10^{-1}	0
	000→120	6761	1.3×10^{-2}	± 1
	000→040	6146	4.3×10^{-3}	± 1
	000→200	7188.1	2.5×10^{-1}	± 1
	000→002	7442.2	2.5×10^{-1}	± 1
	010→111	7212.0	4.8×10^{-4}	0

Region	Transition	ω^* (cm^{-1})	Relative Intensity	ΔK
1.38μ	010→031	6769	4.8×10^{-5}	0
(Cont.)	010→130	6663	6.2×10^{-6}	± 1
	010→050	5990	2.1×10^{-6}	± 1
	010→210	7148.1	1.2×10^{-4}	± 1
	010→012	7402.6	1.2×10^{-4}	± 1

* The wave numbers of the band centers were computed from equation (33) using the following vibrational constants of Darling and Dennison[27] (all in cm^{-1}):

$\omega_1 = 3825.32$, $\omega_2 = 1653.91$, $\omega_3 = 3935.59$,
$x_{11} = -43.89$, $x_{22} = -19.5$, $x_{33} = -46.37$,
$x_{12} = -20.02$, $x_{13} = -155.06$, $x_{23} = -19.81$,

$|\gamma| = 74.46$, where γ is the perturbation constant appearing in the matrix element

$$\langle v_1, v_2, v_3 | W | v_1-2, v_2, v_3+2 \rangle = \frac{\gamma}{2} \sqrt{v_1(v_1-1)(v_3+1)(v_3+2)}$$

for H_2O. The constants of Darling and Dennison were obtained by fitting Eq. (33) to experimental data.[30-32] Slightly different constants have been given by Nielson.[33]

4. Rotational Energy Levels- The expression for the rotational energy levels of an asymmetric top molecule such as water vapor is very complex.[1] In view of this complexity, we shall use a simpler "nearly symmetric top" representation in the form*

$$\frac{E(J,K)}{hC} = \sqrt{BC}\,J(J+1) + (A - \sqrt{BC})K^2, \tag{34}$$

where J is the total angular momentum quantum number, K is the quantum number measuring the projection of J on the symmetry axis, and A, B and C are rotational constants inversely proportional to the three principal moments of inertia of the molecule ($A > B > C$).† The degeneracies of the energy levels are $g_{JK} = 2(2J+1)$ for $K \neq 0$ and $g_{JK} = 2J + 1$ for $K = 0$. For the ground state of the water molecule, the following numerical values apply: $A = 27.8\ cm^{-1}$, $B = 14.5\ cm^{-1}$, and $C = 9.28\ cm^{-1}$.[1]

5. The Infrared Spectrum of Water Vapor. The infrared spectrum of water vapor is composed of spectral lines corresponding to transitions between different vibration-rotation energy levels. The frequency of a spectral line is determined by the difference between the sum of the vibrational and rotational energy levels of the final and initial states.

Selection rules governing the allowed transitions for a triatomic,

---

* See Ref. 1, Eq. (7-123).

† For symmetric top molecules, B = C.

asymmetric molecule such as H_2O, are given by Herzberg.[25] The rotational selection rules, $\Delta J=0, \pm 1$, always apply. In addition, two types of rotational transitions are allowed: $\Delta K= 0$ and $\Delta K= \pm 1$ corresponding to the so-called parallel and perpendicular transitions of a symmetric top molecule, respectively. The vibration-rotation bands of water vapor, composed of one of these types of transitions, will approach, as limits, the parallel or perpendicular bands of the equivalent symmetric top molecule, and will have the same general structure. The K-transition for each of the bands of water vapor is also given in Table 1.

C. EXPERIMENTAL METHOD

1. Definitions - Consider a hemisphere of radius ℓ, filled with a gas at thermal equilibrium at pressure p. A spectral absorption coefficient is defined so that the emitted radiancy from the base of the hemisphere, in the wave number range between ω and $\omega + d\omega$, is

$$R_\omega d\omega = R_\omega^o \left[1-\exp(-P_\omega p\ell)\right], \tag{35}$$

where R_ω^o is the black body radiancy at the wave number ω. The product $p\ell$ is known as the optical depth and is usually expressed in cm-atm.

The expression $\left[1-\exp(-P_\omega p\ell)\right]$ is the hemispherical spectral emissivity and, at thermal equilibrium, is equal to the spectral absorptivity by Kirchoff's law. Therefore, radiation passing through a layer of gas at thermal equilibrium, of length ℓ, and at pressure p,

will be attenuated so that

$$I_\omega = I_\omega^o \exp(-P_\omega p\ell), \tag{36}$$

where I_ω and I_ω^o are the transmitted and incident spectral flux densities, respectively.

For a liquid absorber of length ℓ, it is convenient to define a linear spectral absorption coefficient k_ω, by

$$I_\omega = I_\omega^o \exp(-k_\omega \ell) . \tag{37}$$

The integrated intensity of a gas, a, for an absorption band located between the wave numbers ω_1 and ω_2, is defined as

$$a = \int_{\omega_1}^{\omega_2} P_\omega d_\omega . \tag{38}$$

Likewise, the integrated intensity for an absorption band of a liquid, a', is defined as

$$a' = \int_{\omega_1}^{\omega_2} k_\omega d\omega . \tag{38a}$$

When analyzing the experimental data, one must take into account the finite resolution of the instrument and the resulting slit distortions. We define an instrumental slit function $g(|\omega - \omega'|, b', c')$ for the effective spectral width of the exit slit between $\omega - \Delta\omega^*$ and $\omega + \Delta\omega^*$; ω is the actual wave number setting of the instrument while b' and c' are parameters dependent upon the slit geometry. If the normalization

condition

$$\int_{\omega - \Delta\omega^*}^{\omega + \Delta\omega^*} g\,(|\omega-\omega'|,\ b', c')\ d\omega' = 1 \qquad (39)$$

holds, the slit function gives the fraction of energy at the wave number ω' which the detector senses when the instrument is set at ω. The apparent spectral flux density, I^a_ω, detected by the instrument when it is set at ω, is therefore

$$I^a_\omega = \int_{\omega-\Delta\omega^*}^{\omega+\Delta\omega^*} I_{\omega'}\, g(|\omega-\omega'|,\ b', c')\ d\omega' . \qquad (40)$$

Representative slit functions are triangular for prism instruments and gaussian for grating instruments.

2. The Wilson-Wells-Penner-Weber (W_3P) Method - The effect of the slit function in determining the integrated intensity and spectral absorption coefficient can be eliminated if certain experimental conditions are satisfied. The absorption data were analyzed according to the W_3P method described by Penner.[1]

The method necessitates the smearing out of the rotational fine structure of a vibration-rotation band by means of sufficient pressure broadening. This may be accomplished either by maintaining an adequately high pressure of the absorbing gas (self-broadening) or by pressurizing with a foreign, non-absorbing gas (foreign-gas broadening).

In order to obtain the integrated intensity, we define a parameter $\mathcal{B}$, which equals the integral over the band region of the natural logarithm of the ratio of apparent spectral incident intensity $I_{\omega}^{o,a}$, to the apparent spectral transmitted intensity I_{ω}^{a}, i. e.,

$$\mathcal{B} = \int_{\omega_1}^{\omega_2} \ell n \left(\frac{I_{\omega}^{o,a}}{I_{\omega}^{a}} \right) d\omega = \int_{\omega_1}^{\omega_2} \left[\ell n \frac{\int_{\omega-\Delta\omega^*}^{\omega+\Delta\omega^*} I_{\omega'}^{o} \, g(|\omega-\omega'|, b', c')d\omega'}{\int_{\omega-\Delta\omega^*}^{\omega+\Delta\omega^*} I_{\omega'} \, g(|\omega-\omega'|, b', c')d\omega'} \right] d\omega. \quad (41)$$

Since $I_{\omega'} = I_{\omega'}^{o} \exp(-P_{\omega'}X)$, where X = optical depth = $p\ell$, it follows that, if the incident spectral flux density $I_{\omega'}^{o}$, is constant over the wave number interval between $\omega - \Delta\omega^*$ and $\omega + \Delta\omega^*$, then

$$\mathcal{B} = \int_{\omega_1}^{\omega_2} \left\{ -\ell n \frac{\int_{\omega-\Delta\omega^*}^{\omega+\Delta\omega^*} \left[\exp(-P_{\omega'}X)\right] g(|\omega-\omega'|, b', c')d\omega'}{\int_{\omega-\Delta\omega^*}^{\omega+\Delta\omega^*} g(|\omega-\omega'|, b', c')d\omega'} \right\} d\omega \quad (42)$$

and

$$\frac{d\mathcal{B}}{dX} = \int_{\omega_1}^{\omega_2} \left\{ \frac{\int_{\omega-\Delta\omega^*}^{\omega+\Delta\omega^*} P_{\omega'} \left[\exp(-P_{\omega'}X)\right] g(|\omega-\omega'|, b', c')d\omega'}{\int_{\omega-\Delta\omega^*}^{\omega+\Delta\omega^*} \left[\exp(-P_{\omega'}X)\right] g(|\omega-\omega'|, b', c')d\omega'} \right\} d\omega. \quad (43)$$

From Eq. (43) we see that the integrated intensity is

$$a = \int_{\omega_1}^{\omega_2} P_\omega \, d\omega = \frac{d\mathcal{B}}{dX} \quad , \tag{44}$$

as long as P_ω, can be considered constant over the wave number range of the effective slit width $2\Delta\omega^*$. This condition is satisfied by sufficient pressure broadening.

In a similar fashion, we find that if sufficient pressure broadening is achieved,

$$P_\omega = \frac{d\ell n(I_\omega^{o,\,a}/I_\omega^{a})}{dX} \quad . \tag{45}$$

Equations (44) and (45) are the desired results.

3. Analysis of Data - A sample of the experimental data showing the absorption of 1.22 cm of water vapor at 200°C and 5.18 atm is shown in Fig. 3; the signal was recorded on 0 to ∞ log paper. The experimental data, along with the calibration curve of the monochromator prism, was input to an IBM 7090.* The computer was programmed to perform the integration designated by Eq. (41), and to execute a least square fit of the resultant values for $\mathcal{B}$ to Eq. (44) in order to determine the integrated intensity. In addition, the computer carried out a least square fit of the experimental points to Eq. (45) in order to determine the spectral absorption coefficients.

The computer printed out the determined values of the integrated intensity (from Eq. (44)), the experimental and fitted values of $\mathcal{B}$ along

---

* The author is indebted to M. Thomas for writing the program.

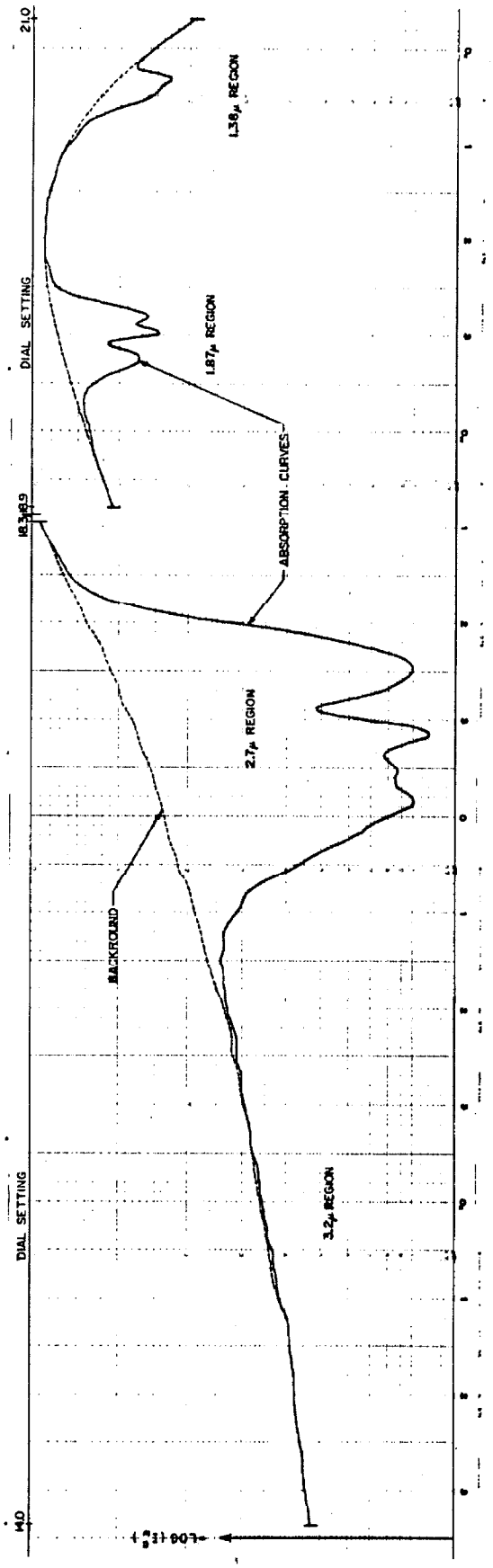

Fig. 3. Sample of the experimental data showing the absorption by water vapor; spacer = 1.22 cm; T = 200°C; p = 5.19 atm.

with the percent error for each point, the experimental values of $\ell n(I_{(\omega)}^{o,a}/I_{(\omega)}^{a})$ at previously designated wave number intervals, and the slope-determined values of the spectral absorption coefficients (from Eq. (45)) at the same wave number intervals.

D. EXPERIMENTAL FACILITIES* AND PROCEDURES

1. Introduction - An overall view of the apparatus appears in Fig. 4. Situated on the table, from left to right, are the constant temperature bath, the potentiometer with ice bath, the control panel containing the electrical switches and meters, the thermocouple selector, and the pressure gage. Below the table are the oven temperature control unit, the 220 volt switch, and variac. At the right are the vacuum tank, spectrometer, and recorder.

Figure 5 is a view of the inside of the vacuum tank containing the globar, chopper, mirrors and oven; a schematic diagram of the apparatus is shown in Fig. 6.

2. Vacuum System - The 2-ft. diameter by 5-ft. long vacuum tank, which can be seen in Figs. 4 and 6, contains the absorption cell, light source, chopper, oven, and associated optics. A pressure of 50μ was achieved in the tank by using a CEC Type MCF-60 oil diffusion pump backed up by a Kinney Model KC-8 mechanical pump. This system was

---

* The apparatus used in the present studies is an improved version of equipment first assembled by D. Weber and subsequently modified by U. P. Oppenheim and A. Guttman.

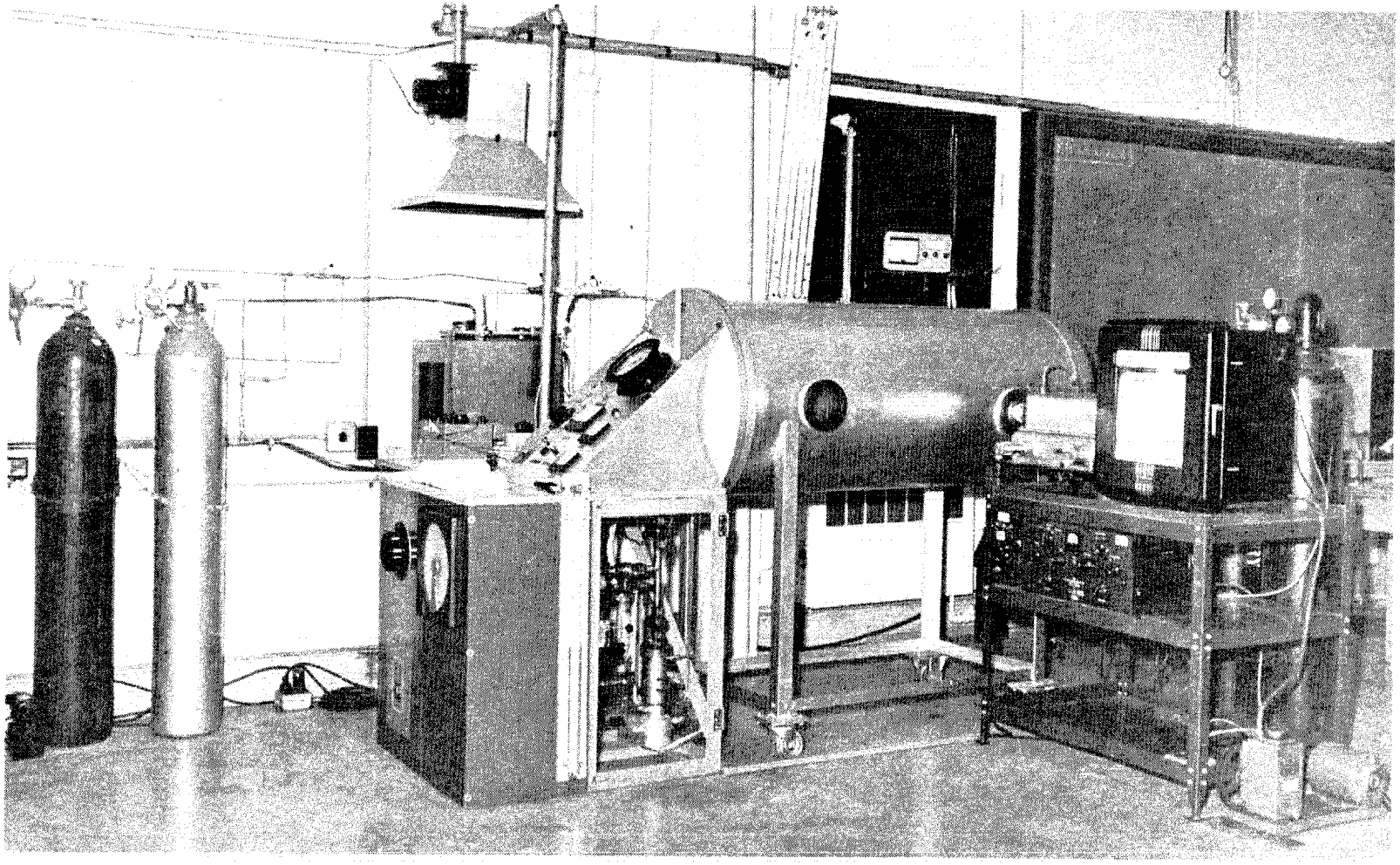

Fig. 4. Overall view of experimental facilities.

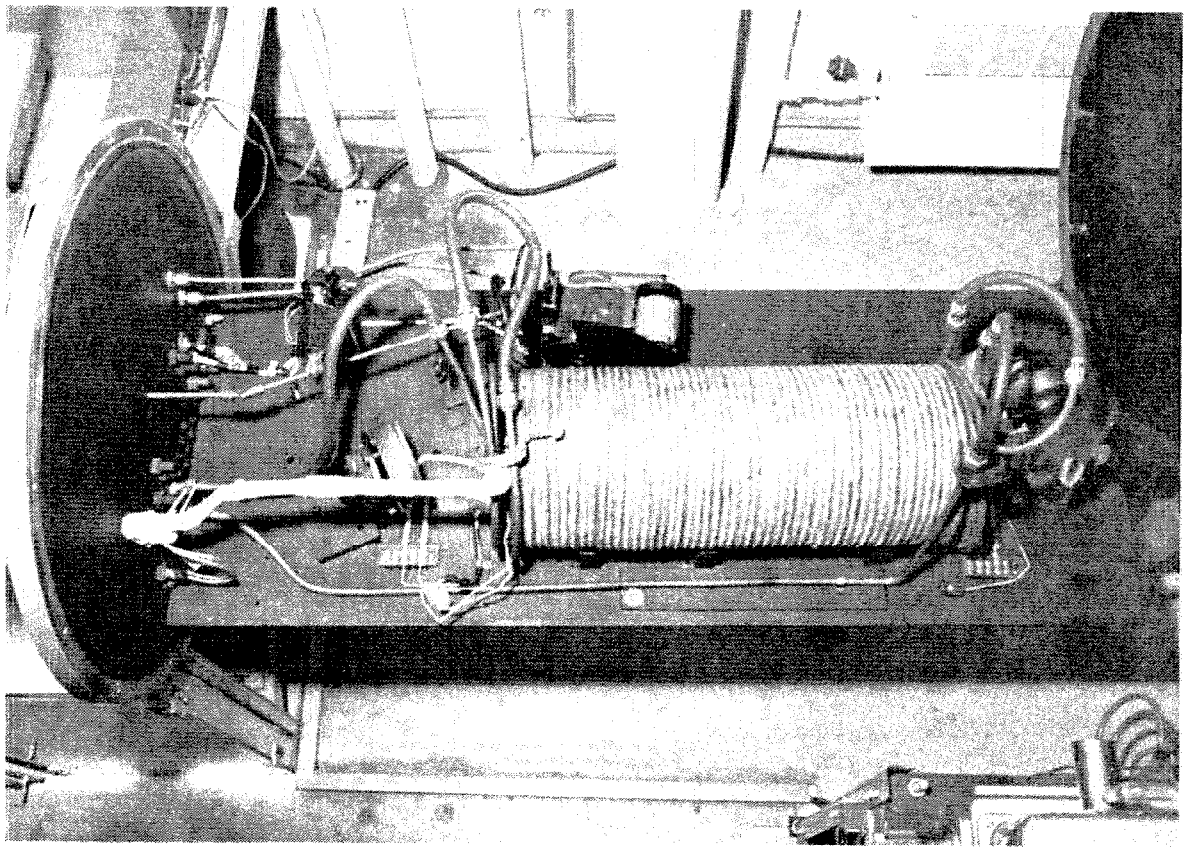

Fig. 5. View of inside of vacuum tank.

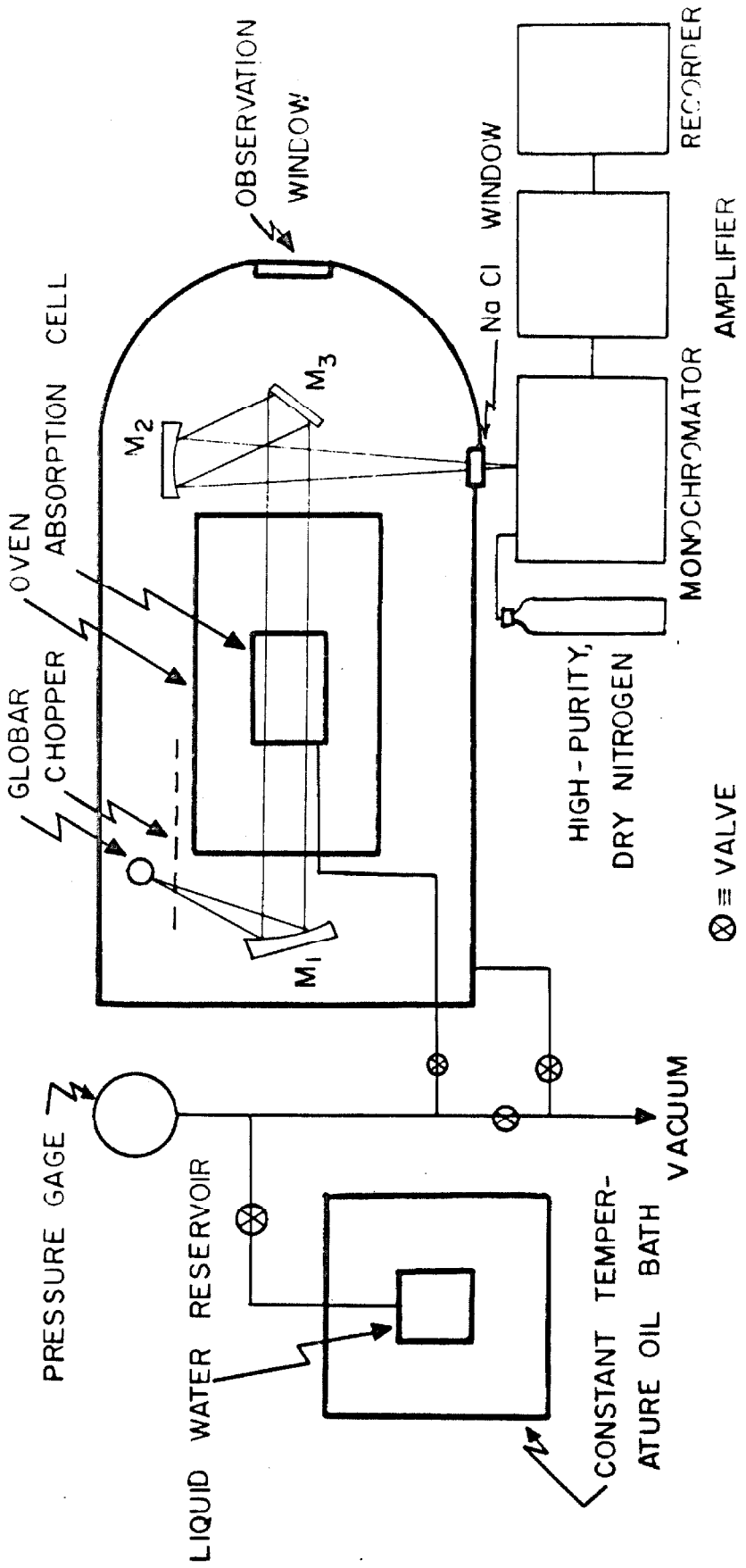

Fig. 6. Schematic diagram of the experimental apparatus.

also used to evacuate the gas supply lines and absorption cell.

3. Optical System - A water-cooled globar was used, operated at about 1400°K, as an infrared light source. Stable radiation output was accomplished by placing a number of 10 - 25 Amperite ballast tubes in series with the globar, and supplying the voltage from a Sola constant-voltage transformer; regulation of the voltage was achieved by using a variac.

The radiation was modulated at 13 cps by a Perkin-Elmer chopper (see Fig. 6), passed through the absorption cell by using a parabolic mirror (M_1) and focused onto the exit slit of the monochromator with the aid of another parabolic mirror (M_2). The light beam left the vacuum tank through a 2-inch diameter by 1/4-inch thick sodium chloride window.

The signal was measured by a Perkin-Elmer Model 98 spectrometer with a 13 cps amplifier, and put onto a Leeds and Northrup Speedomax Type G recorder; logarithmic chart paper No. 578, supplied by Technical Charts Incorporated, was used.

Standard procedures were used to calibrate the monochromator. The calibrations for the LiF and Na Cℓ prisms are shown in Figs. 7 and 8, respectively.

4. Heating Unit and Temperature Measurement - The oven was made with a Norton cylindrical refractory core (inside diameter $\simeq$ 3.1-inch,

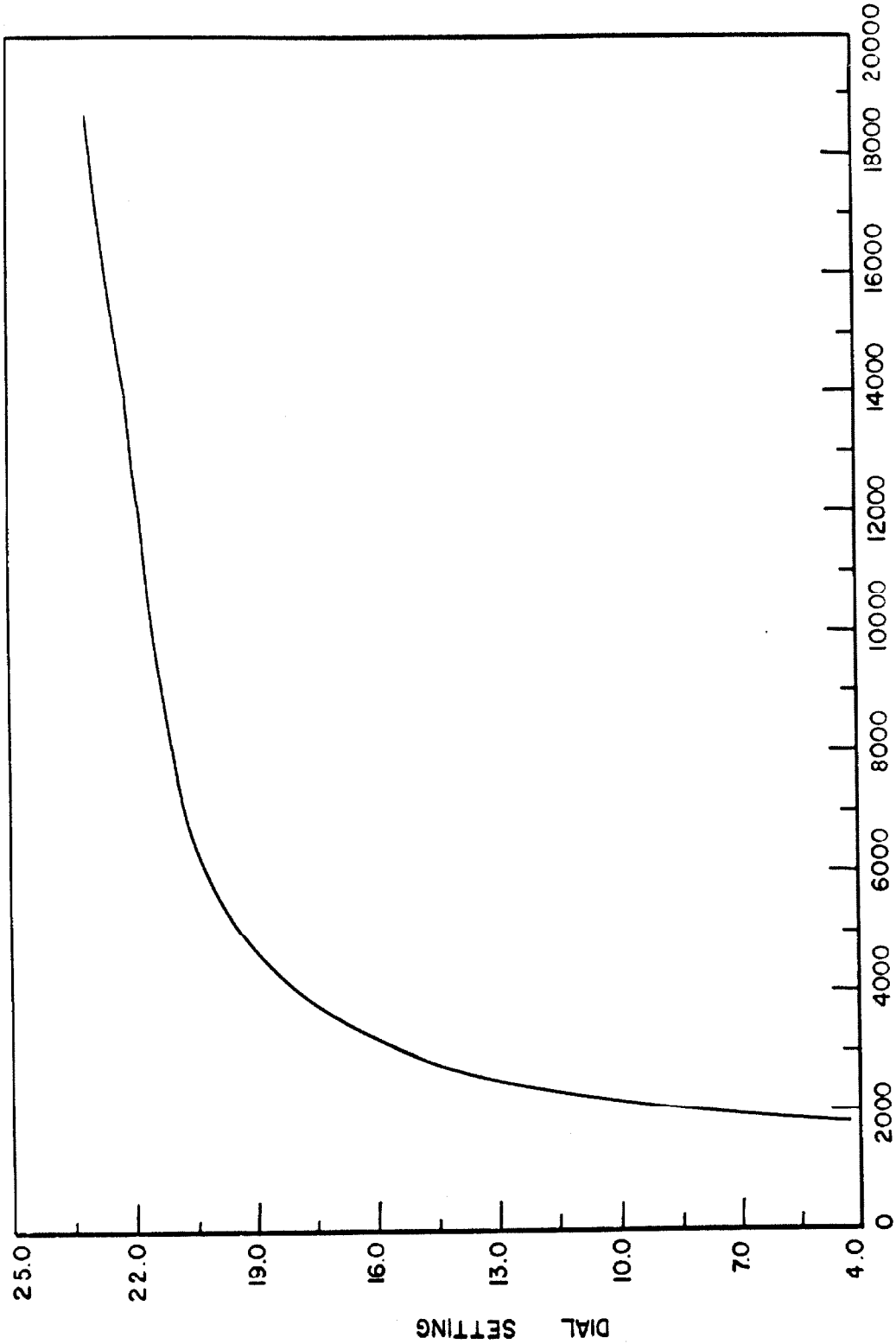

Fig. 7. Lithium fluoride prism calibration.

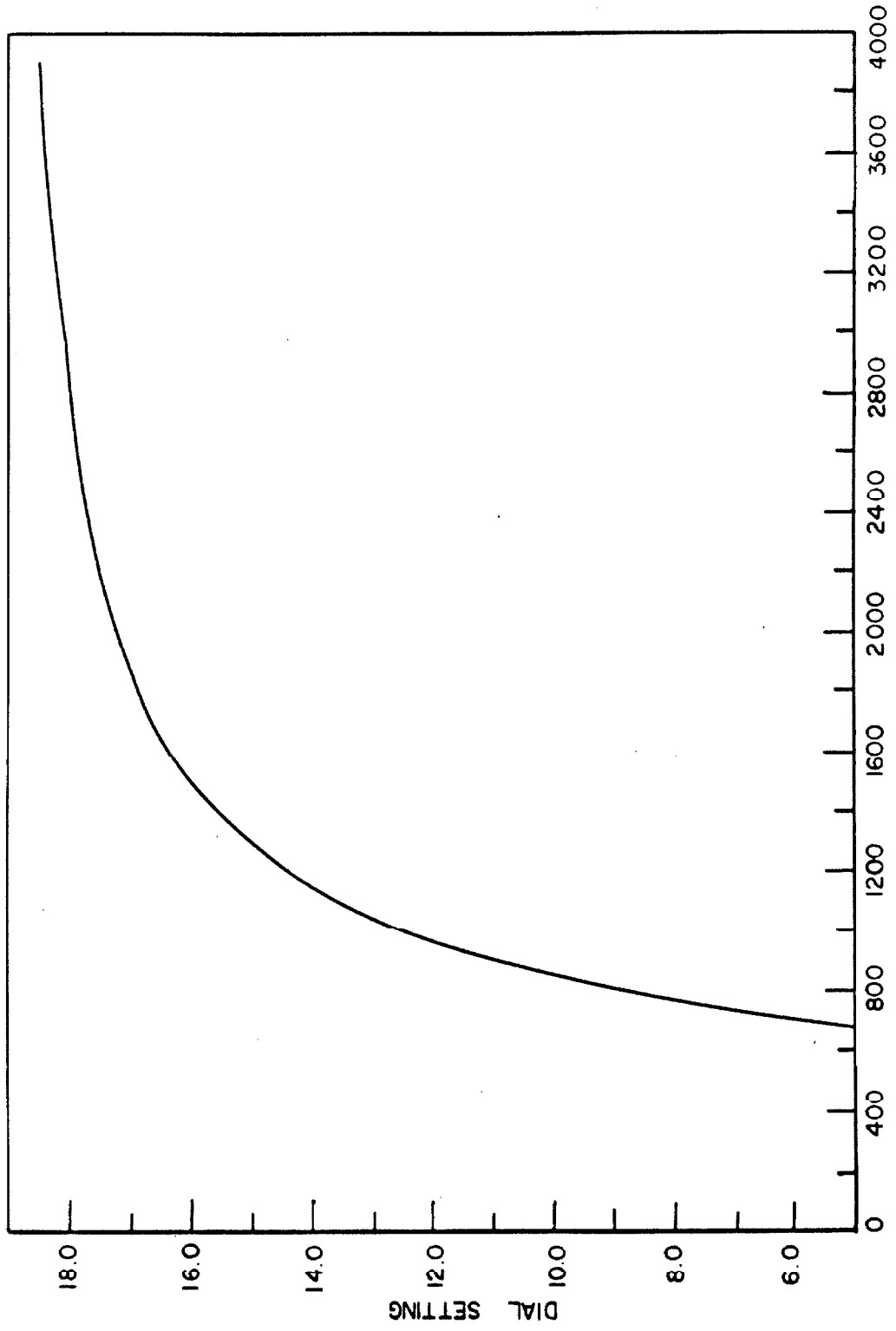

Fig. 8. Sodium chloride prism calibration.

length $\simeq$ 20-inch) and Jelliff Alloy K resistance wire. Water-cooled copper tubing surrounded the oven. Current was passed through the heating coils from a 220-volt A. C. source, regulated by a variac. An oven temperature of 1200°K was easily achieved with a current of about 16 amperes. Temperatures were kept within $\pm$ 2°C of the desired value ($\pm$ 1°C below 210°C) by controlling the oven current with a Leeds and Northrup Speedomax Type H temperature – control unit, which monitored the absorption cell temperature through an alumel-chromel thermocouple. Precise measurement of the cell temperature was accomplished by a second alumel-chromel thermocouple and a Leeds and Northrup N. 8657-C double range potentiometer.

5. Gas Supply and Constant Temperature Reservoir - The water vapor was supplied from a stainless steel liquid water reservoir, submerged in a constant — temperature oil bath. A cross-sectional view of the oil bath is shown in Fig. 9. The current through the copper heating elements was controlled by a Cenco-DeKhotinsky DPST, Bimetallic Thermoregulator and a SPST, Non-Induction Load Relay obtained from Central Scientific Company; the oil used was Mar-Temp Oil No. 2, purchased from E. F. Houghton and Co. Temperatures up to 215°C could be held in the bath with an accuracy of $\pm$ 0.5°C. Water-cooled copper tubing was submerged in the bath so that the oil temperature could be reduced in a reasonable amount of time (without cooling, the oil temperature decreased 10°C/hour). The temperature of the oil bath and reservoir was measured by an alumel-chromel thermocouple connected to the potentiometer through a thermocouple selector switch.

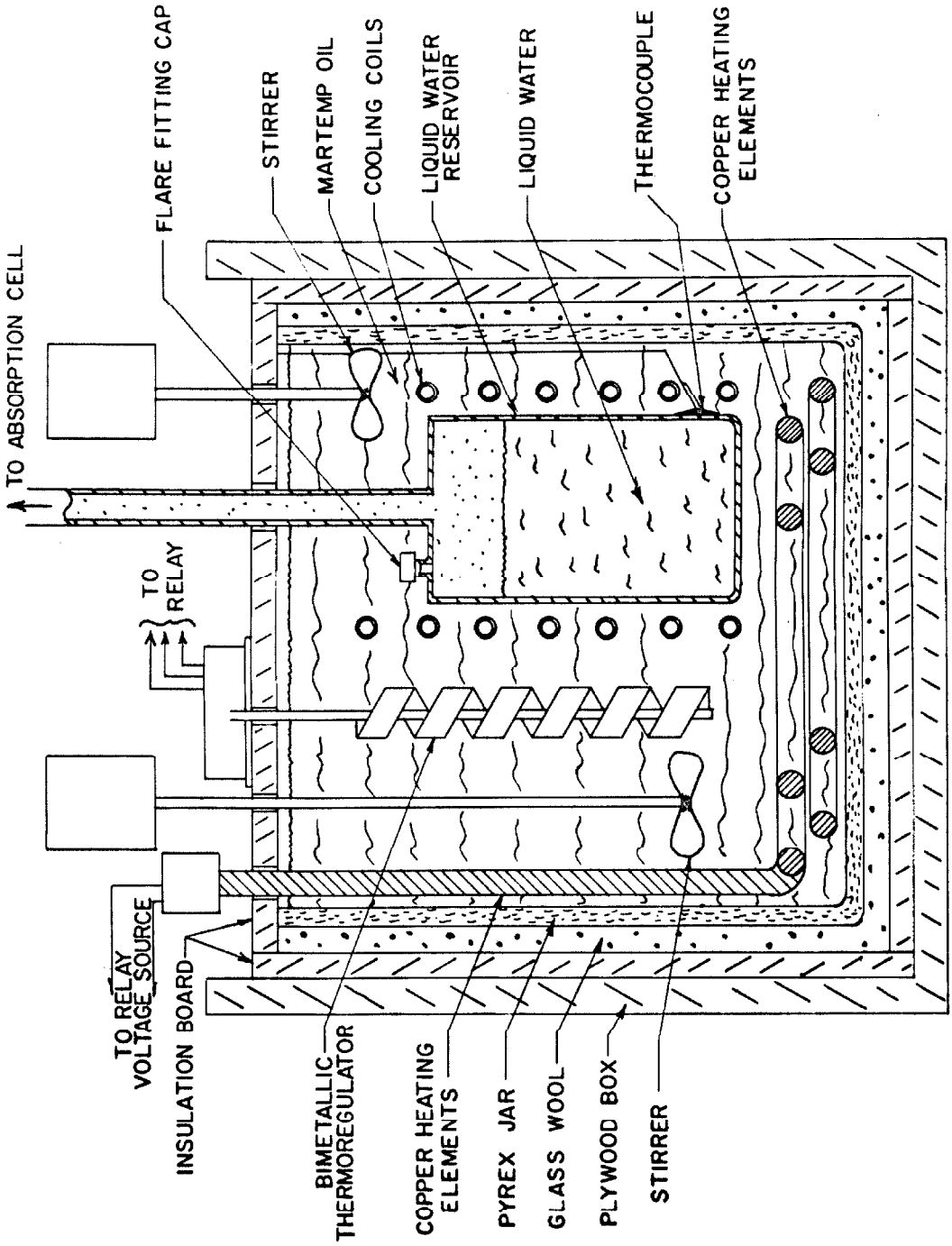

Fig. 9. Cross-sectional view of constant-temperature bath.

The gas supply lines were made of 1/4-inch stainless steel tubing, kept at about 80°C by heating tapes to reduce condensation, connected with stainless steel flare fittings; the valves were 1/4-inch Circle Seal plug valves. A pressure of less than 1μ could be pulled in the gas lines and absorption cell.

6. Pressure Measurement - The water vapor pressure was measured with an Ashcraft 0 to 400 psi pressure gage, which was calibrated using both a dead weight tester and static pressure tests of the water vapor pressure above liquid water at a known temperature.[34] The resulting calibration, shown in Fig. 10, was accurate to ± 1 psi.

Vacuum pressures were measured with a Pirani tube and gage (0 to 2000μ), supplied by Consolidated Electrodynamics Corporation.

7. Absorption Cell with Variable Spacers* - A view of the absorption cell with variable spacers is shown in Fig. 11. The cell was used in two ways. In the preliminary experiments on water vapor absorption (Chapter II), and in the experiments on saturated water vapor absorption (Chapter V), the vapor was supplied from a liquid reservoir attached to the cell and placed in the oven with the cell (see Fig. 12). With this setup, the water vapor pressure in the cell corresponded to the vapor pressure above liquid water at the cell temperature, as long as liquid remained in the reservoir, and pressure equilibrium was achieved.

For the experiments on liquid water (Chapter IV) and in the

* This cell was built by A. Guttman.

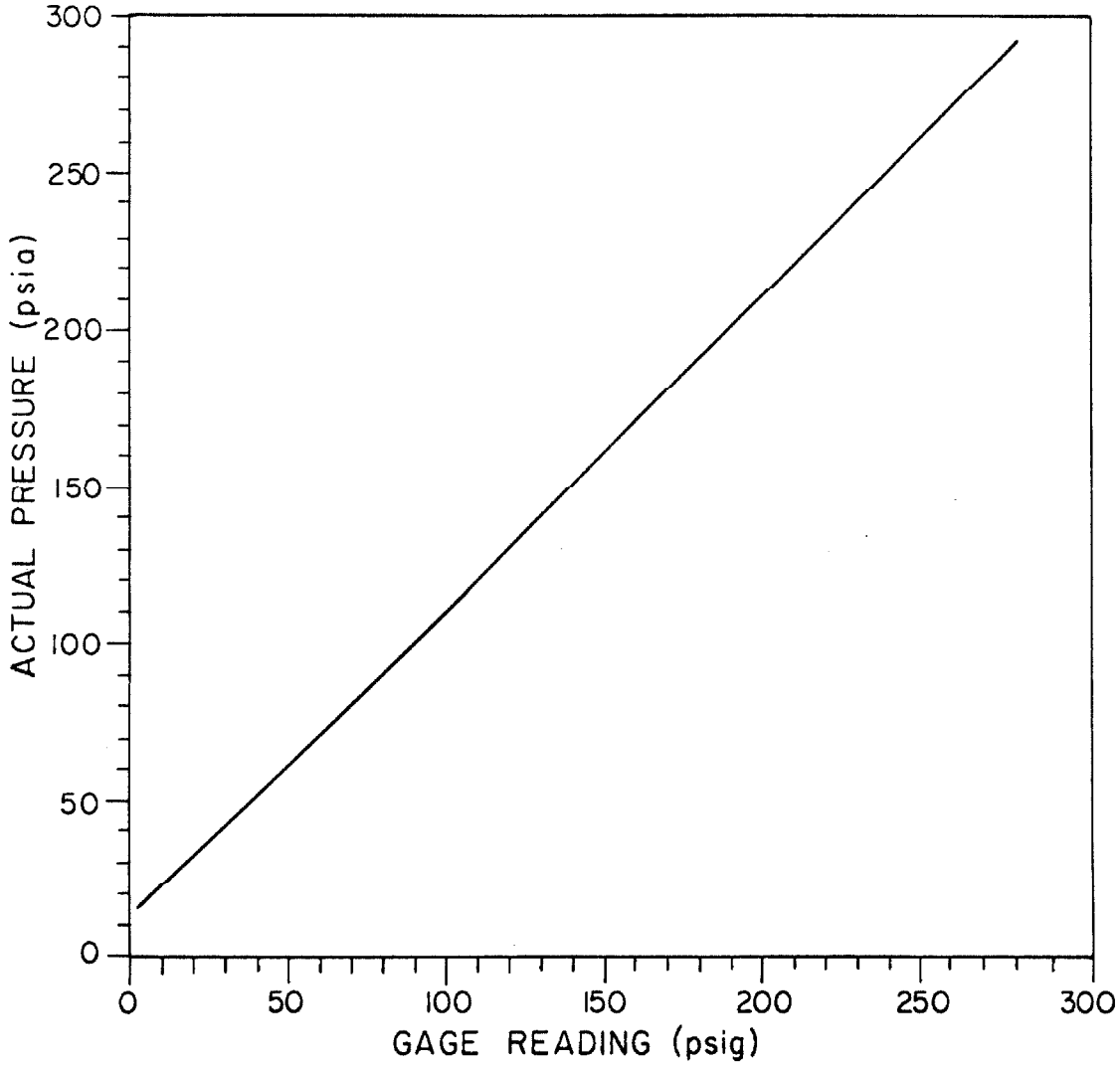

Fig. 10. Pressure gage calibration.

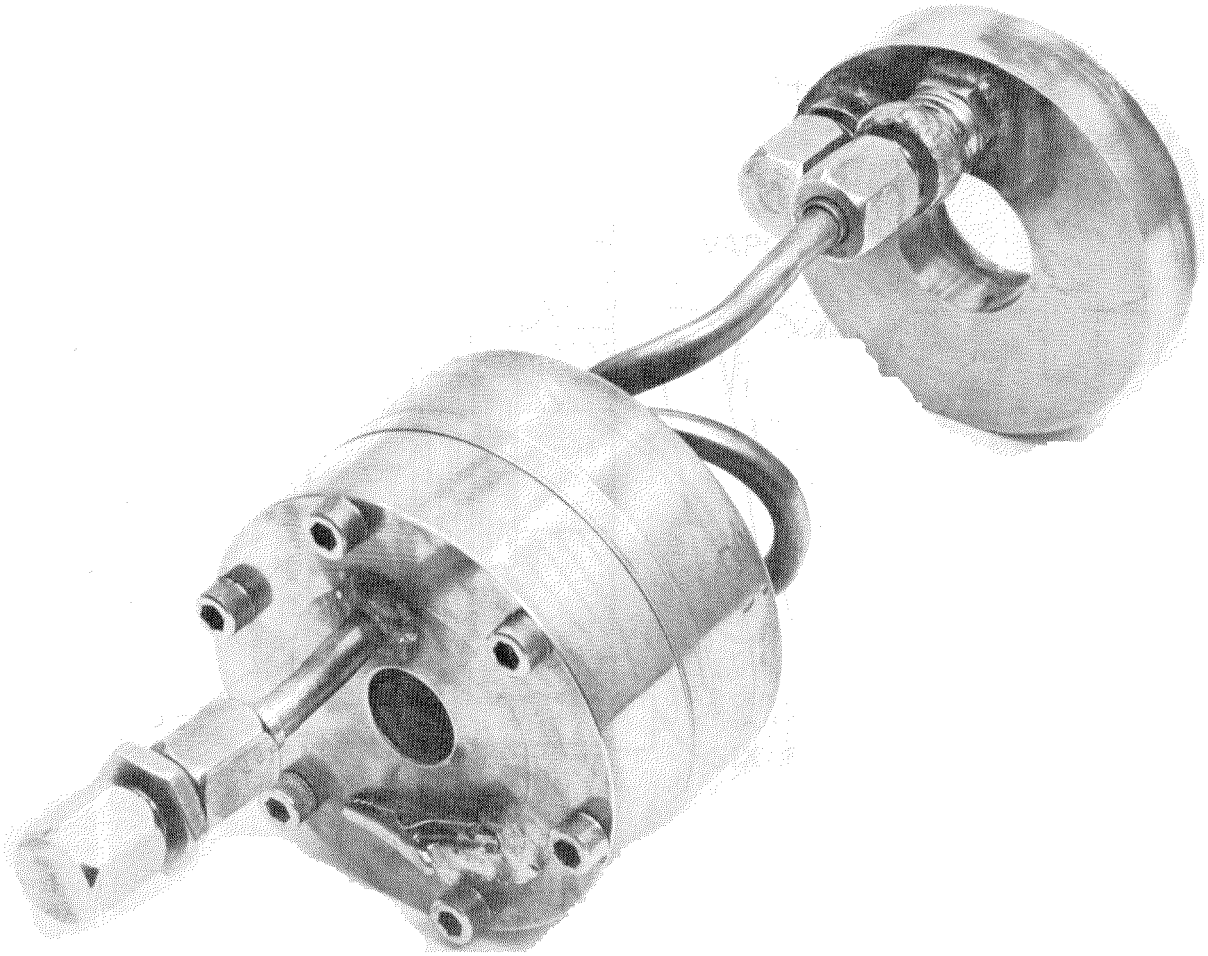

Fig. 11. Absorption cell with variable spacers.

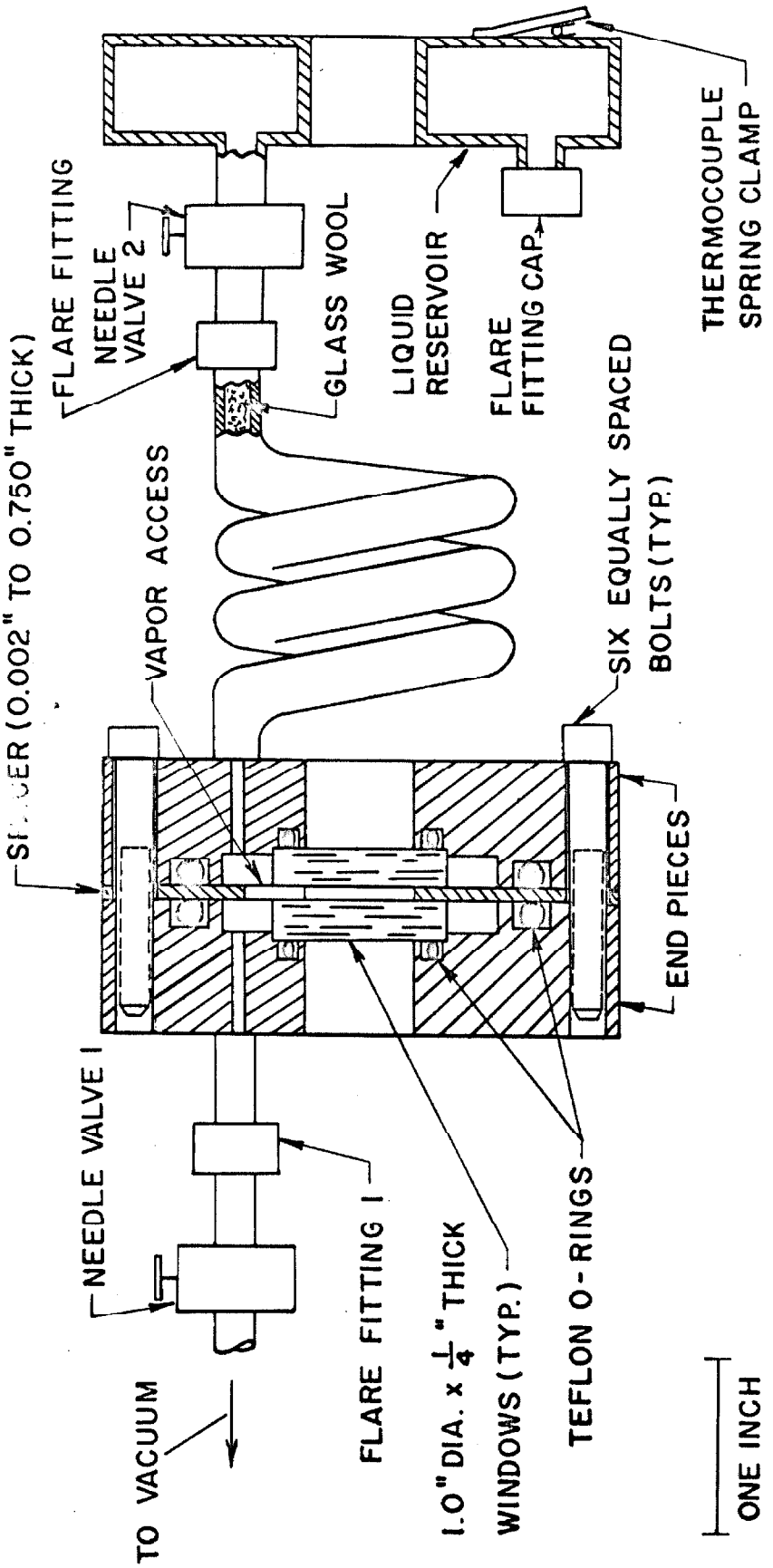

Fig. 12. Cross-sectional view of the variable-spacer absorption cell with self-contained liquid reservoir.

experiments on saturated vapor (Chapter V), the water vapor was supplied to the cell from the liquid reservoir submerged in the constant temperature bath outside the vacuum tank (see Fig. 13).

Because of the teflon O-rings, the cell could only be used to a temperature of 210°C. Thicknesses of available spacers ranged from 0.002 to 0.750-inches. The thermocouples were attached by means of spring clamps silver-soldered to the body of the cell and to the self-contained liquid reservoir.

8. High-Temperature Absorption Cell - An absorption cell (see Figs. 14 and 15) to hold pressure at 1000°K was specially designed and built with the help of Instra-Tech Seals in Pasadena and Neel Industries in Northridge, California. The material used was Haynes-25, a high cobalt alloy which resists oxidation and carburization up to 1300°K; it was obtained from the Haynes Stellite Company of Kokomo, Indiana. The portion of the 1/4-inch tubing that was exposed to the high temperature was also made of the Haynes-25 alloy. The assembled cell consisted of nine pieces: the two end pieces; the center spacer; the adapter seal; the adapter with the tubing arc-welded to it; two platinum O-rings; and two optical windows, as well as 8 bolts, washers and nuts.

The pressure seal between the adapter and the center spacer was achieved by tightening down the adapter screw to squeeze the adapter seal. The platinum O-rings were made in our laboratory from 0.020-inch platinum wire and No. 1500 platinum solder. A seal was formed between the spacer and windows by squeezing each of the O-rings to a width of 0.010-inch by means of the eight equally spaced

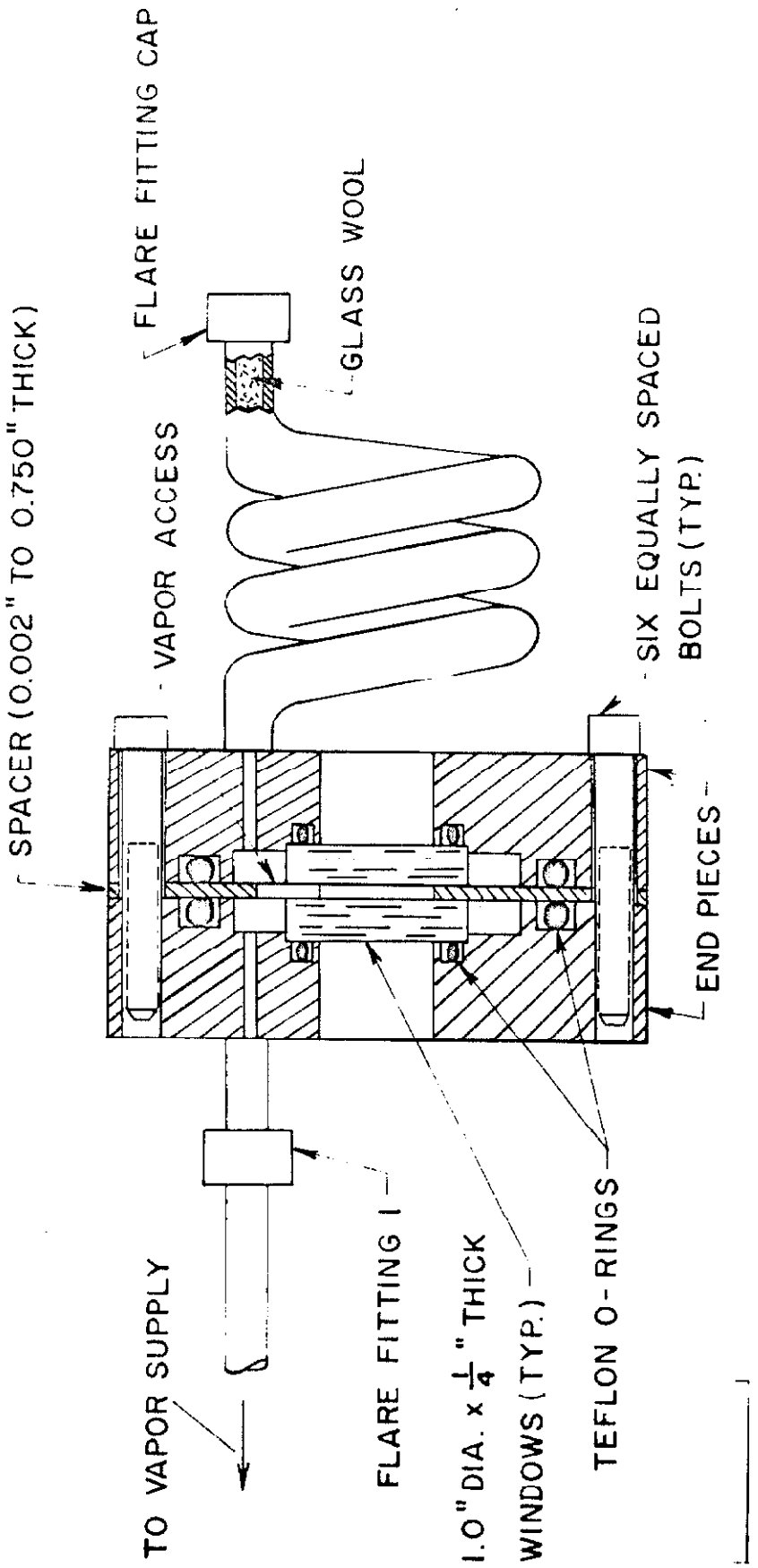

Fig. 13. Cross-sectional view of the variable-spacer absorption cell; the vapor was supplied from a reservoir located outside of the vacuum tank.

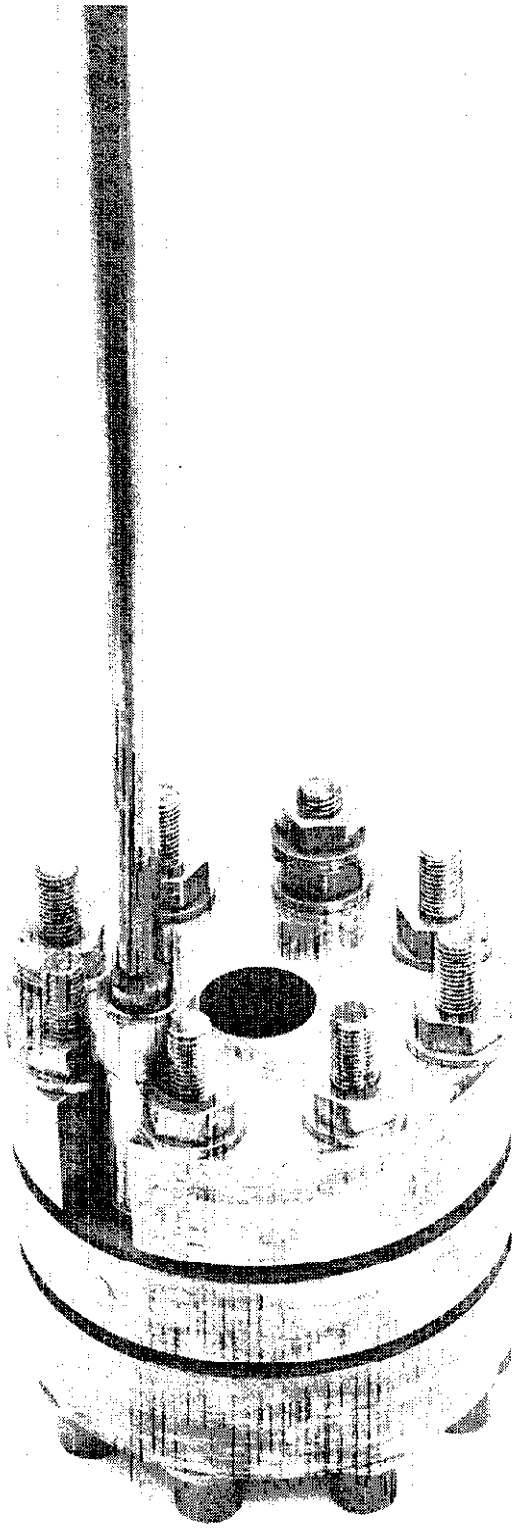

Fig. 14. High-temperature absorption cell.

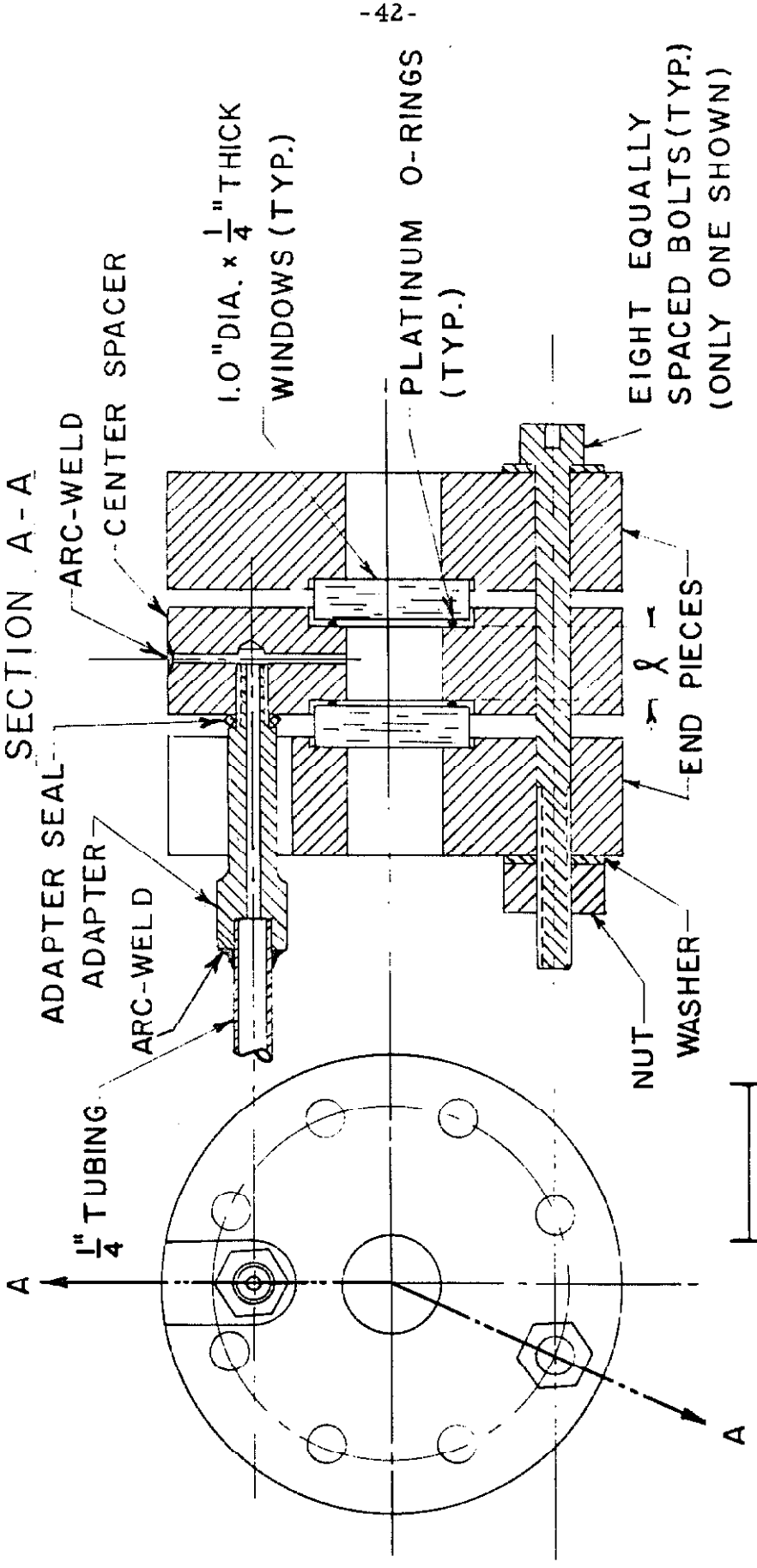

Fig. 15. Cross-sectional view of the high-temperature absorption cell.

bolts. The geometric length of the gas was ℓ (see Fig. 15) plus twice the thickness of the squeezed O-rings (= 0.020-inch). For the cell used, ℓ + 0.020 x 2.54 was 1.22-cm.

The cell held a pressure of 250 psi at 600°C with two 1-inch diameter by 1/4-inch thick sapphire windows. The pressure seal failed above this temperature because of the large difference between the coefficients of expansion of the Haynes-25 and sapphire, 17.7×10^{-6} and 8.4×10^{-6} cm/cm-°C, respectively. Pressure tightness was achieved up to 1100°K (tested with 200 psi) by using magnesium oxide windows, which have a coefficient of expansion of 13.8×10^{-6} cm/cm-°C.

After exposure to temperatures above 1000°K for five days, the cell was covered with a dark green residue, probably cobalt and nickel oxides. But the residue was not found on the windows, and there was only a slight reduction in the transmission through the windows during the five-day period.

The thermocouples were attached to the cell body by using an extra nut and two washers on one of the bolts.

9. Elimination of Atmospheric Absorption - The strong atmospheric absorption due to water vapor and carbon dioxide was eliminated by the 50μ pressure in the vacuum tank, and by continuously flushing the monochromator and the short tube between the monochromator entrance slit and vacuum tank window, with high-purity, dry nitrogen.

10. Standard Operating Procedure for Absorption Experiments:

1) The cell was placed in the oven and connected to the supply line.

2) The vacuum tank and absorption cell were evacuated to a pressure of about 50μ.

3) The cell was heated to the desired temperature.

4) With high-purity, dry nitrogen being flushed through the monochromator, the background radiation was recorded.

5) The constant temperature oil bath was heated to the desired temperature; for the water vapor experiment, the temperature corresponded to the vapor pressure desired; for the liquid water experiment, the bath temperature was held above the cell temperature to insure condensation in the cell.

6) The transmission spectrum was automatically scanned. During the 20 to 30 minutes of this operation, we monitored the cell temperature and vapor pressure constantly.

7) Either the cell temperature or the vapor pressure was appropriately changed and the transmission spectrum rescanned.

CHAPTER II

APPROXIMATE MEASUREMENTS OF THE INTEGRATED INTENSITIES OF WATER VAPOR BETWEEN 125 AND 200°C

A. INTRODUCTION

A preliminary investigation on the integrated intensities of the 1.38μ, 1.87μ and 2.7μ bands of water vapor at temperatures between 125 and 200°C has been performed, using sufficient self-broadening to smear out the rotational fine structure.

B. APPARATUS AND PROCEDURE

The experimental facilities are described in Chapter I; the variable spacer absorption cell with the self-contained liquid reservoir (see Fig. 12) was used. Variation of the optical depth was accomplished by using spacers of 0.060, 0.150, 0.250, 0.375, 0.500, and 0.750-inches; the pressure was assumed to be the vapor pressure above liquid water at the temperature of the cell. This technique for monitoring the vapor pressure was previously employed for NO_2-N_2O_4 mixtures found above N_2O_4;[35, 36] it appears to be particularly useful for the type of studies performed in the present investigations.

After liquid water was put in the reservoir, the cell was evacuated by closing needle valve (2) and connecting needle valve (1) to the vacuum pump; needle valve (2) was opened for a moment to remove the atmospheric pressure from the reservoir. The cell was

then placed in the oven and the vacuum tank pressure reduced to 50μ. The background radiation was recorded before the cell was heated; no measurable absorption was found in the background record.

After the cell and reservoir were heated to the desired temperature, pressure equilibrium in the cell was assumed when repeated scanning of an absorption peak showed no change in absorption.

C. RESULTS AND DISCUSSION OF RESULTS

The parameter β (see Eq. (41)) is shown in Figs. 16 to 18 as a function of spacer thickness at temperatures between 125 and 200°C for the 1.38μ, 1.87μ and 2.7μ bands of water vapor, respectively. It can be observed that there is a large scattering of the experimental points when fitting the results to the straight line designated by Eq. (44).

A summary of the values of the integrated intensities of water vapor determined from Figs. 16 to 18 and Eq. (44) is presented in Table 2. Because of the error due to the uncertainty of measuring the cell temperature, with the resulting uncertainty in the vapor pressure, and the large scattering of experimental points evident in Figs. 16 to 18, the uncertainty of the values for the integrated intensity is estimated at ± 20%.

Reference to Chapter V shows that the absorption spectra of saturated water vapor is different from that of water vapor below the saturation pressure. Because of the experimental setup in this investigation, the water vapor is at a saturated or near-saturated condition; this introduces a definite source of error and may partially explain the large scattering of the experimental points.

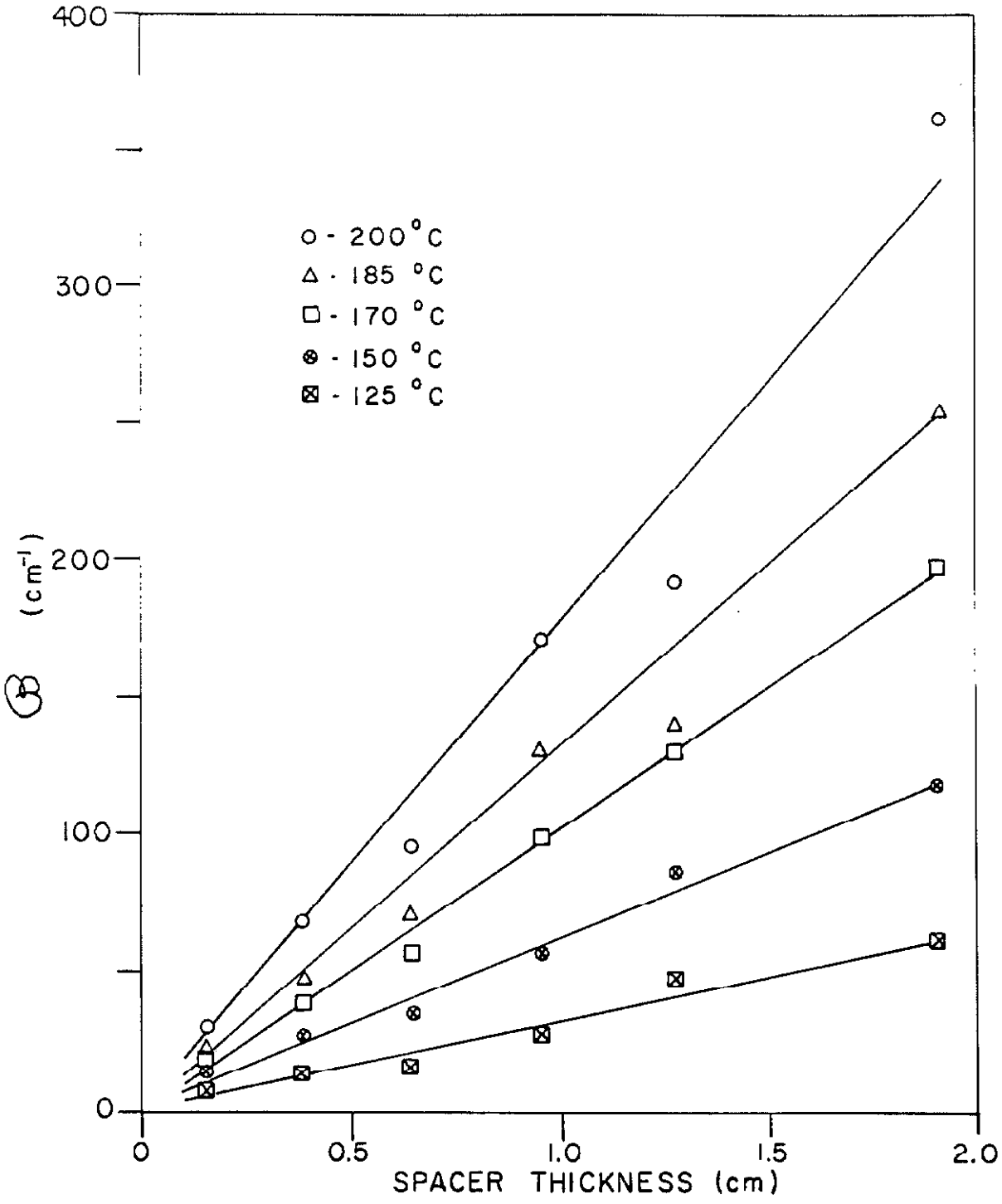

Fig. 16. β plotted as a function of spacer thickness for the 1.38μ band of water vapor at 125, 150, 170, 185, and 200°C.

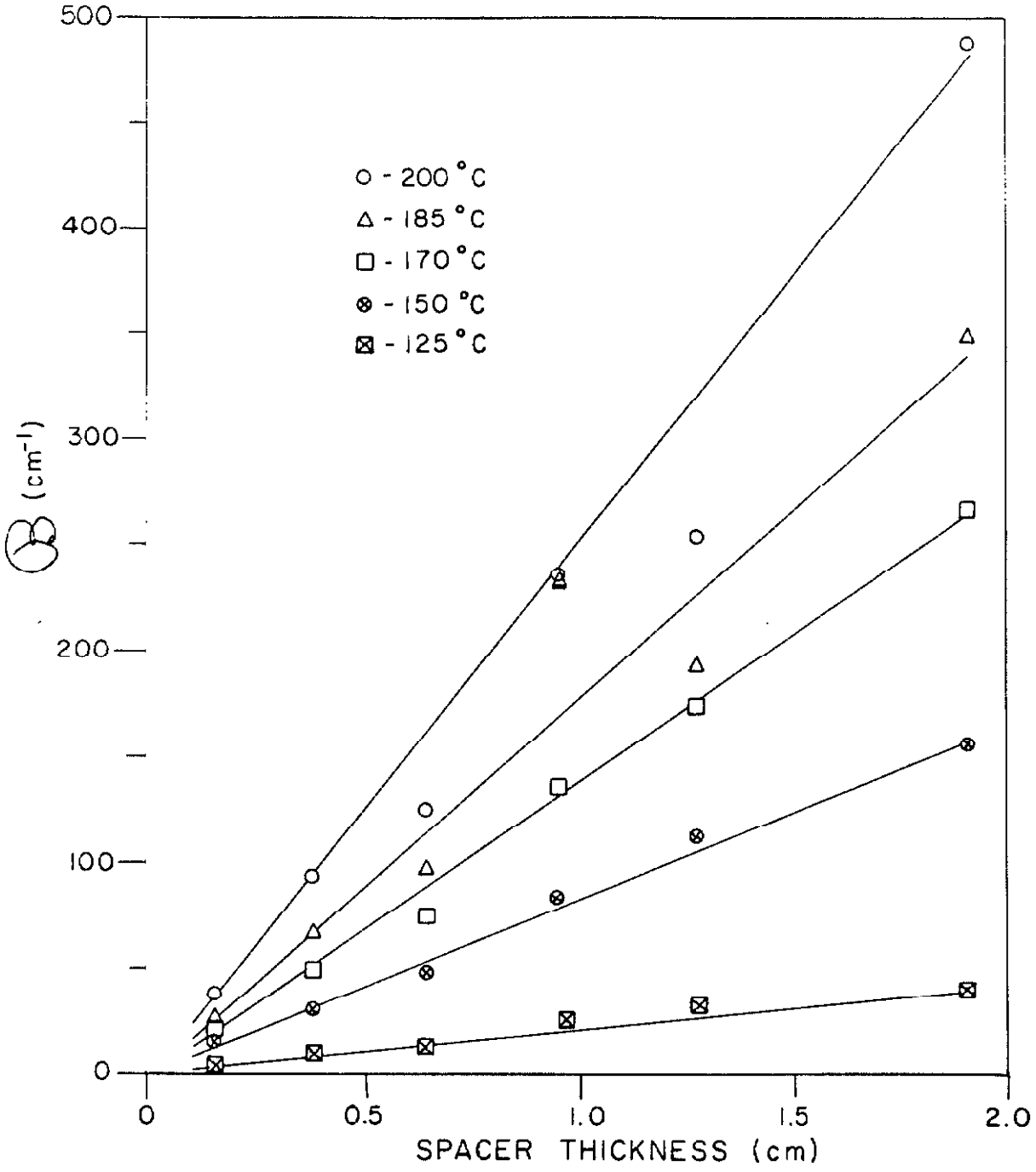

Fig. 17. β plotted as a function of spacer thickness for the 1.87μ band of water vapor at 125, 150, 170, 185, and 200°C.

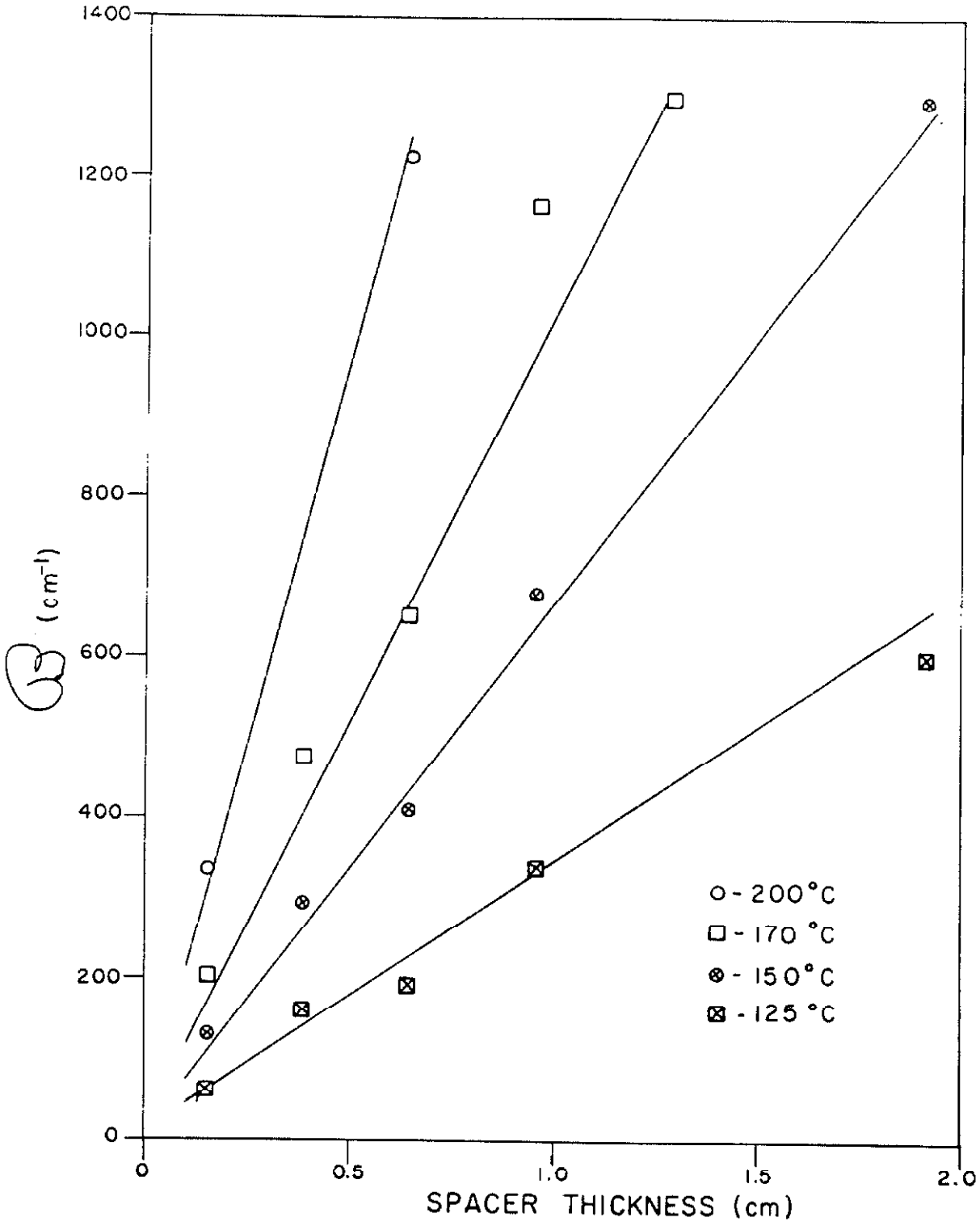

Fig. 18. β plotted as a function of spacer thickness for the 2.7μ band of water vapor at 125, 150, 170, and 200°C.

Table 2. Approximate Values for the Integrated Intensities of Water Vapor Between 125 and 200°C (± 20%)

Temperature (°C)	Pressure (atm)	a (cm^{-2}-atm^{-1}) for the band region near					
		1.38μ		1.87μ		2.7μ	
		a^*	$a^{o\dagger}$	a	a^o	a	a^o
125	2.29	13.3	17.7	17.8	23.6	136	180
150	4.70	12.2	17.3	16.4	23.1	144	203
170	7.82	12.8	18.9	17.2	25.4	132	195
185	11.08	11.6	17.7	15.7	24.0	-	-
200	15.34	11.7	18.5	15.2	24.0	126	199

* Integrated intensity at temperature of experiment.

† Integrated intensity normalized to 300°K assuming inverse relationship with temperature.

CHAPTER III

MEASUREMENTS OF THE INTEGRATED INTENSITIES AND SPECTRAL ABSORPTION COEFFICIENTS OF WATER VAPOR BETWEEN 200 AND 727°C

A. INTRODUCTION

Measurements have been made of the integrated intensities and spectral absorption coefficients of water vapor in the 1.38μ, 1.87μ, 2.7μ and 6.3μ regions, at temperatures between 200 and 727°C, using sufficient self-broadening to remove the rotational fine structure. In each spectral region, several bands contribute to the absorption, but usually only one or two of the bands are of dominant importance. By using estimates of the relative intensities of the bands in each region,[29,37] individual f-numbers can be calculated for each of the bands from the integrated intensities found in our experiment.

B. APPARATUS AND PROCEDURE

The apparatus is described in Chapter I. The 1.38μ, 1.87μ and 2.7μ bands of water vapor were studied with the high temperature absorption cell (see Fig. 15); two 1-inch diameter by 1/4-inch thick sapphire windows were used for the measurements at 200, 400 and 600°C, while magnesium oxide windows were used for the study of the 2.7μ band at 1000°K. The 6.3μ band of water vapor was studied with the variable spacer cell (see Fig. 13) using a 0.500-inch spacer and two silver chloride windows. With slit widths varying between

100 and 1000μ, the resulting resolutions were about 50, 20, 15, and 200 cm^{-1} for the 1.38μ, 1.87μ, 2.7μ, and 6.3μ bands, respectively.

Water vapor, at known pressures, was supplied to the cell from the liquid water reservoir outside the vacuum tank. The optical depth was varied by raising the water vapor between 2.5 and 18 atm. Smearing out of the rotational fine structure was accomplished by self-broadening, which is achieved for water vapor at a pressure of 3 atm. at 300°K[1]; the pressure required for self-broadening should decrease with temperature because of the increased number of bands and lines.

The computer was programmed to print out the values of the spectral absorption coefficients at 5 cm^{-1} intervals.

C. EXPERIMENTAL RESULTS

Figures 19 to 22 show β (see Eq. (41)) as a function of optical depth for the 1.38μ, 1.87μ, 2.7μ, and 6.3μ regions of water vapor, respectively, at temperatures of 200, 400, 600 and 727°C. The integrated intensities of the bands determined from Eq. (44) and Figs. 19 to 22, are given in Table 3 in units of cm^{-2}-atm^{-1} and g^{-1}-cm. Table 3 also includes the values for the integrated intensities normalized to 300°K, assuming an inverse relationship with temperature, and the integrated intensities found by numerically integrating the graphs of the spectral absorption coefficient P_ω as a function of wave number. The latter values agree within 2% with the integrated intensities determined from Figs. 19 to 22. Plots of

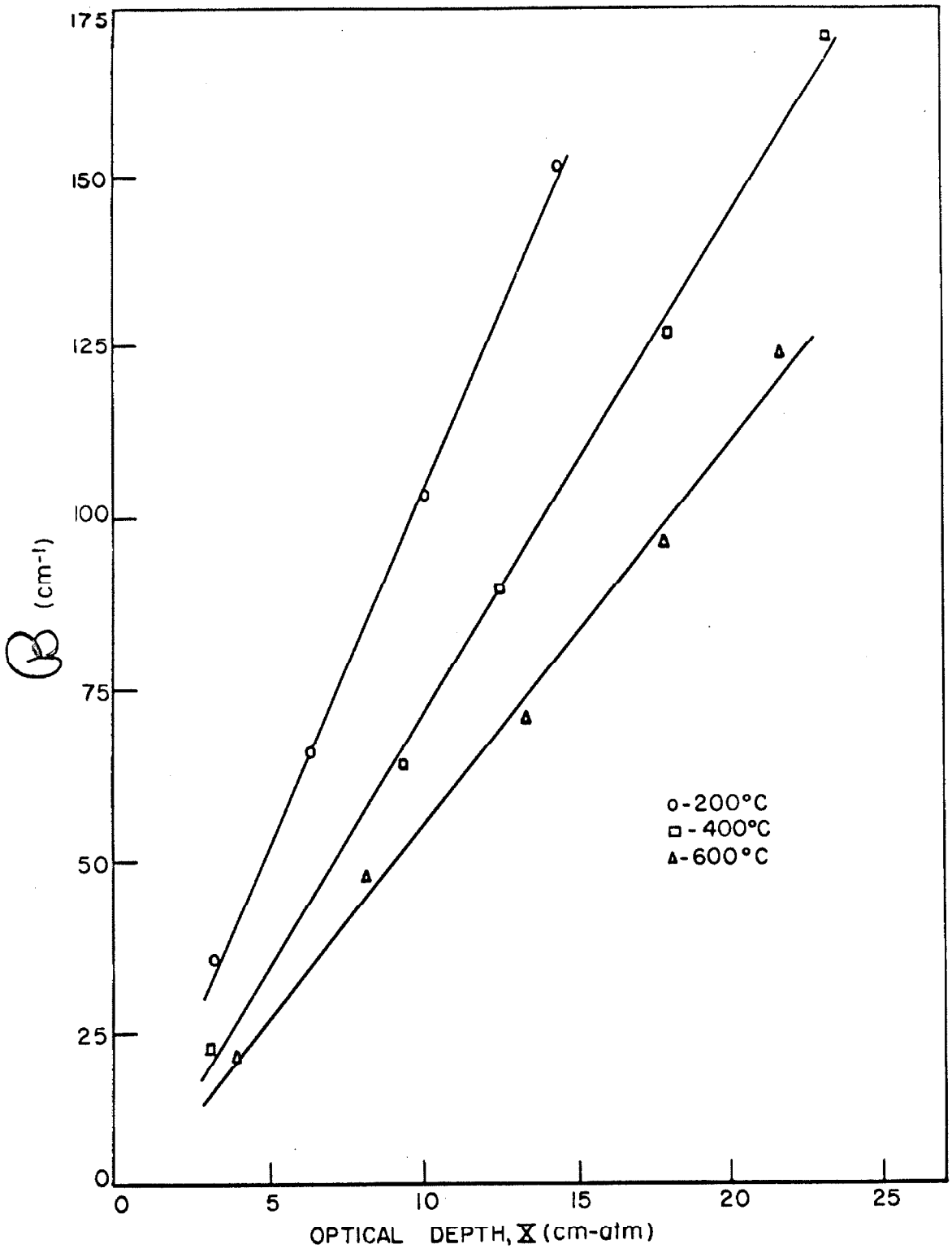

Fig. 19. β plotted as a function of optical depth for the 1.38μ band of water vapor at 200, 400, and 600°C.

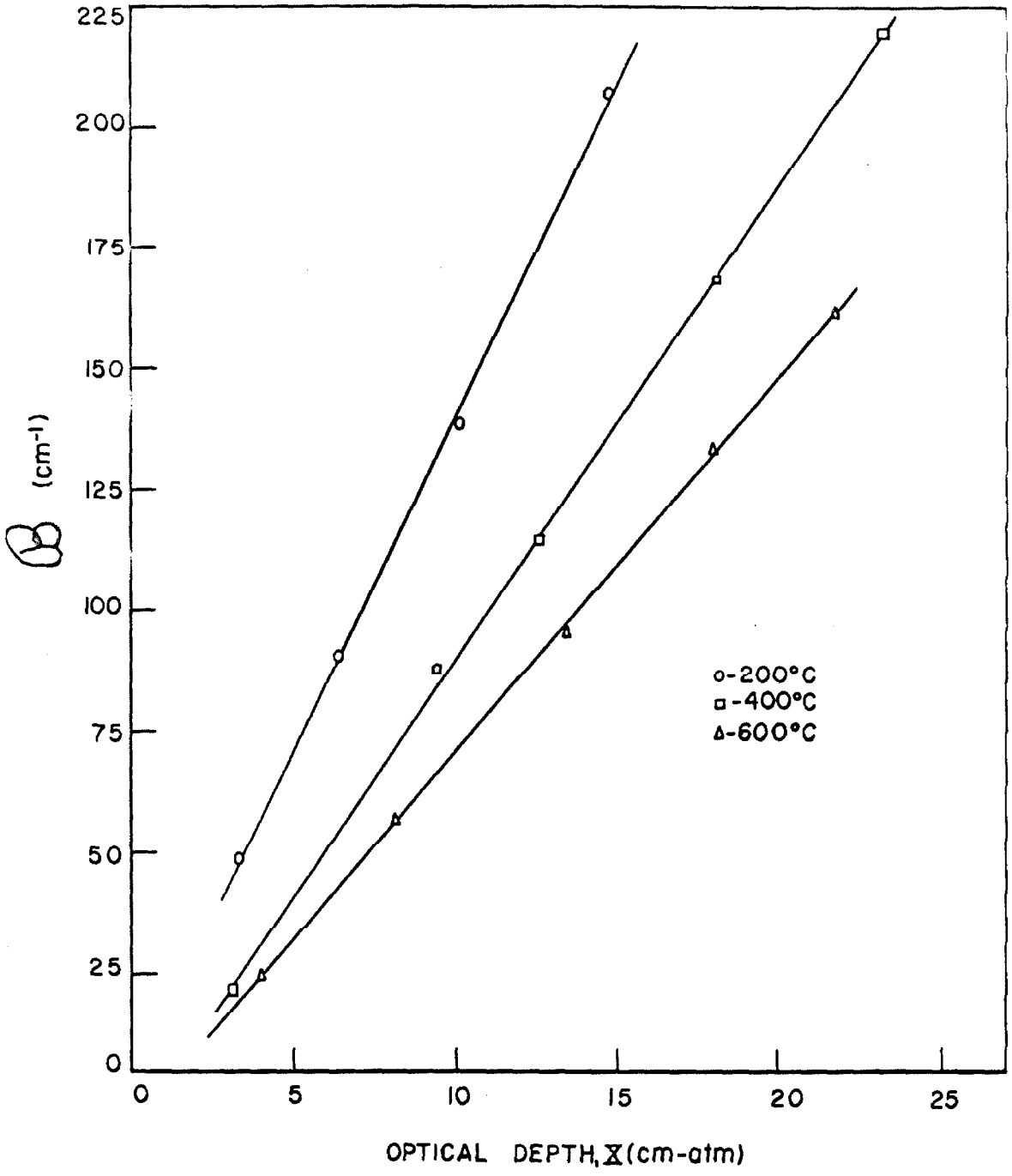

Fig. 20. β plotted as a function of optical depth for the 1.87μ band of water vapor at 200, 400, and 600°C.

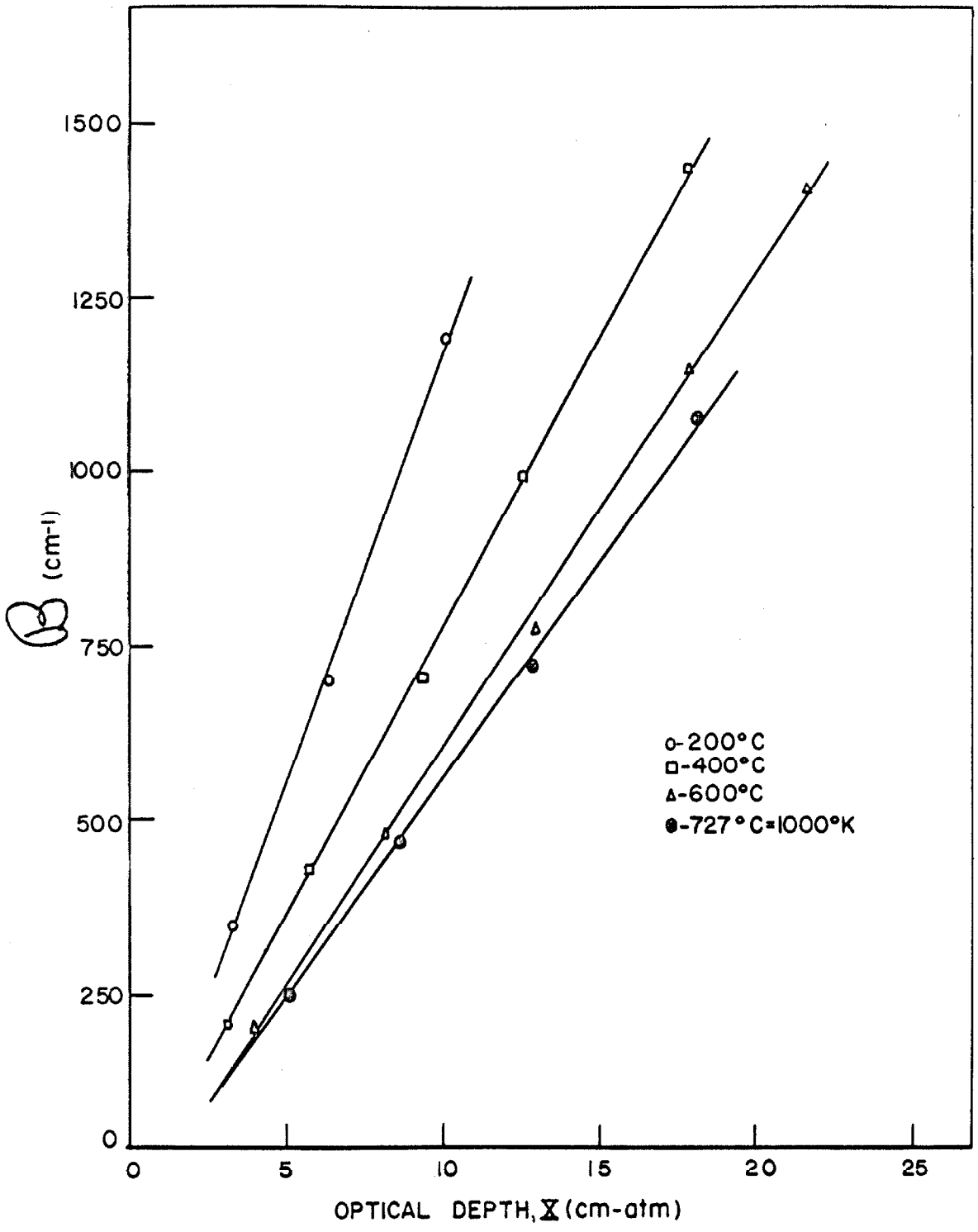

Fig. 21. β plotted as a function of optical depth for the 2.7μ band of water vapor at 200, 400, 600, and 727°C.

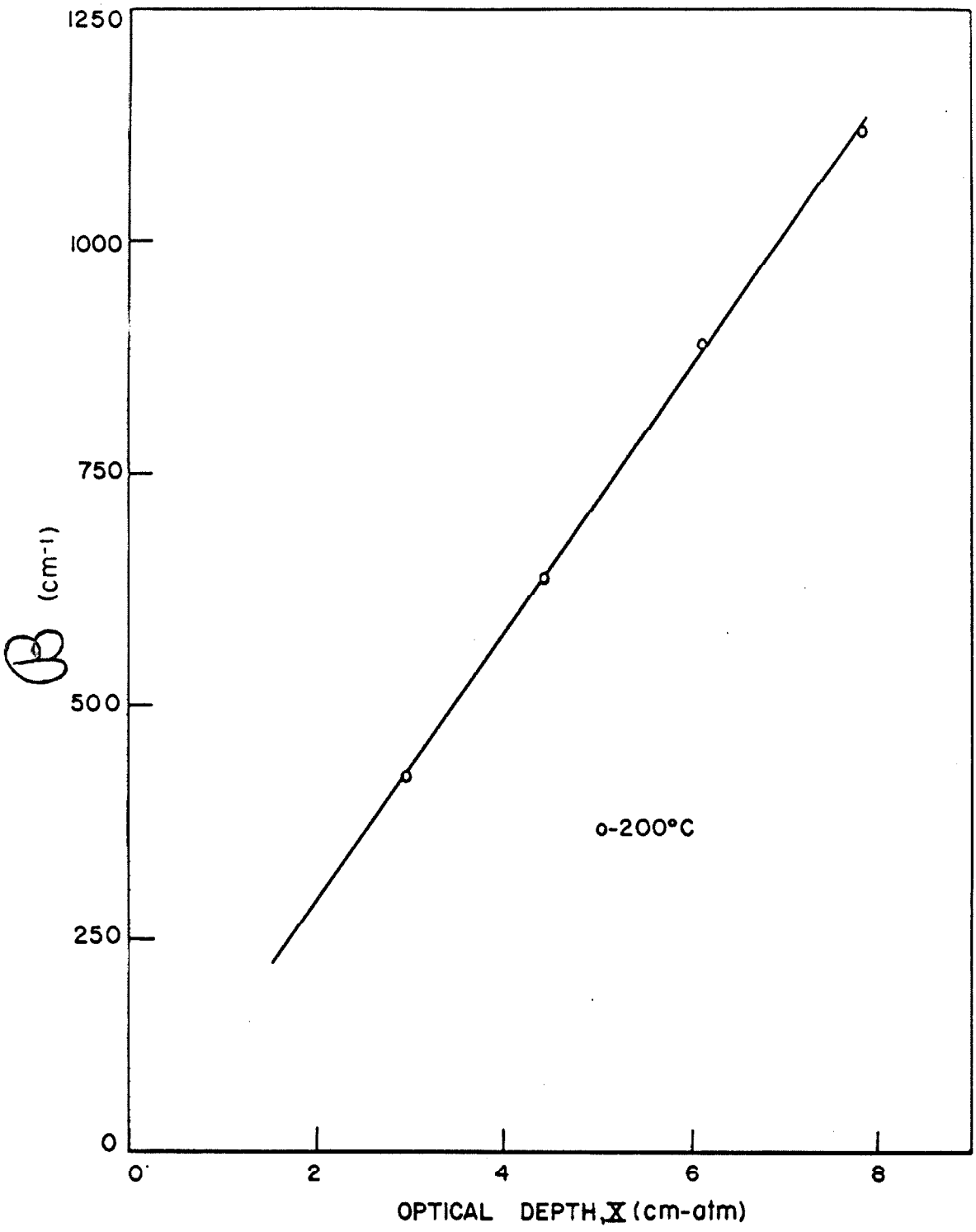

Fig. 22. β plotted as a function of optical depth for the 6.3μ band of water vapor at 200°C.

Table 3. Integrated Intensities of Water Vapor (± 10%)

Band Region Near	Temperature	a_{slope} *	$a_{num.}$ †	a_{slope} *	a^{o}_{slope} **
	°C	cm^{-2}-atm^{-1}	cm^{-2}-atm^{-1}	g^{-1}-cm	normalized to 300°K, cm^{-2}-atm^{-1}
1.38μ	200	10.2	9.9	22,000	16.1
	400	7.3	7.3	22,300	16.3
	600	5.5	5.5	21,800	16.0
1.87μ	200	13.7	13.9	29,600	21.6
	400	9.7	9.7	29,800	21.8
	600	7.7	7.7	30,500	22.3
2.7μ	200	123.	125.	266,000	194.
	400	82.4	83.3	253,000	185.
	600	67.3	67.6	268,000	196.
	727	61.6	62.1	281,000	206.
6.3μ	200	143.	143.	308,000	225.

* a_{slope} determined using Figs. 19 to 22 and Eq. (44).

† $a_{num.}$ determined from numerical integration of the plots of P_{ω} as a function of wave number (Figs. 23 to 33).

** a^{o}_{slope} is a_{slope} normalized to 300°K assuming an inverse variation of integrated intensity with temperature.

the experimentally determined values of the spectral absorption coefficient of water vapor (from Eq. (45)) as a function of wave number, are shown in Figs. 23 to 33; the theoretical values of the spectral absorption coefficients, which were calculated by using a just-overlapping line model, are also shown on these figures. Details of the theoretical calculations are described in Chapter VI.

The integrated intensities of water vapor (in cm^{-2}-atm^{-1}) are plotted in Fig. 34 as a function of temperature. If we assume that a varies as T^x, the values of x derived from Fig. 34, for the 1.38μ, 1.87μ, and 2.7μ bands of water vapor, are -0.99, -0.93 and -0.93, respectively.

A table of the experimentally determined values for the spectral absorption coefficients of water vapor at 5 cm^{-1} intervals is given in Appendix B; graphs showing $\ell n(I_\omega^{o,a}/I_\omega^a)$ as a function of wave number for all the experimental conditions is given in Appendix A.

D. DISCUSSION OF RESULTS

The cell spacer was measured with an uncertainty of ± 1%; the uncertainty of the pressure was about ± 2%. Small sources of error were also contributed by the reading of the data, the slight variation of the background, the uncertainty of ± 2°C in the cell temperature, and the fitting of the experimental points to a straight line, as designated by Eqs. (44) and (45). With regard to the latter uncertainty, reference to Figs. 19 to 22 shows that the points determine a straight line, well

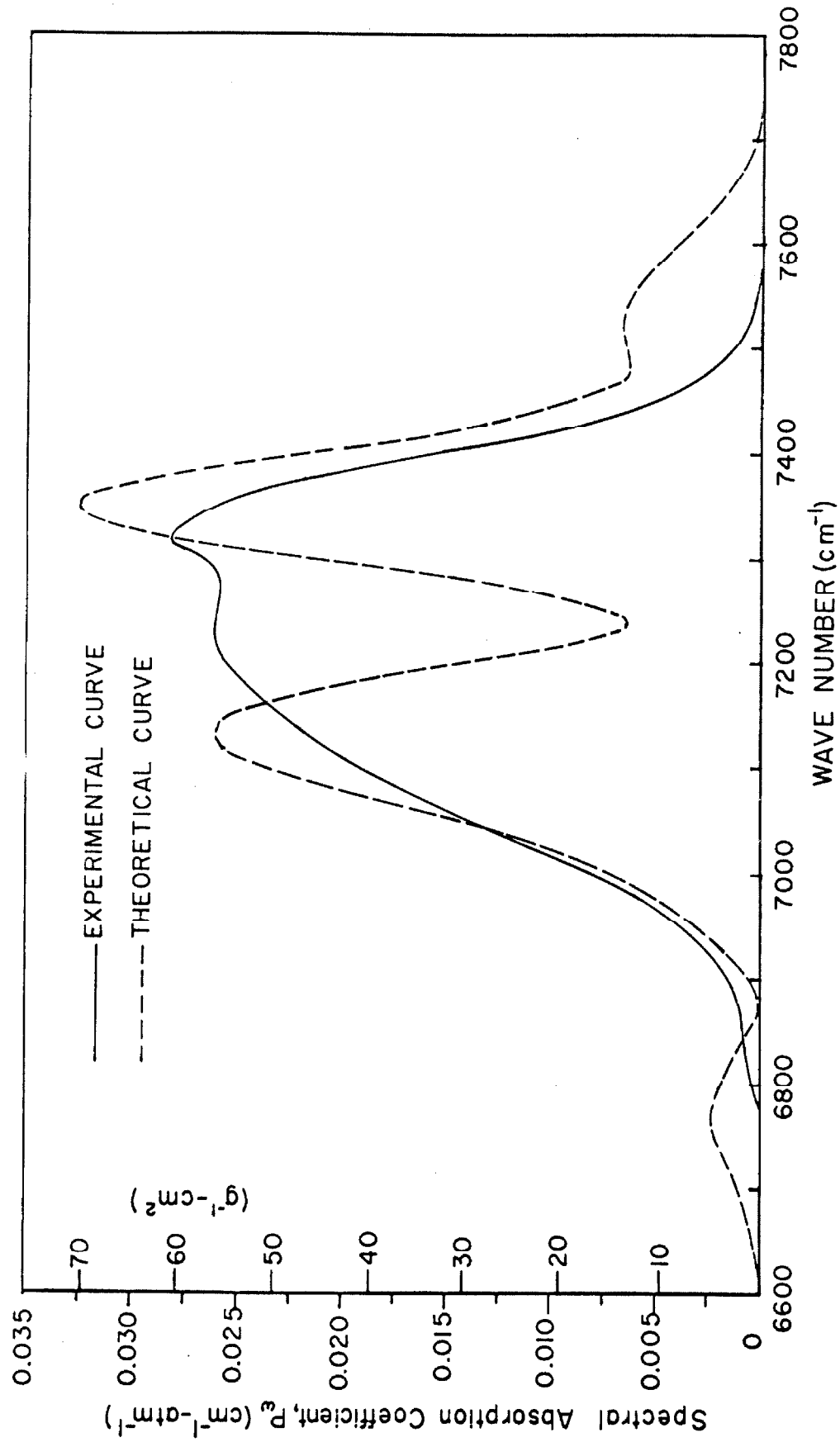

Fig. 23. The spectral absorption coefficient of water vapor in the 1.38μ region at 200°C as a function of wave number. The experimental points were determined at 5 cm^{-1} intervals.

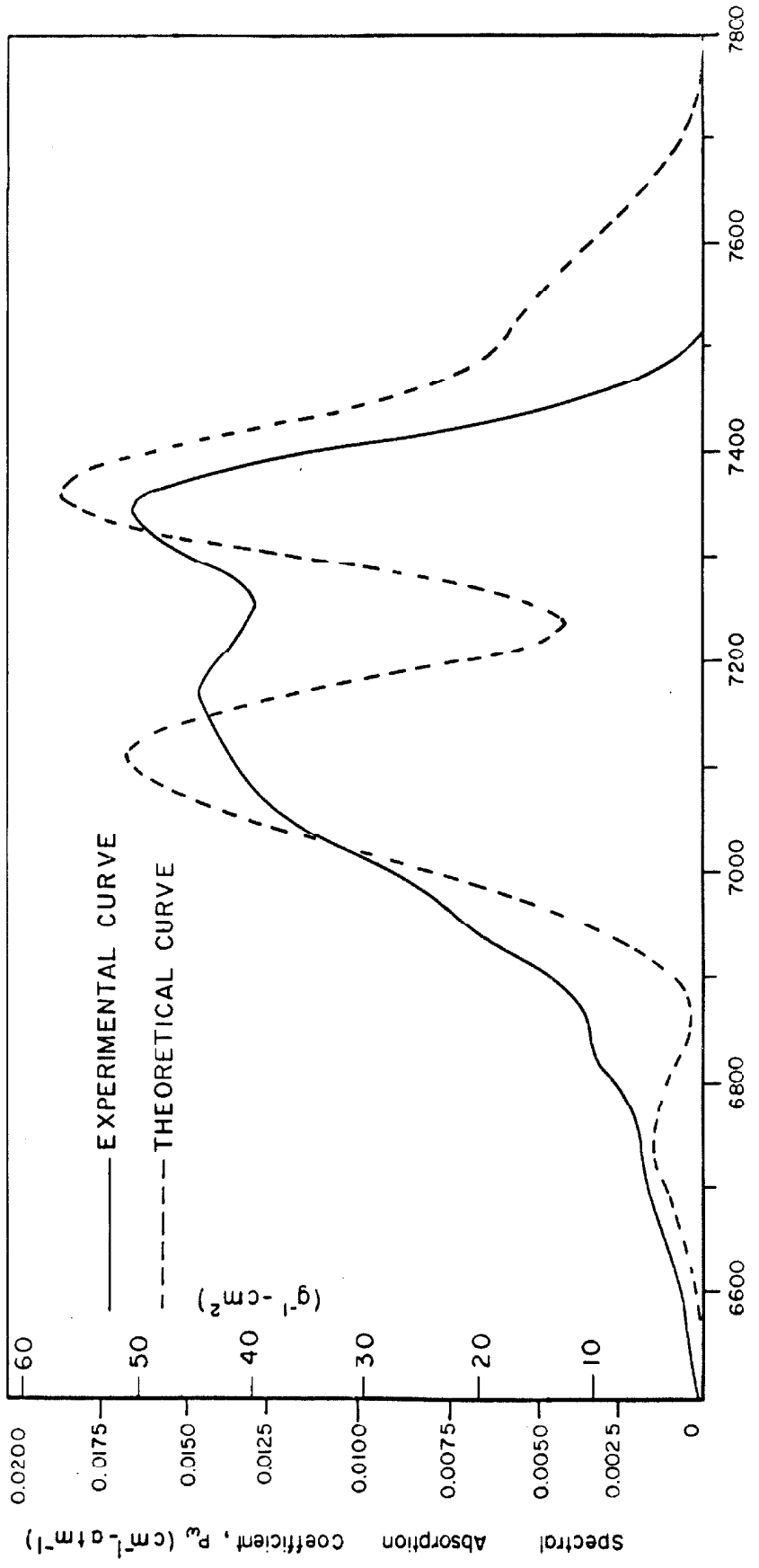

Fig. 24. The spectral absorption coefficient of water vapor in the 1.38μ region at 400°C as a function of wave number. The experimental points were determined at 5 cm^{-1} intervals.

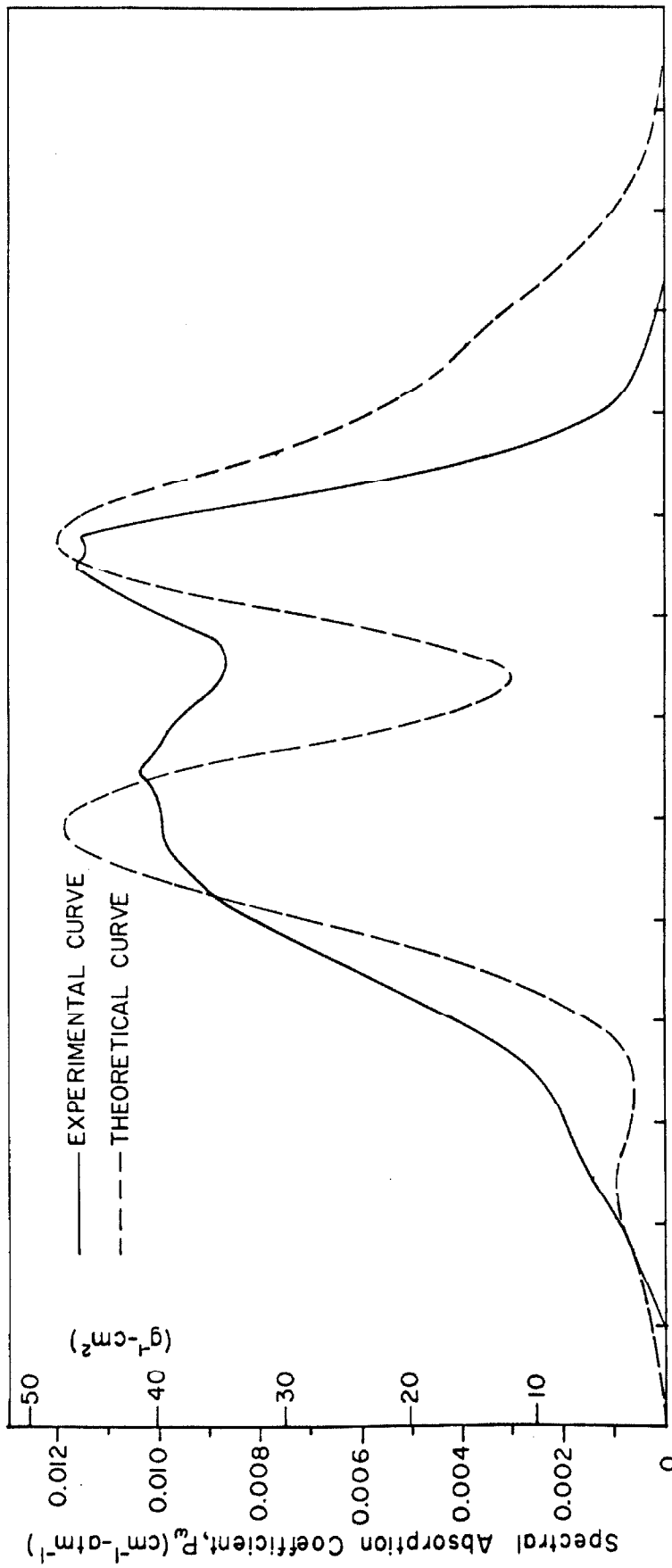

Fig. 25. The spectral absorption coefficient of water vapor in the 1.38μ region at 600°C as a function of wave number. The experimental points were determined at 5 cm^{-1} intervals.

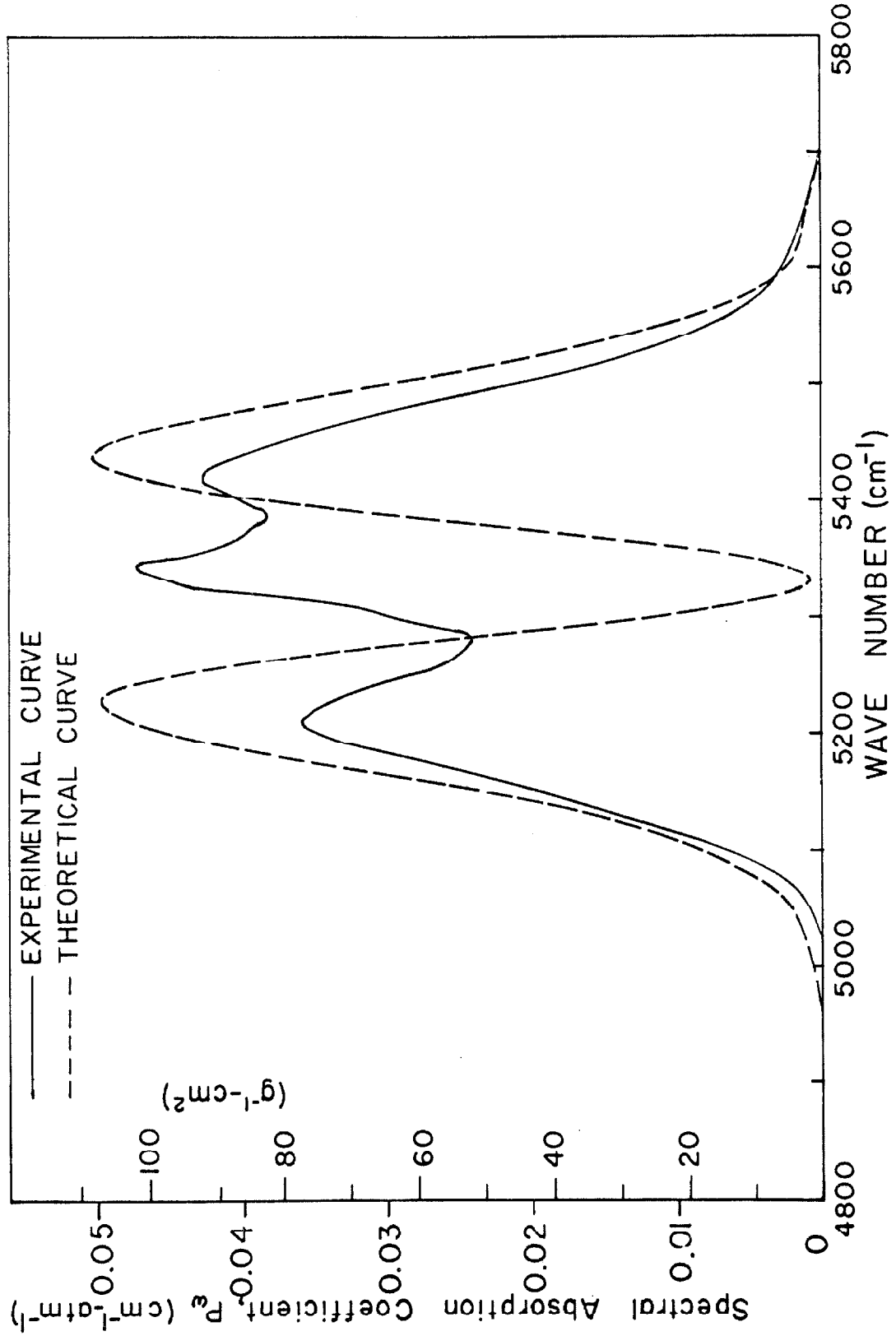

Fig. 26. The spectral absorption coefficient of water vapor in the 1.87μ region at 200°C as a function of wave number. The experimental points were determined at 5 cm^{-1} intervals.

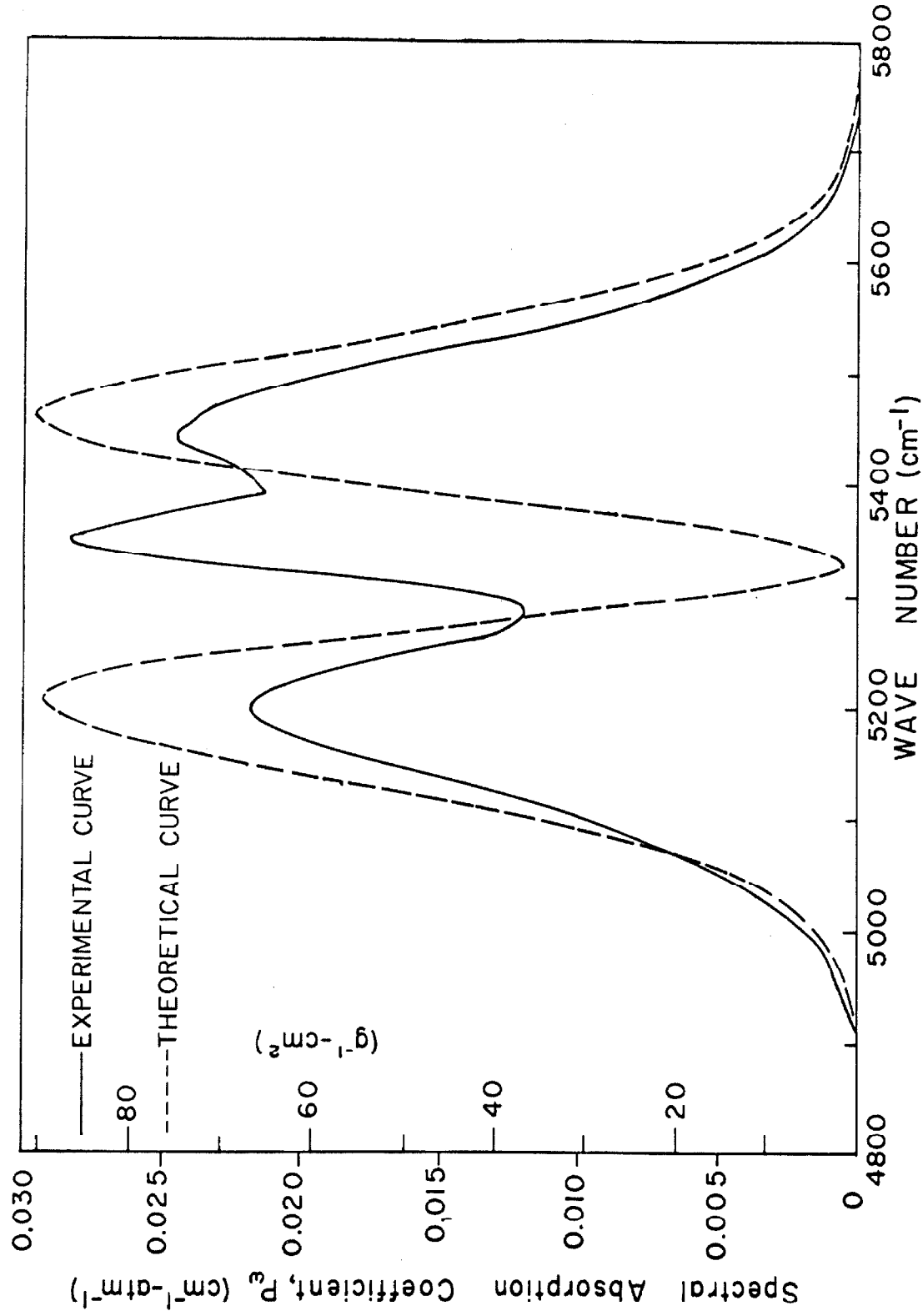

Fig. 27. The spectral absorption coefficient of water vapor in the 1.87μ region at 400°C as a function of wave number. The experimental points were determined at 5 cm^{-1} intervals.

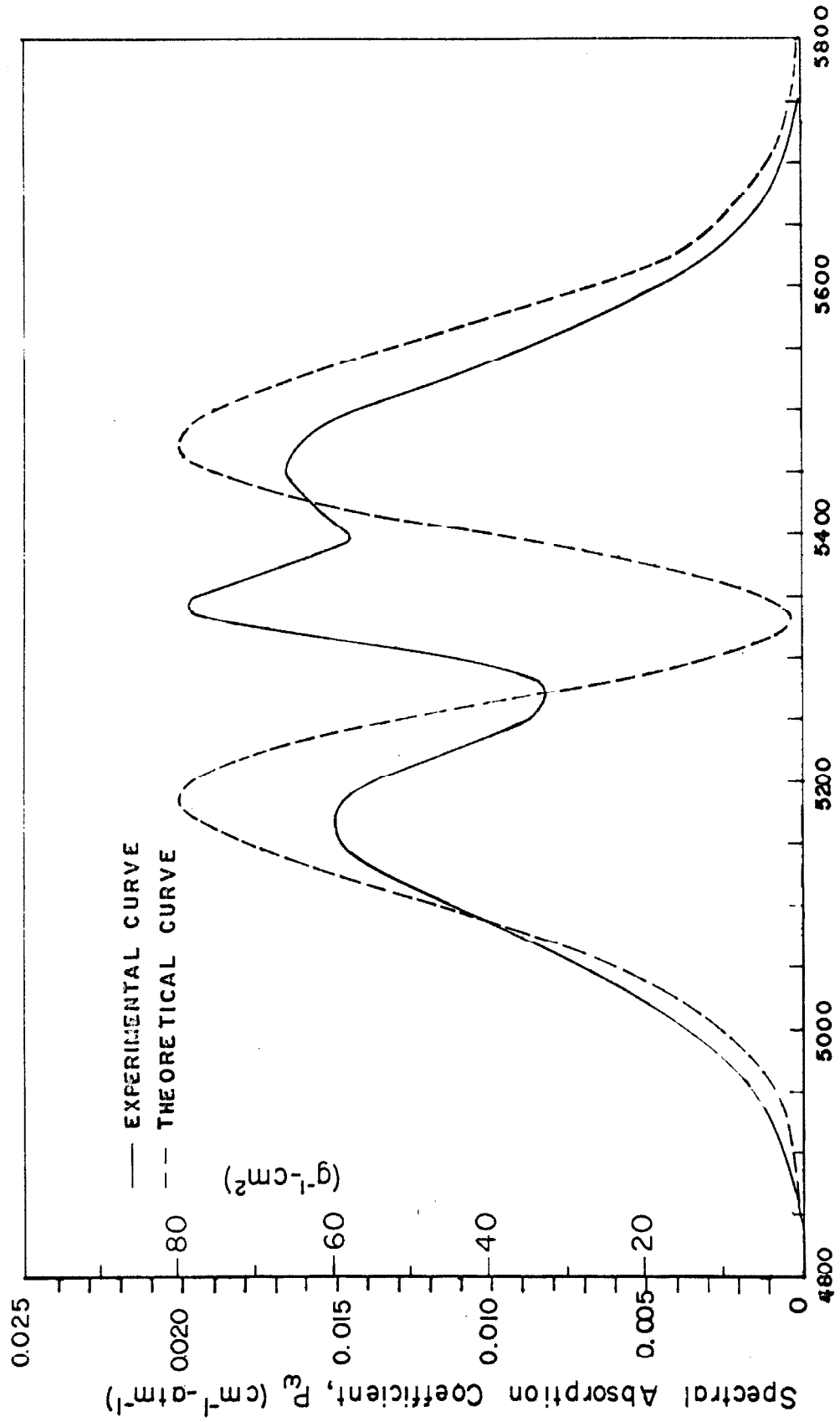

Fig. 28. The spectral absorption coefficient of water vapor in the 1.87μ region at 600°C as a function of wave number. The experimental points were determined at 5 cm^{-1} intervals.

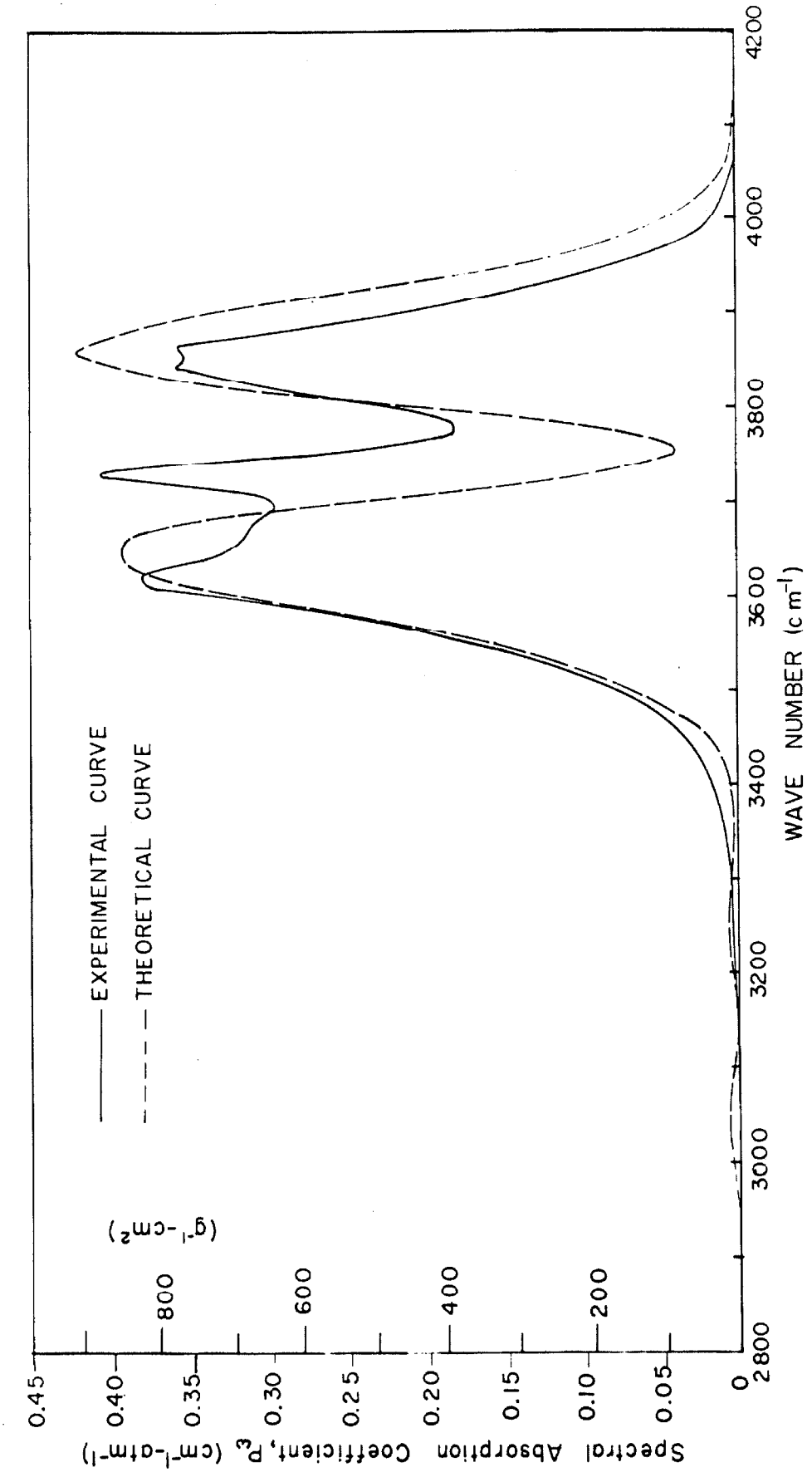

Fig. 29. The spectral absorption coefficient of water vapor in the 2.7μ region at 200°C as a function of wave number. The experimental points were determined at 5 cm^{-1} intervals.

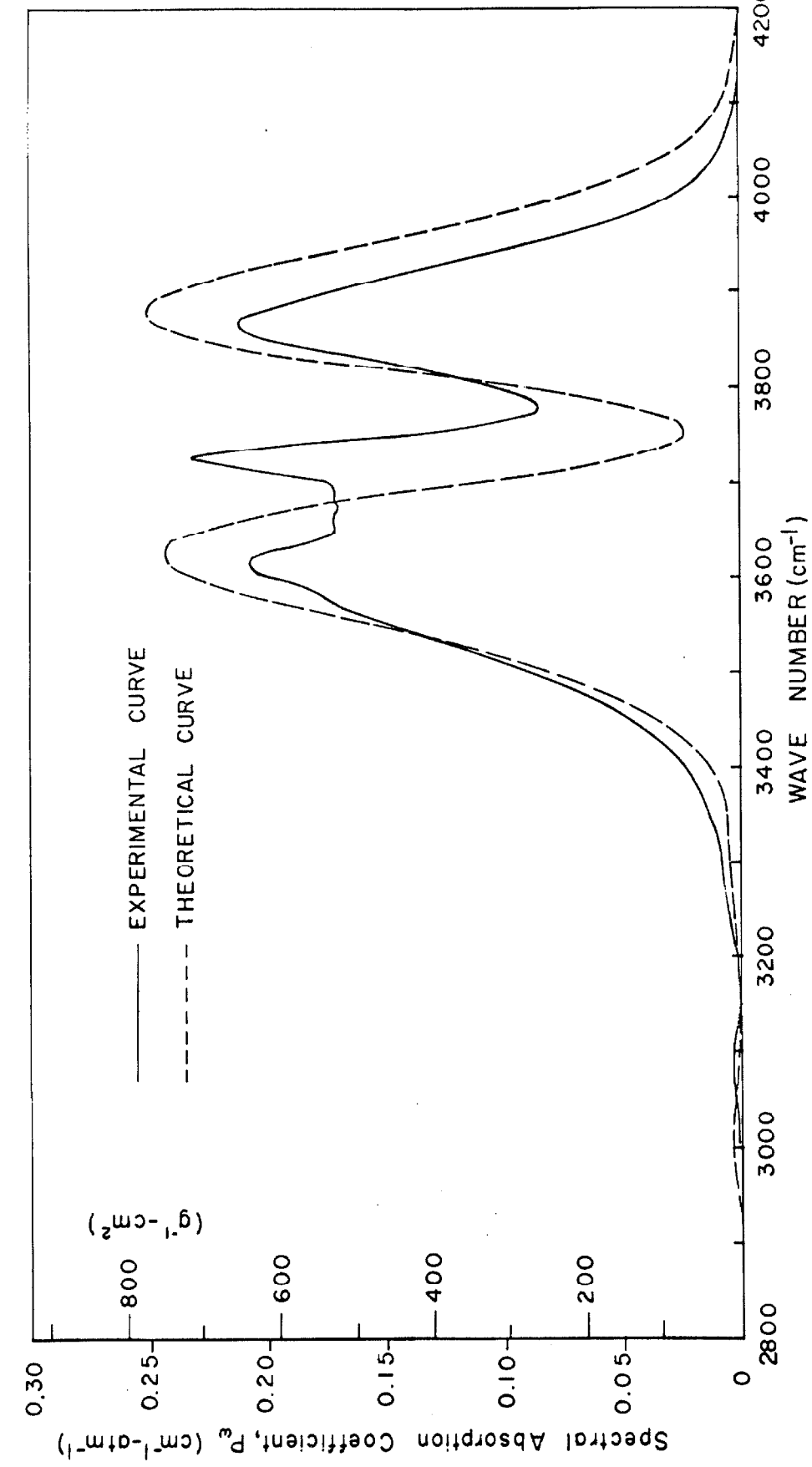

Fig. 30. The spectral absorption coefficient of water vapor in the 2.7μ region at 400°C as a function of wave number. The experimental points were determined at 5 cm^{-1} intervals.

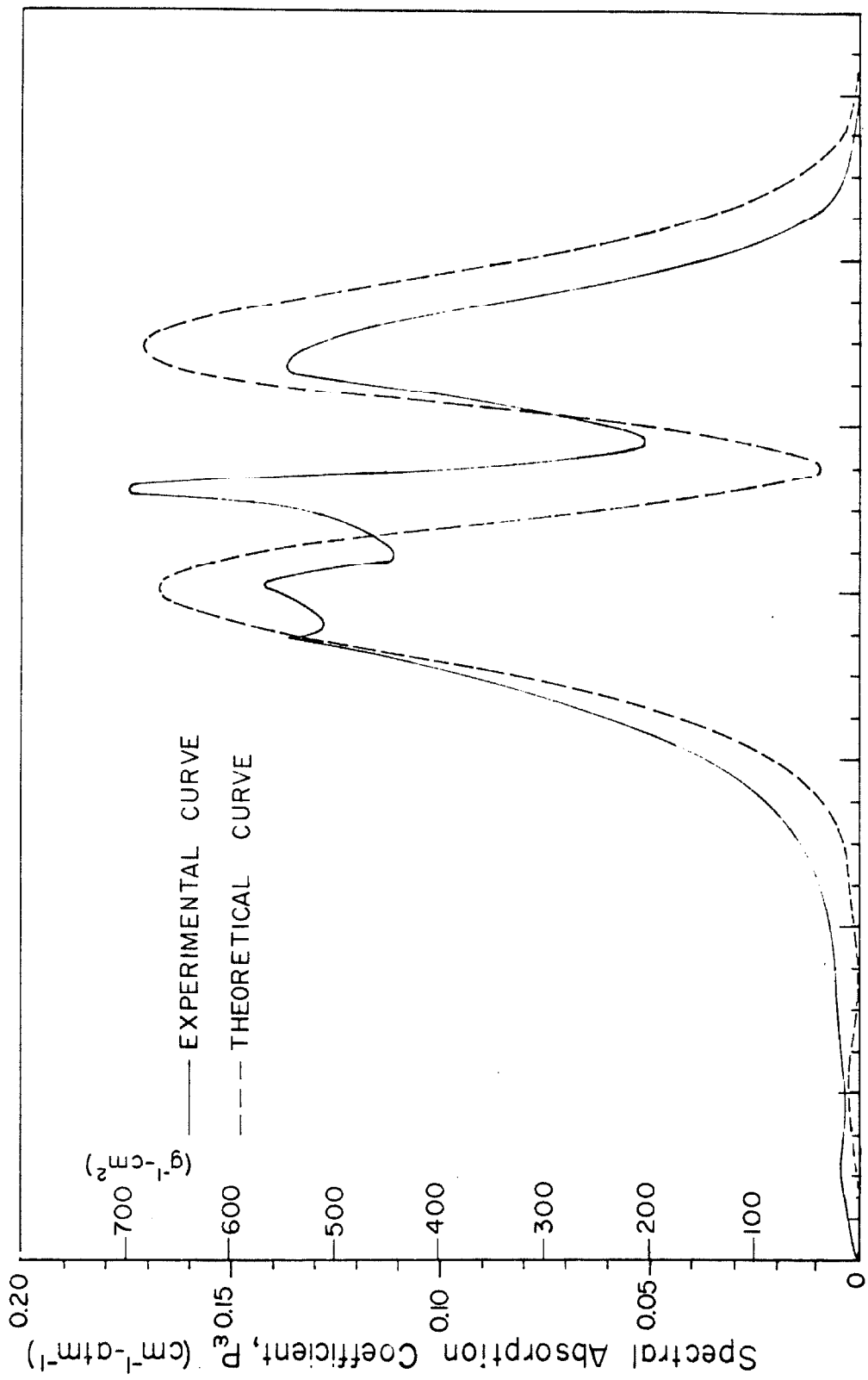

Fig. 31. The spectral absorption coefficient of water vapor in the 2.7μ region at 600°C as a function of wave number. The experimental points were determined at 5 cm^{-1} intervals.

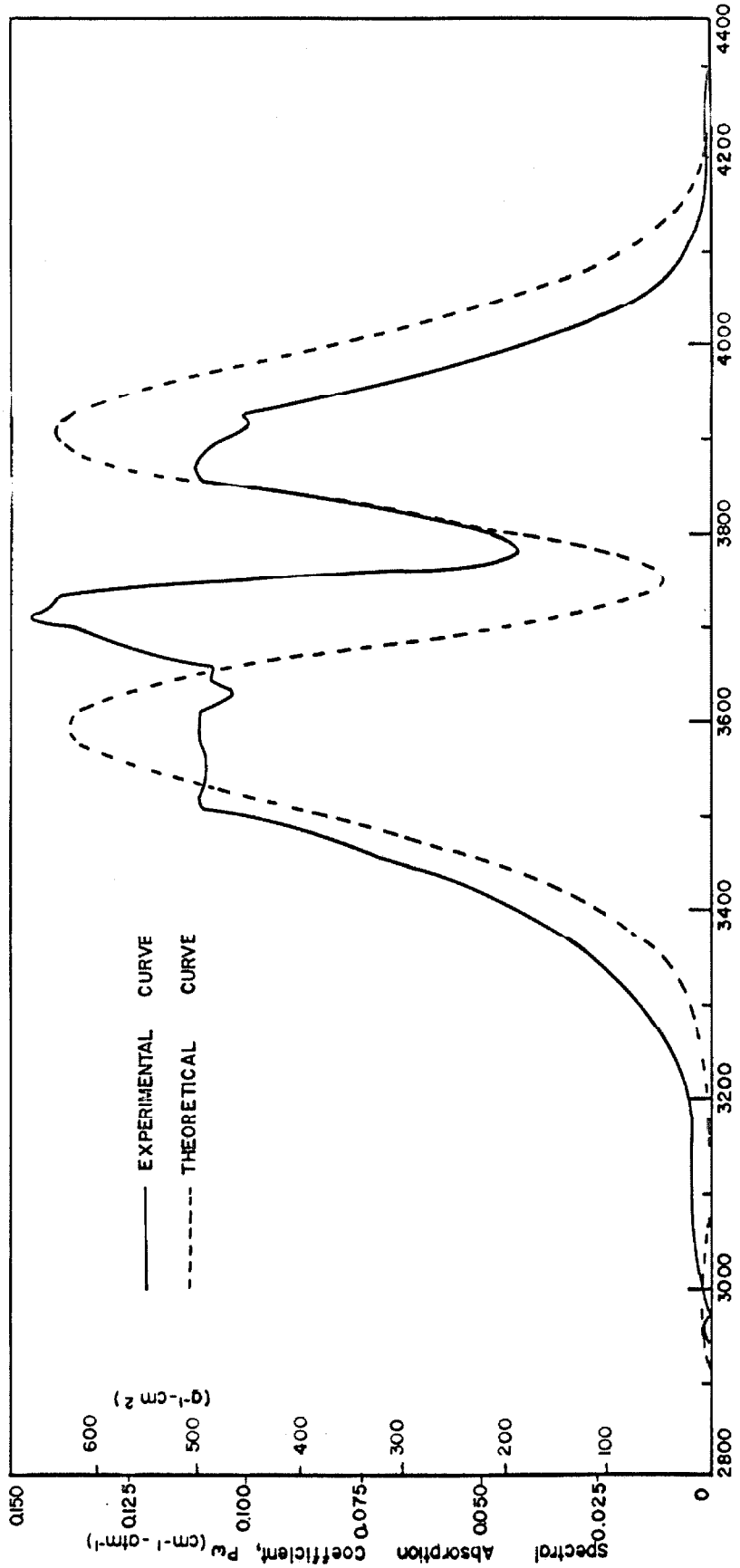

Fig. 32. The spectral absorption coefficient of water vapor in the 2.7μ region at 727°C as a function of wave number. The experimental points were determined at 5 cm^{-1} intervals.

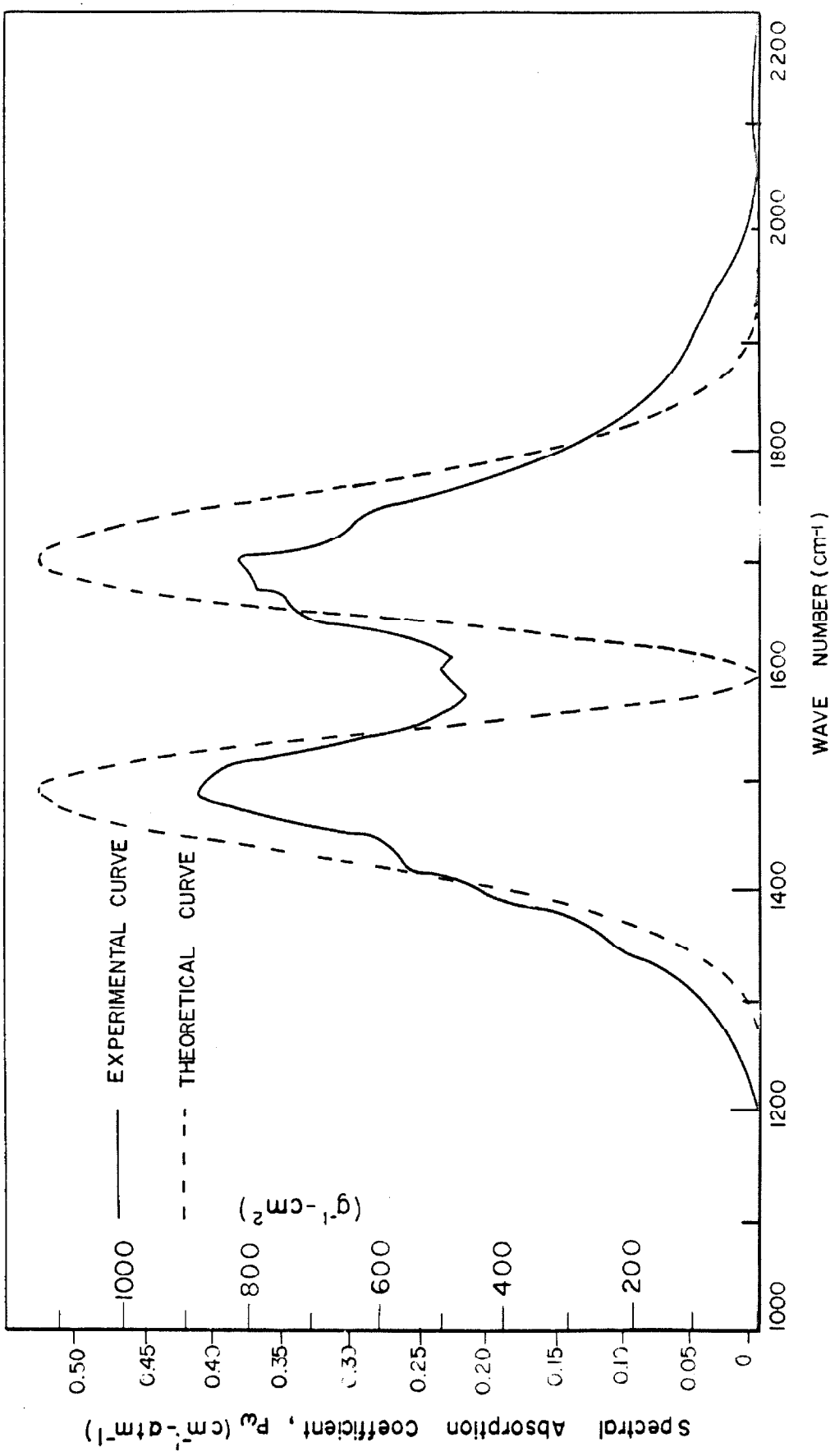

Fig. 33. The spectral absorption coefficient of water vapor in the 6.3μ region at 200°C as a function of wave number. The experimental points were determined at 5 cm^{-1} intervals.

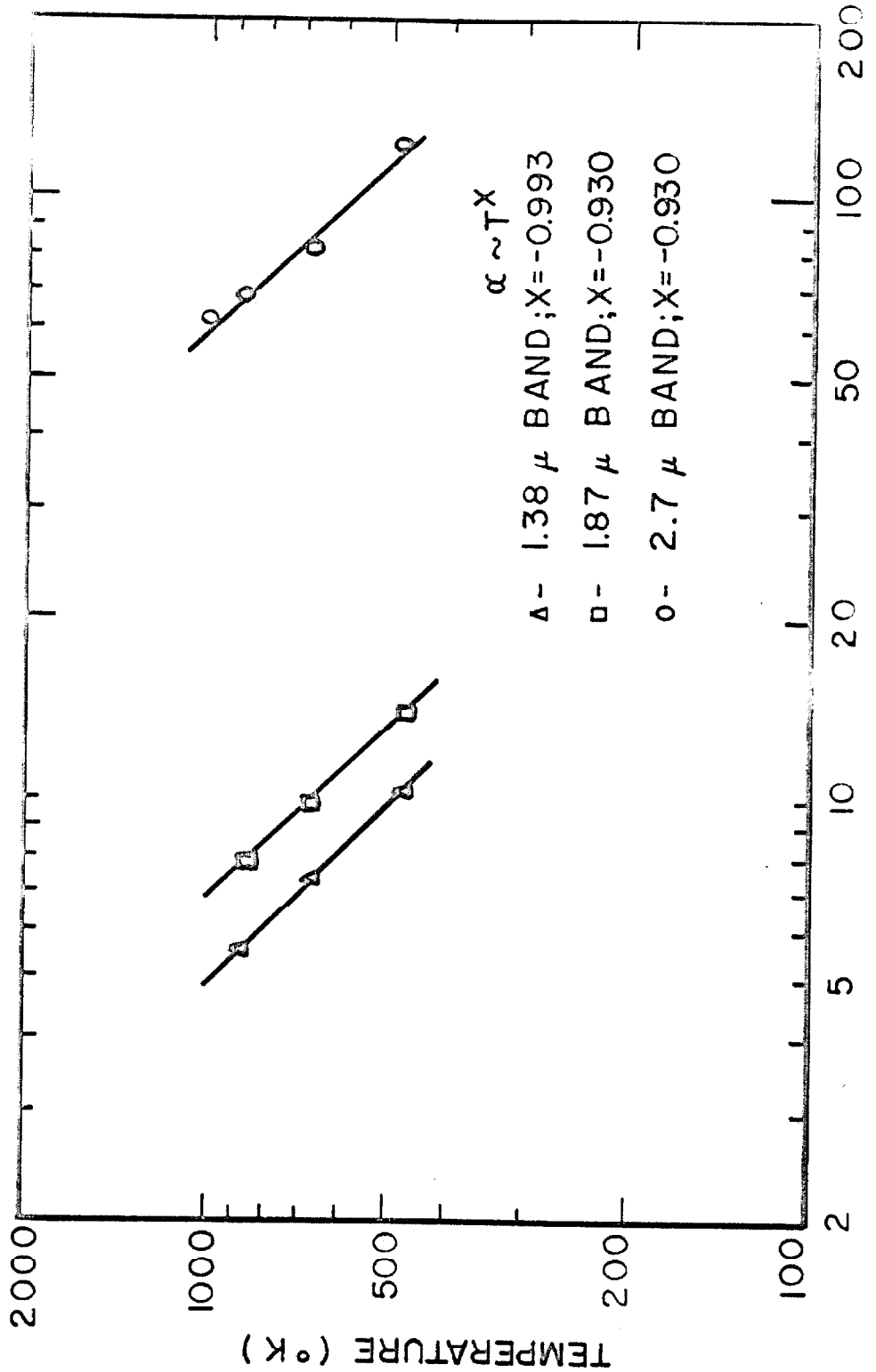

Fig. 34. The integrated intensities of the 1.38μ, 1.87μ, and 2.7μ bands of water vapor plotted as a function of temperature.

within the uncertainty due to the optical depth and the reading of the data, even though most of the straight lines do not pass through the origin. This behavior is known to be produced by a slight malalignment of the monochromator but may also result when inadequate pressure-broadening is achieved and the low-pressure data are weighted too heavily. The integrated intensities obtained by using only the data at the highest pressure varied from the values determined from the slope method by less than 5%. In evaluating the integrated intensities and spectral absorption coefficients, no corrections were made for gas imperfections, which introduced a maximum variation of the density, for the highest pressure runs, of 6.0, 1.7 and 0.5% at 200, 400, and 600°C, respectively.

A conservative estimate for the overall uncertainties in the integrated intensities and spectral absorption coefficients is ± 10%.

The values of x taken from Fig. 34 show that the simplified theory, according to which the integrated intensity for a band varies inversely with temperature because of the change of density, is approximately correct for the 1.38μ band but that some deviations may be present for the 1.87μ and 2.7μ bands.

The value for the ν_3-fundamental band strength at 300°K, calculated from the data in Table 3 and using estimated relative band intensities,[29] is 177 ± 18 cm^{-2}-atm^{-1}. This value is consistent with the results mentioned in Chapter I, Section A and agrees, in particular, with the estimate of Jaffe and Benedict[5] of 192 ± 28 cm^{-2}-atm^{-1}.

Figure 35 shows the values of the integrated intensity of the 2.7μ region, determined by several investigators, at various temperatures. The values have been normalized to 300°K by assuming an inverse variation of integrated intensity with temperature. There is general agreement for the normalized value of the integrated intensities within the acknowledged experimental uncertainties. The data of Ferriso and Ludwig,[4] and of Burch and Grynak,[38] are slightly lower than that obtained in the present investigations. This deviation is to be expected because of the difficulty of achieving adequate pressure-broadening in their experiments.

Ferriso and Ludwig[4] stated that the normalized integrated intensity for the 2.7μ region is approximately constant at 180 cm^{-2}-atm^{-1} between 300 and 2200°K. Our results are in agreement with this observation, but give the value of 195 ± 20 cm^{-2}-atm^{-1} at 300°K.

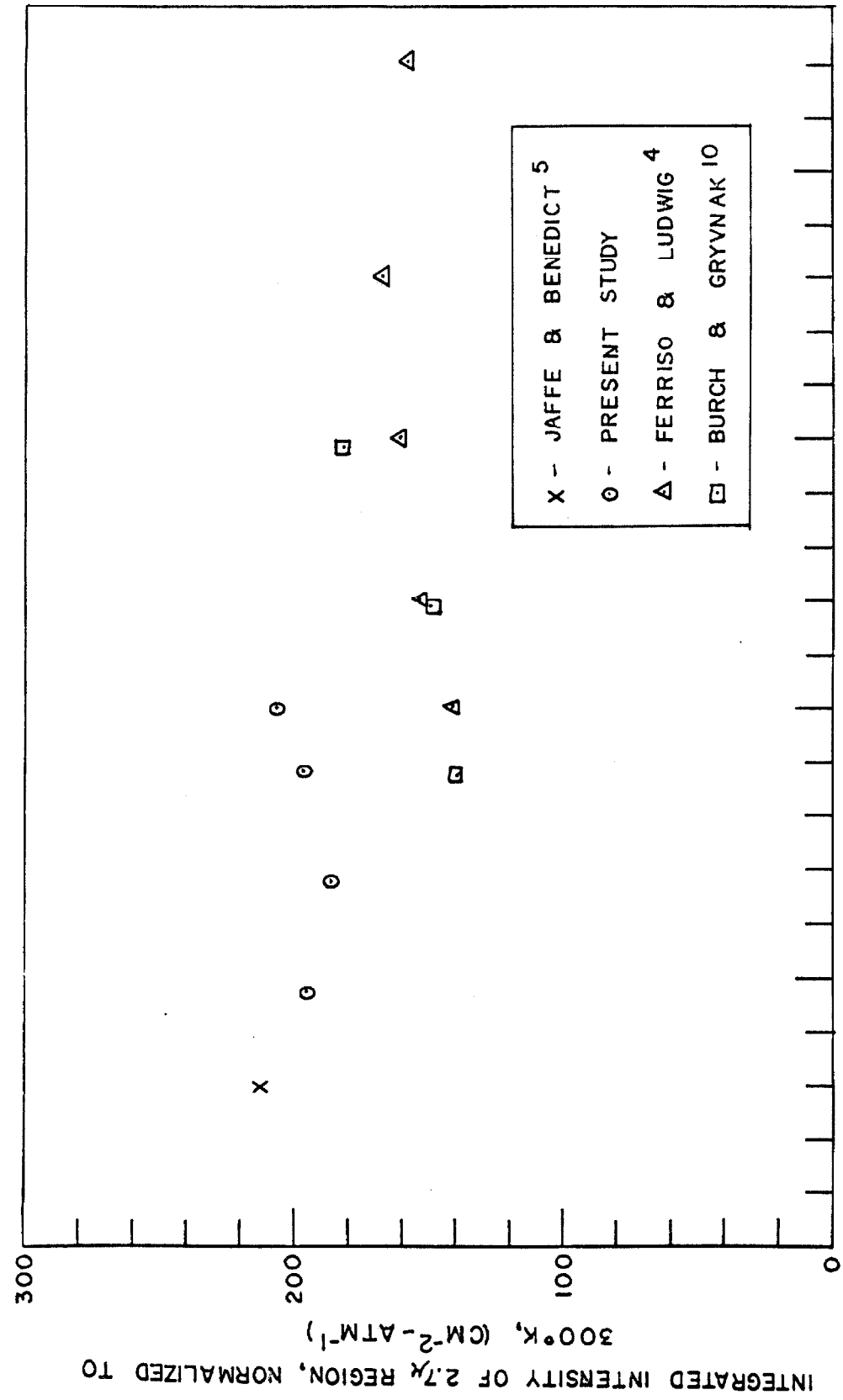

Fig. 35. The integrated intensity of the 2.7μ region as a function of temperature determined by various investigators (normalized to 300°K by assuming an inverse relationship between α and T).

CHAPTER IV

MEASUREMENTS OF THE SPECTRAL ABSORPTION COEFFICIENTS OF LIQUID WATER BETWEEN 27 AND 209°C

A. INTRODUCTION

The spectral absorption coefficients of liquid water have been measured between 2200 and 3000 cm^{-1} and between 3700 and 7600 cm^{-1} at temperatures of 27, 89, 159, and 209°C. The integrated intensitics for the entire spectral regions extending from 4600 to 5900 cm^{-1} and from 5900 to 7600 cm^{-1} have also been determined at each of the specified temperatures. Following Buijs and Choppin,[18] the experimental data have been used, in a highly simplified analysis, for the determination of hydrogen bonding in liquid water on the assumption that water consists of clusters containing only zero, one or two hydrogen bonds per molecule. We have also indicated briefly a more complete analysis of the experimental measurements in which the full range of results on spectral absorption coefficients as a continuous function of frequency is properly utilized.

B. APPARATUS AND PROCEDURE

The experimental facilities are described in Chapter I. The variable-spacer absorption cell was used with 1/4-inch thick sapphire windows for the present investigations (see Fig. 13).

Liquid water was introduced into the cell from the external liquid water reservoir which was submerged in the constant temperature oil bath. By raising the temperature of the oil bath above the

temperature of the cell, liquid water could be made to condense in the cell. The liquid was kept in the cell during the absorption runs by maintaining a higher vapor pressure in the supply lines than in the cell. The slit width of the Perkin-Elmer model 98 monochromator, which was used with a lithium fluoride prism, was set at 100μ with a resulting spectral resolution of 5 to 50 cm^{-1} for the 5.0 to 1.3μ spectral regions, respectively.

The data were analyzed according to the method described in Chapter I; the optical depth was varied by using spacers of 0.00508, 0.0132, 0.0264, and 0.0391-cm. A least square fit of the four experimental points was performed to Eq. (45) with the aid of an IBM 7090 and the spectral absorption coefficients were printed out at 10 cm^{-1} intervals. By using suitable reference points to superimpose the background (observed with a non-absorbing gas pressure of 50μ in the absorption cell) and absorption records, the effect of window reflection was eliminated. The reference data were measured at 10300, 9750, 9250, and 8850 cm^{-1}, where the absorption was too small to be discernible with the spacers used.

C. EXPERIMENTAL RESULTS

A normalized linear spectral absorption coefficient k_ω^o, is defined by

$$\frac{I_\omega}{I_\omega^o} = \exp(-k_\omega^o \ell^o) , \tag{46}$$

where I_ω and I_ω^o refer to the transmitted and incident spectral flux density, respectively, and ℓ^o is the geometric thickness that the

absorbing liquid would have at 300°K. Thus

$$\ell^{o} = \frac{\rho}{\rho^{o}} \ell \ , \tag{47}$$

where ℓ is the geometric thickness of the absorbing liquid, and ρ and ρ^{o} are the densities of liquid water at the temperature of the absorption run, and at 300°K, respectively. It is apparent that k_{ω}^{o} is directly proportional to the absorptive power per unit mass.

Figure 36 shows the normalized spectral absorption coefficients for liquid water in the spectral region from 2200 to 7600 cm^{-1} for temperatures of 27, 89, 159 and 209°C. Reference to Fig. 36 shows that strong absorption is localized in the regions between 2500 and 4600 cm^{-1}, between 4600 and 5900 cm^{-1} (region I) and between 5900 and 7600 cm^{-1} (region II). Figures 37 and 38 show details of the normalized absorption coefficients, and indicate more clearly the variations with temperature. The linear spectral absorption coefficients in Figs. 34 to 36 are expressed per precipitable cm of liquid water at 27°C. They may be converted to mass spectral absorption coefficients by dividing by the water density at 27°C of 0.9965 g/cm^{3}.

The quantity $\mathcal{B}$ (see Eq. (41)) is plotted as a function of spacer thickness in Fig. 39 for regions I and II. The integrated intensity of the normalized spectral absorption coefficient

$$a^{o}_{\text{slope}} = \int_{\text{band}} k_{\omega}^{o} \, d\omega \ , \tag{48}$$

has been determined from the slopes of the "best" lines through the points shown in Fig. 39. The values of a^{o}_{slope} are presented in Table

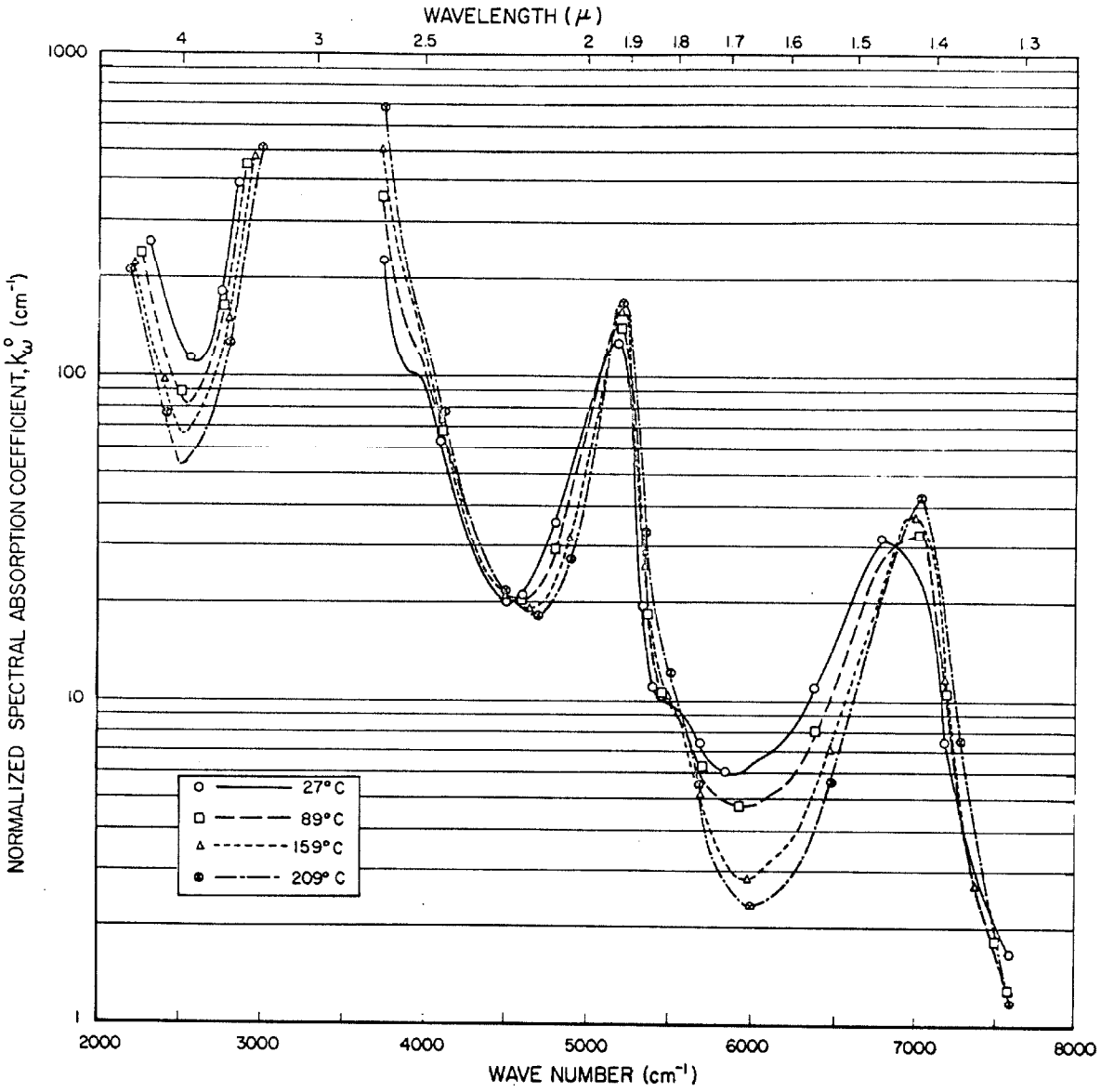

Fig. 36. The normalized spectral absorption coefficient of liquid water, k_ω°, as a function of wave number at temperatures of 27, 89, 159, and 209°C. The absorption coefficients were measured at 10 cm^{-1} intervals.

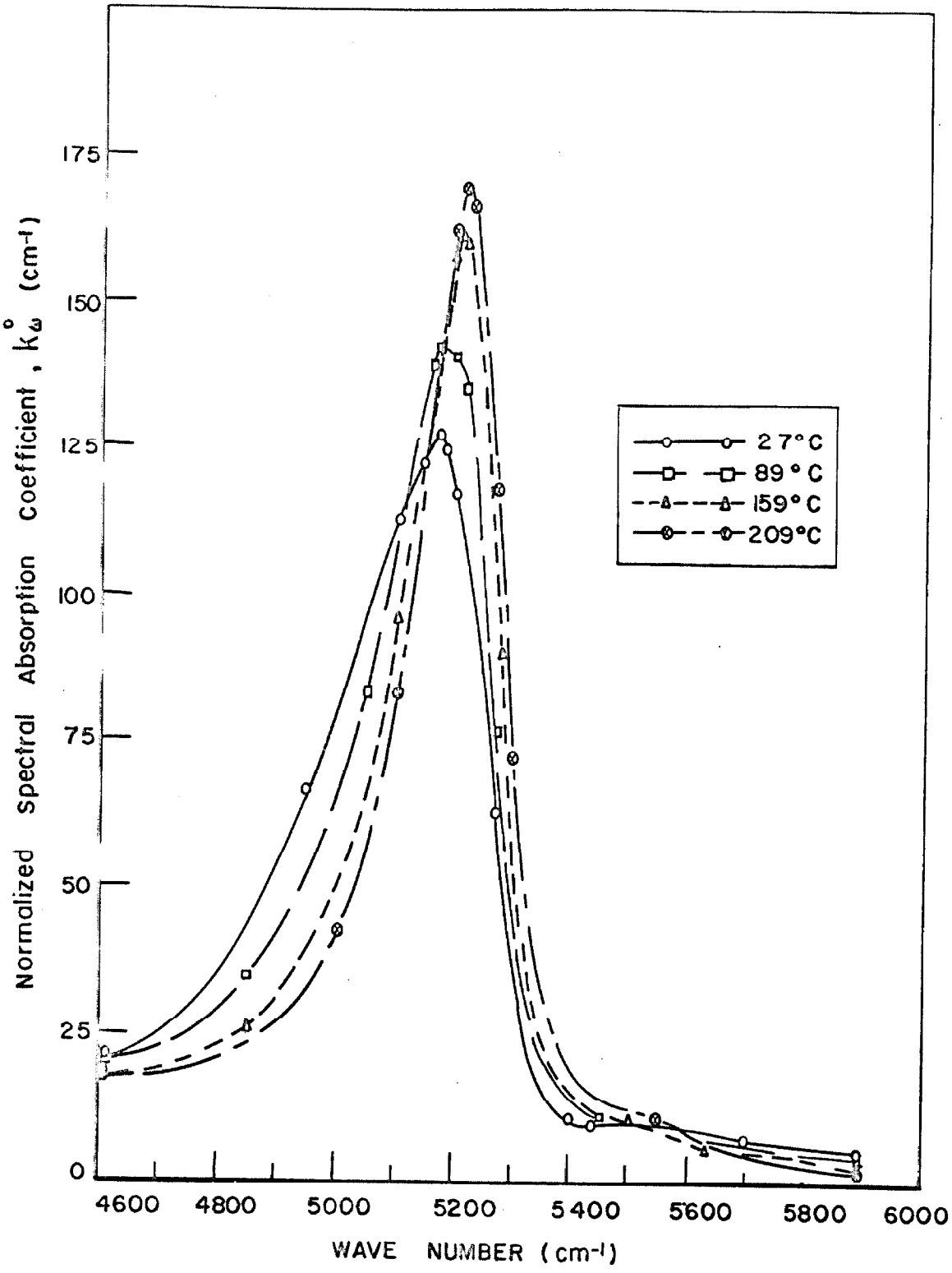

Fig. 37. The normalized spectral absorption coefficients of liquid water, k_ω°, in region I(4600-5900 cm^{-1}) at temperatures of 27, 89, 159, and 209°C.

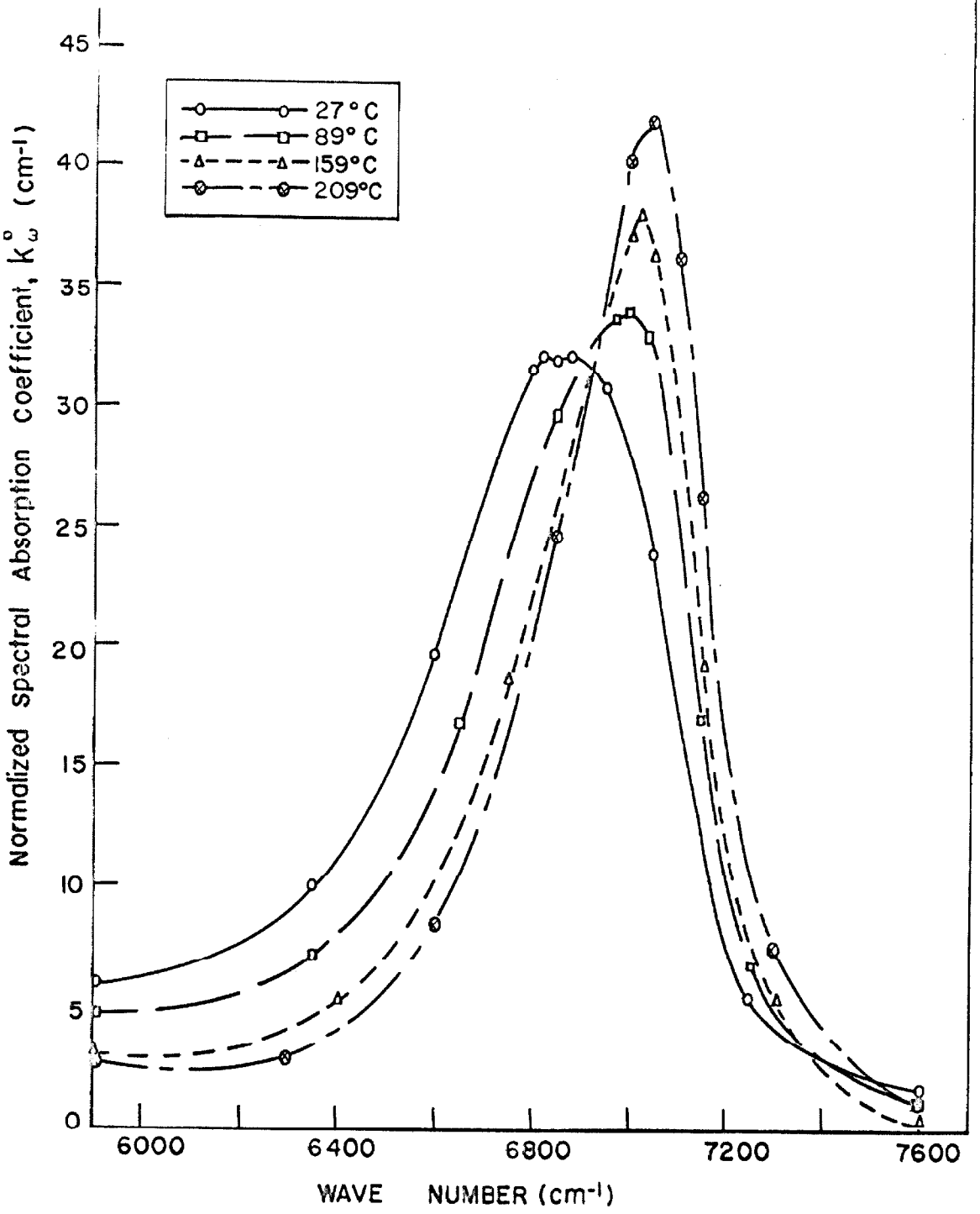

Fig. 38. The normalized spectral absorption coefficients of liquid water, k_ω°, in region II (5900-7600 cm^{-1}) at temperatures of 27, 89, 159, and 209°C.

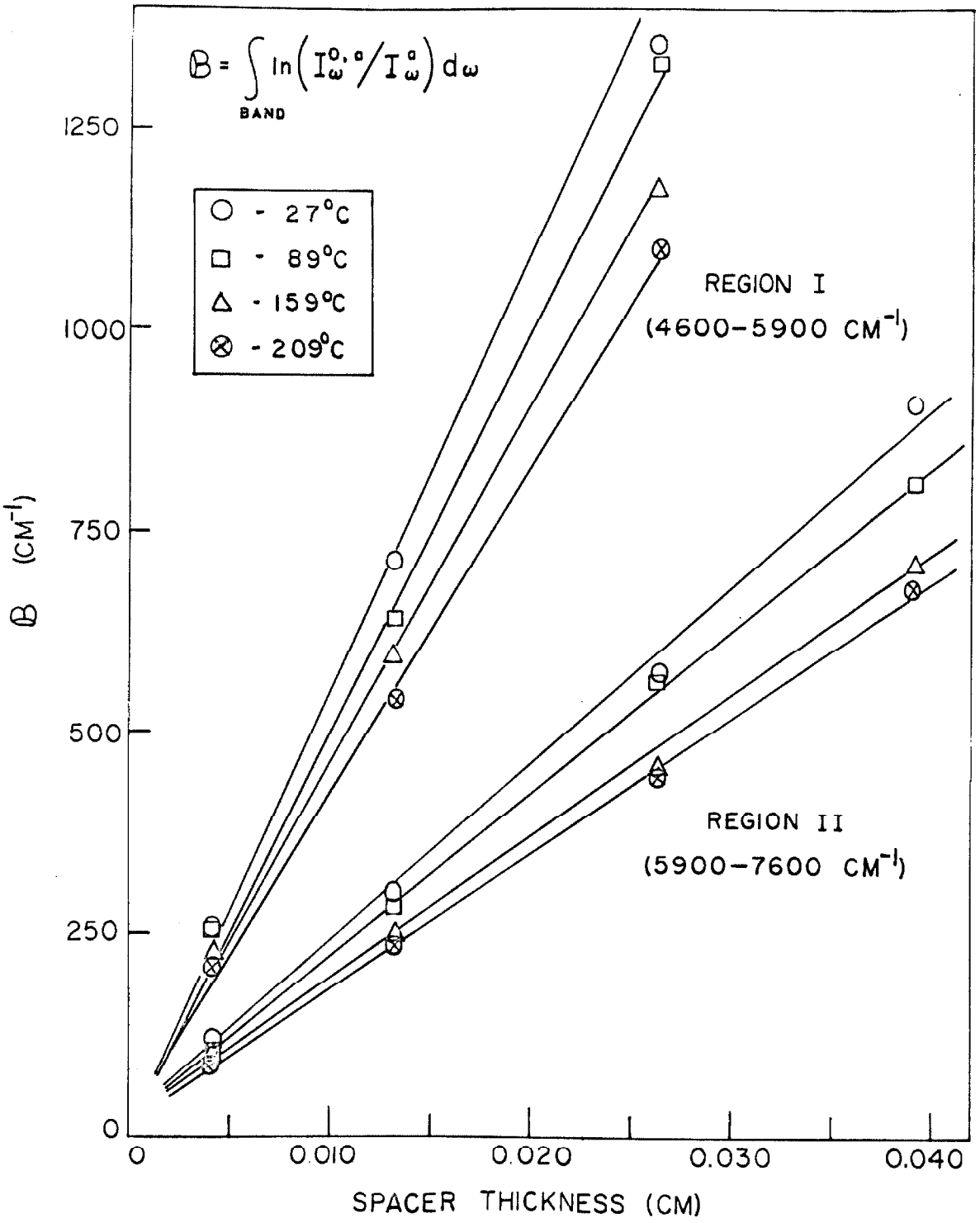

Fig. 39. The quantity $\mathcal{B}$ for liquid water in regions I and II plotted as a function of spacer thickness at temperatures of 27, 89, 159, and 209°C.

4, along with the values of the integrated intensity obtained by integrating Figs. 37 and 38 numerically.

Reference to Figs. 36, 37 and 38 shows that liquid water absorbs strongly in some spectral regions where water vapor at moderate optical depths has no measurable absorption. There is no evidence of rotational fine structure with the spectral resolution of 5 to 50 cm^{-1}. In addition, the infrared absorption of liquid water has a strong dependence on temperature which is different for different spectral regions. Furthermore, as the temperature is raised, there is a displacement of the absorption band centers to higher frequencies; k_ω^o increases at the absorption peaks; the absorption peaks move toward higher frequencies; k_ω^o decreases strongly between absorption peaks; the absorption bands become narrower, especially on the low frequency side of the bands; and weak absorption peaks (for example, at 3900, 5500 and 6100 cm^{-1}) may tend to disappear. A summary of the location of absorption peaks, and of the corresponding values of k_ω^o, is given in Table 5; the peak absorption in the 2500 to 4600 cm^{-1} spectral region was too great to be measured with the spacers used.

A table of the experimental values for the normalized linear spectral absorption coefficients of liquid water at 10 cm^{-1} intervals is given in Appendix C.

D. DISCUSSION OF RESULTS

There are small errors introduced in measuring the spacer thicknesses, in superimposing the background and absorption runs,

Table 4. Integrated Intensities of Liquid Water Bands (cm^{-2}) For Various Temperatures

Temperature °C	$\frac{\rho}{\rho_o}$	Region I (4600-5900 cm^{-1})		Region II (5900-7600 cm^{-1})	
		a^o_{slope} *	$a^o_{num.}$ †	a^o_{slope}	$a^o_{num.}$
27°C	1.000	52,000	52,000	22,600	23,000
89°C	0.9694	51,800	51,300	21,600	21,600
159°C	0.9117	48,500	49,200	19,700	19,700
209°C	0.8543	47,100	49,000	20,200	20,100

* $a^o_{slope} = \int_{band} k^o_\omega d\omega$ calculated by using Eq. (44) and the data shown in Fig. 39.

† $a^o_{num.} = \int_{band} k^o_\omega \, d\omega$ determined by direct integration of the data shown in Figs. 37 and 38.

Table 5. Change of the Absorption Peaks of Liquid Water With Temperature

27°C			89°C			159°C			209°C		
ω (cm^{-1})	λ (μ)	$k^o_{\omega, max}$ (cm^{-1})	ω (cm^{-1})	λ (μ)	$k^o_{\omega, max}$ (cm^{-1})	ω (cm^{-1})	λ (μ)	$k^o_{\omega, max}$ (cm^{-1})	ω (cm^{-1})	λ (μ)	$k^o_{\omega, max}$ (cm^{-1})
5175	1.932	128.3	5170	1.934	142.7	5205	1.921	162.3	5215	1.918	169.6
6880	1.453	32.1	7000	1.429	34.0	7020	1.425	37.8	7050	1.418	42.0

and in analyzing the data. We estimate the uncertainty of the spectral absorption coefficients and the integrated intensities to be ± 10%.

This experiment was done in conjunction with the experiments on the infrared absorption of water vapor (Chapter III) and saturated vapor (Chapter V). Comparison of the results shows that, as the water vapor condenses, the rotational fine structure is smoothed out, the absorption bands become much wider and are displaced to lower frequencies, and absorption occurs in regions where the water vapor has no measurable absorption. But, as the temperature of the liquid water is raised, the absorption spectra of liquid water more closely approximates the absorption spectra of the vapor.

The new experimental measurements confirm and, to some extent, amplify previously reported information on the relation between absorption spectra of water in the liquid and vapor phase. For example, the frequency shifts of the absorption peaks for unbonded molecules in the liquid phase relative to those in the vapor phase may be determined[18] from the following rule: -60 cm^{-1} for ν_1, + 30 cm^{-1} for ν_2, and -150 cm^{-1} for ν_3. Thus the liquid water band in region I peaks at 5220 cm^{-1} at elevated temperatures (see Fig. 37) whereas the corresponding absorption maximum in the vapor phase occurs at 5340 cm^{-1} (see Chapters III and V), as is to be expected for the $(\nu_2 + \nu_3)$-band; similarly, the $(\nu_1 + \nu_3)$-band has an absorption peak at 7050 cm^{-1} at elevated temperatures in the liquid phase (see Fig. 38) whereas the corresponding vapor phase maximum lies at about 7260 cm^{-1} (see Chapters III and V).

The abrupt change in the character of the spectral absorption coefficient near 6900 cm^{-1} between 27°C and 89°C is in accord with previously reported discontinuities in such parameters as the rate of change with temperature of refractive index, viscosity, thermal expansion, etc.[18, 39-41]

Reference to the data listed in Table 4 shows that α^{o}_{slope} decreases about 10% in region I and about 13% in region II as the temperature is increased from 27 to 209°C. The integrated intensities for water vapor at 200°C are 30,000 cm^{-2} and 22,400 cm^{-2} for regions I and II, respectively (see Chapter III). The corresponding values for liquid water at 209°C are seen to be 47,100 cm^{-2} and 20,200 cm^{-2}, respectively. Thus the integrated absorption in region I is much more strongly affected by a phase change than the integrated absorption in region II.

Table 5 shows the positions and magnitudes of the absorption coefficients at the absorption peaks. The position of the absorption peak at 6880 cm^{-1} agrees with that observed by Collins[9] (at both 27°C and 89°C) and also with that of Curcio and Petty;[11] the position of the peak at 5175 cm^{-1} agrees with that of Curcio but is about 50 cm^{-1} higher than the peak observed by Collins. In general, the spectral absorption coefficients of Curcio and Petty are about 15% lower than the estimates derived in the present study, while the data of Collins are about 10% lower, except in the 1.75 to 1.90μ region, where both the present investigations and Curcio's data show lower absorption

coefficients by 10 to 30% than Collins. It should be noted that Collins[9] and Curcio and Petty[11] used single spacers to determine the absorption coefficients in each spectral region, whereas a variety of spacers was employed in the present investigations. The presence of a "shoulder" on the 1.93μ absorption band at 5550 cm^{-1} was found by Curcio and Petty[11] but not by Collins.[9] As the temperature is increased, this "shoulder" tends to disappear.

The quantitative variation of spectral absorption coefficients with wave number (ω) and with temperature (T) provides important information on the change in hydrogen bonding with temperature. Following Buijs and Choppin,[18] we may use the new experimental results to estimate the mass fractions (Y_0, Y_1 and Y_2) of unbonded (S_0), singly hydrogen-bonded (S_1), and doubly hydrogen-bonded (S_2) water molecules in the liquid phase on the assumption that these species are sufficient to explain the quantitative variations of k_ω^o with ω and T. Thus we select the wave numbers ω_0, ω_1, and ω_2 at which the spectral absorption coefficients for the unbonded, the singly hydrogen-bonded, and the doubly hydrogen-bonded species have their respective maxima. We then identify ω_0 with the location of the absorption peak in the liquid phase at the highest temperature for which we have experimental data, choose ω_2 equal to the wave number at which the corresponding absorption coefficient in ice has a maximum value,[7, 8] and assume that the ratio $(\omega_1-\omega_0)/(\omega_2-\omega_1)$ is the same in regions I and II as for the 1.20μ band studied by Buijs and Choppin.[18] Next we consider the following set of four simultaneous equations:

$$
\begin{aligned}
k_{\omega_0}^{(0)} Y_0 + k_{\omega_0}^{(1)} Y_1 + k_{\omega_0}^{(2)} Y_2 &= k_{\omega_0}^{o} , \\
k_{\omega_1}^{(0)} Y_0 + k_{\omega_1}^{(1)} Y_1 + k_{\omega_1}^{(2)} Y_2 &= k_{\omega_1}^{o} , \\
k_{\omega_2}^{(0)} Y_0 + k_{\omega_2}^{(1)} Y_1 + k_{\omega_2}^{(2)} Y_2 &= k_{\omega_2}^{o} ,
\end{aligned} \tag{49}
$$

and

$$Y_0 + Y_1 + Y_2 = 1,$$

where $k_{\omega_j}^{(i)}$ is the spectral absorption coefficient of the i^{th} species at wave number ω_j. The quantities $k_{\omega_0}^{o}$, $k_{\omega_1}^{o}$, and $k_{\omega_2}^{o}$ are read directly from Figs. 37 and 38 and Appendix C (after the necessary correction for the background absorption from the 3μ region is taken into account); the values of $k_{\omega_0}^{(2)}$, $k_{\omega_1}^{(2)}$ and $k_{\omega_2}^{(2)}$ represent previously determined[7,8] absorption coefficients for ice at ω_0, ω_1, and ω_2, respectively. We assume that the term $k_{\omega_2}^{(0)} Y_0$ is negligibly small because the unbonded species has a strongly peaked absorption maximum and the value of $k_{\omega_2}^{(0)}$ decays rapidly for large values of $\omega - \omega_0$; we also assume that $k_{\omega_2}^{(1)} = k_{\omega_0}^{(1)}$, i.e., that the singly hydrogen-bonded species has an absorption coefficient which is nearly symmetric and has decayed to the same value at ω_0 and at ω_2. If the absorption coefficients are assumed to be independent of temperature,[18] there are sixteen unknowns ($k_{\omega_0}^{(0)}$, $k_{\omega_0}^{(1)} = k_{\omega_2}^{(1)}$, $k_{\omega_1}^{(0)}$, $k_{\omega_1}^{(1)}$; and Y_0, Y_1 and Y_2 at each of the four temperatures) and 16 non-linear equations (Eqs. (49) at each of the four temperatures) for each of the two regions.* A set of values was found for the unknowns that satisfied all 28 equations to better than 10%, i.e., within the experimental limits of uncertainty. The results for

*Since the values of Y_0, Y_1, and Y_2 must be the same in the two chosen spectral regions, only four of the equations $Y_0 + Y_1 + Y_2 = 1$ (one at each of the four temperatures) are independent and the problem therefore reduces to 28 non-linear equations in 20 unknowns.

the spectral absorption coefficients are listed in Table 6 and those obtained for the mass fractions are presented in Table 7, together with the values extrapolated from the data of Buijs and Choppin[18] (who performed their experiments between 6 and 72°C).

If ice is assumed to have 100% hydrogen-bonding, the fraction of hydrogen bonds at any temperature is $Y_H = 1.0 - Y_0 - 0.5Y_1$; the values of Y_H defined in this manner are also presented in Table 7. The mass fraction of bonded hydrogen is seen to decrease from 60 to 20% in the temperature range 27 to 209°C. Extrapolation of the data allows 68% hydrogen bonding in liquid water at 0°C. Reference to the data shown in Table 7 indicates that our results show a much stronger dependence of the mass fraction of unbonded species on temperature than do those of Buijs and Choppin. However, the values of Y_H are seen to be in fair agreement.

Following Buijs and Choppin,[18] we assume that the following equilibria obtain:

$$S_1 \rightleftarrows S_0 \quad \text{with } k_1 = Y_0/Y_1 ,$$
$$S_2 \rightleftarrows S_1 \quad \text{with } k_2 = Y_1/Y_2 , \tag{50}$$

and

$$k_3 \equiv k_1 k_2 = Y_0/Y_2 .$$

The heats of reaction may then be derived from plots of $\ell n\, k_i$ vs. $1/T$ (see Fig. 40). The resultant enthalpy changes do not agree well with those of Buijs and Choppin, whose estimates are identified by the subscript BC, viz.,

for $S_1 \rightleftarrows S_0$, we find $\Delta H^1 = 3.0$ kcal/mole whereas $\Delta H^1_{BC} = 1.1$ kcal/mole;

for $S_2 \rightleftarrows S_1$, we find $\Delta H^2 = 2.0$ kcal/mole whereas $\Delta H^2_{BC} = 1.6$ kcal/mole;

Table 6. Spectral Absorption Coefficients Used in Calculations of Species Concentrations (Per Precipitable cm of Liquid Water at 27°C)

	Region I			Region II		
	ω_0	ω_1	ω_2	ω_0	ω_1	ω_2
	5220 cm^{-1}	5120 cm^{-1}	5000 cm^{-1}	7050 cm^{-1}	6870 cm^{-1}	6660 cm^{-1}
$k_\omega^{(0)}$	190	55	0	45	15	0
$k_\omega^{(1)}$	110	175	110	21	33	21
$k_\omega^{(2)}$	41.5	44.6	46.4	18.8	29.5	32.6

Table 7. Species Mass Fractions as a Function of Temperature

Present Experiments					Buijs and Choppin[18]			
T(°C)	Y_0	Y_1	Y_2	Y_H	Y_0	Y_1	Y_2	Y_H
0	0.09†	0.46†	0.45†	0.68†	0.26*	0.41*	0.33*	0.54*
27	0.15	0.50	0.35	0.60	0.32	0.43	0.25	0.47
89	0.37	0.45	0.18	0.41	0.42*	0.42*	0.16*	0.37*
159	0.53	0.37	0.10	0.29	0.50*	0.39*	0.11*	0.30*
209	0.645	0.315	0.06	0.20	0.55*	0.37*	0.08*	0.27*

† Extrapolated from present data.

* Extrapolated from data obtained between 6 and 72°C.

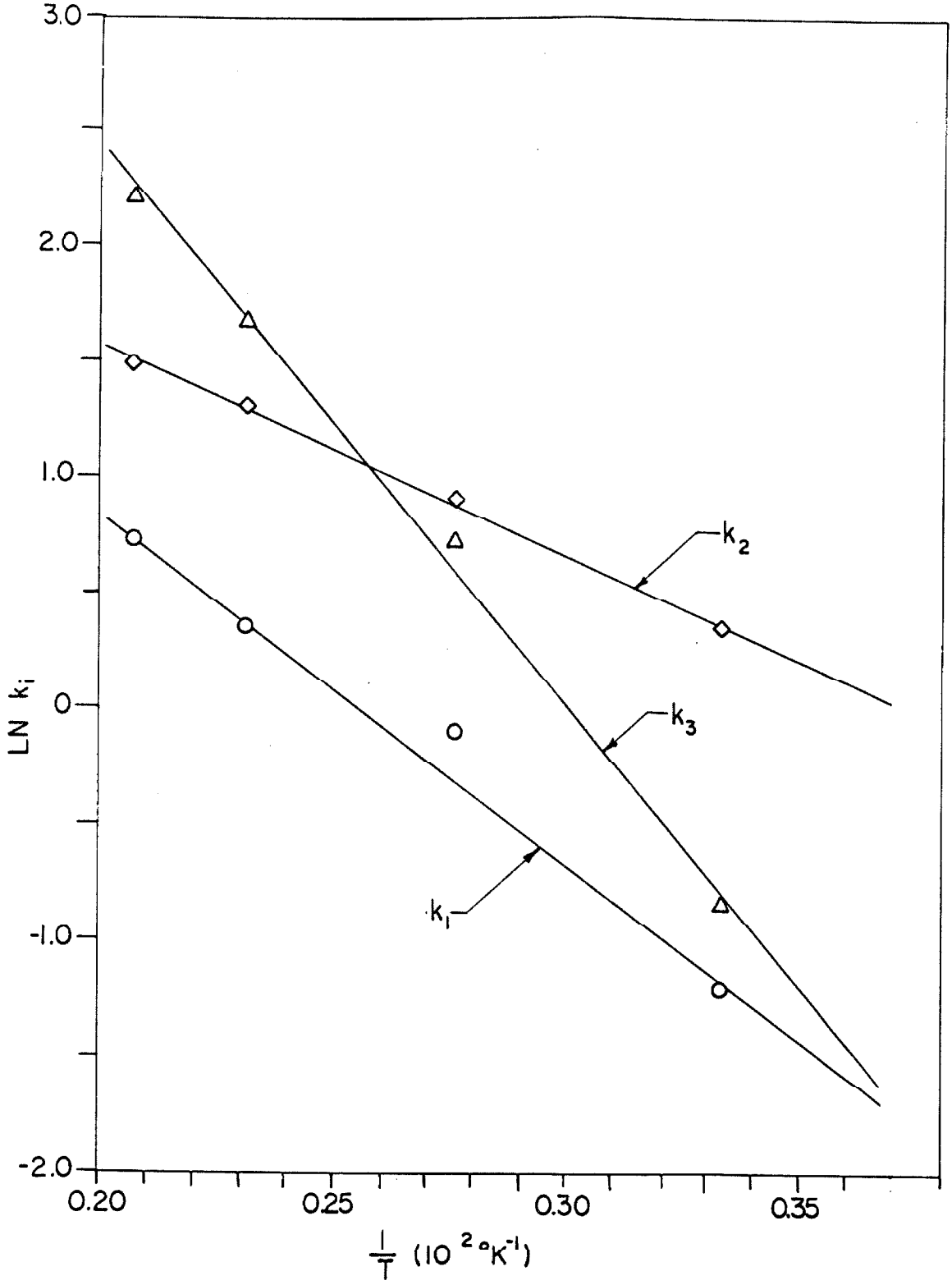

Fig. 40. The quantity $\ell n\, k_i$ plotted as a function of (1/T) for the equilibrium between various species of water molecules in liquid water.

for $S_2 \rightleftarrows S_0$, we find $\Delta H^3 = 5.0$ kcal/mole whereas $\Delta H^3_{BC} = 2.7$ kcal/mole. Since we had to introduce some rather arbitrary assumptions, in addition to the model of Buijs and Choppin, the differences in the calculated heats of dissociation are not surprising. Furthermore, because our experimental data cover a much wider temperature range, the assumed constancy of the $k_{\omega_j}^{(i)}$ may lead to larger discrepancies.

Again following Buijs and Choppin,[18] we may make an estimate for the heat of fusion by using the heats of reaction and the relation $\Delta H^f = Y_0(0^\circ C)\, \Delta H^3 + Y_1(0^\circ C)\, \Delta H^2$. The result is identical with that of Buijs and Choppin, namely, 1.36 kcal/mole compared with the experimental value of 1.44 kcal/mole.[34]

Further discussion of our data on hydrogen bonding would follow closely the work of Buijs and Choppin,[18] except for the changes in the numerical estimates of Y_0, Y_1, and Y_2 at various temperatures (see Table 7).

The discussion of the implications of our measurements on water structure is not definitive because of the inadequacy of the model used and because of the rather arbitrary nature of some of the assumptions made by us. In this connection, it should be noted particularly that our method of data analysis, like that of Buijs and Choppin,[18] is incomplete since full utilization was not made of the wealth of experimental information that is provided by the fact that spectral absorption coefficients are measured as <u>continuous</u> functions of frequency. Thus it is apparent that we could assume band contours for the unbonded and for the hydrogen-bonded species in water and

then use the available data on k_w^o to construct concentration estimates for the five unbonded and hydrogen-bonded species of water that have been considered, for example, by Némethy and Scheraga.[19] We defer this ambitious programme of data analysis to a later date when more exhaustive measurements will have been performed, particularly on ice and on liquid water under saturation conditions.

CHAPTER V

INVESTIGATIONS OF THE ABSORPTION BY SATURATED WATER VAPOR AT 209°C

A. INTRODUCTION

Measurements have been performed in the wave number range between 3600 and 7600 cm^{-1} on the transmission through equal optical depths of liquid water and through water vapor near the limits of saturation. This experiment was carried out at 209°C, because a high water vapor saturation pressure was required in order to obtain equal optical depths of liquid and gaseous water.

B. APPARATUS AND PROCEDURE

The apparatus is described in Chapter I. The transmission spectra of liquid water was studied with a 0.0052-inch spacer in the variable spacer absorption cell (see Fig. 15); the liquid was introduced into the cell from the constant temperature liquid reservoir outside the vacuum tank as described in Chapter IV.

Two absorption cell setups were used to investigate the transmission through water vapor near and at saturation. The first employed the variable spacer cell (spacer = 0.500 inch) with the vapor supplied from the liquid water reservoir outside the vacuum tank (see Fig. 13); the vapor pressure was held constant (± 0.5 psi) at a value below the pressure at which condensation occurred, while the absorption spectra was scanned. The measured nominal saturation

pressure was slightly above 277 psi at 209 ± 1°C. This value is somewhat larger than the known vapor pressure of 271. 2 psi at 209°C;[34] however, the observed discrepancy is within the limits of uncertainty corresponding to the accuracy of the temperature measurements in the cell. Scannings of the absorption spectra were taken with vapor pressures of 271, 276 and 277 psi. The fact that condensation or droplet formation did not occur was determined by visual observation of the windows (from outside the vacuum tank) and by continuous observation of the signal.

The second setup used the variable spacer absorption cell (spacer = 0. 500-inch) with the vapor supplied from the self-contained liquid reservoir (see Fig. 12); the procedure was the same as that described in Chapter II, and is assumed to have given saturated water vapor. Two 1-inch diameter by 1/4-inch thick sapphire windows were used in all the present investigations.

The background was recorded and superimposed to the absorption spectra in the same way as described in Chapter IV.

C. RESULTS AND DISCUSSION OF RESULTS

Figure 41 presents the fractional transmission through the liquid water and near saturated vapor in the wave number region between 3600 and 8000 cm^{-1}; the data shown in Fig. 41 refer to a fixed amount (0. 0108 g/cm^2 + 5%) of precipitable water in the light path. They may, therefore, be used directly for illustrating the dependence of infrared transmission on the proximity to saturation conditions.

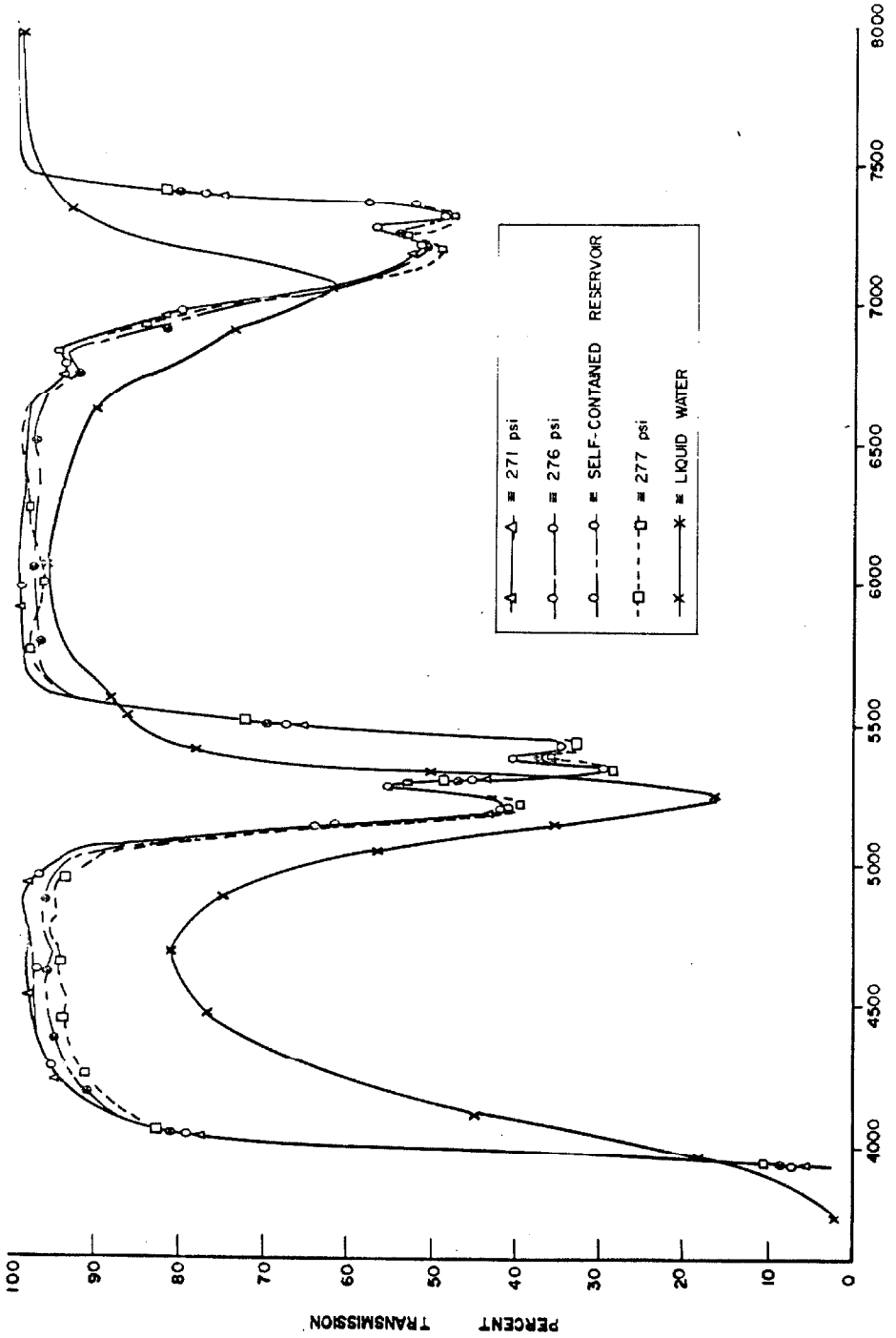

Fig. 41. The fractional transmission as a function of wave number (between 3500 and 8000 cm^{-1}) for liquid water and for water vapor near saturation conditions; 0.0108 g/cm^2 of precipitable water (within ± 5%); T = 209°C (± 1°C); spectral resolution ≈ 20 cm^{-1}; experimental points determined at 10 cm^{-1} intervals; condensation occurred just above 277 psi.

Reference to the experimental data shows that the vapor phase, at a pressure which differs from saturation conditions by a microscopic amount, has a transmission spectrum that is noticeably different from that of the liquid phase. It is interesting to observe the rather abrupt change in transmission just before saturation conditions are reached; the transmission spectra of water vapor at 271 and 276 psi are almost completely identical in the spectral region studied, but differ markedly from the transmission spectra of the two conditions considered to be at, or near, saturation (277 psi and self-contained reservoir runs). As condensation occurs, the remaining rotational structure (which is observed with about 10 to 50 cm^{-1} resolution) disappears, the absorption peaks are notably shifted, and the absorption coefficients are markedly increased in some spectral regions, and decreased in others.

The observed experimental results are consistent with the view that molecular aggregates in liquid and gaseous water, at the highest vapor pressures which we were able to maintain without condensation, are significantly different. Further discussion on this subject is presented in Chapter IV.

CHAPTER VI

APPROXIMATE CALCULATIONS OF THE SPECTRAL ABSORPTION COEFFICIENTS OF WATER VAPOR BETWEEN 200 AND 727°C

A. INTRODUCTION

The basic spectroscopic constants for water vapor, required for an a priori calculation of spectral absorption coefficients, have been measured and are described in Chapter III. Thomson[42] was able to correlate the total emissivity data of water vapor, in terms of a just-overlapping line model in the temperature range between 333 and 1666°K, by assuming "reasonable" values for the integrated intensities of the various bands. In addition, Gray[6] used the same model, with approximate values for the integrated intensities of water vapor, to correlate emissivity data at 1111°K. Therefore, it appears justified to employ a just-overlapping line model, combined with the quantitative data of Chapter III, in order to perform approximate spectral absorption coefficient calculations.

The just-overlapping line model assumes that there is sufficient pressure-broadening to smear out the rotational structure of the band. For water vapor, this occurs at room temperature at a pressure of 3 atm; the pressure required for self-broadening should decrease with temperature because of the increased number of bands and lines. This condition was satisfied in obtaining the data in Chapter III.

Calculations of the spectral absorption coefficients of water vapor have been performed for all of the experimental conditions in Chapter III

and the results have been compared to the experimental data.

B. THEORY

The integrated intensity of an individual spectral line is given by*

$$S_{\ell u} = \frac{8\pi^3 \omega_{\ell u}}{3hcp} \frac{N}{Q_T} \left| \Re_{\ell u} \right|^2 \exp(-E_\ell/kT) \left[1-\exp\left(- \frac{hc\omega_{\ell u}}{kT} \right) \right], \qquad (51)$$

where N is the number of molecules per unit volume, Q_T is the total partition function, $\omega_{\ell u}$ is the wave number of the transition, $\Re_{\ell u}$ is the electric dipole matrix element corresponding to the transition and E_ℓ is the sum of the vibrational and rotational energies of the lower (initial) state; the other symbols have their usual meanings.

For an asymmetric top molecule such as water vapor, the matrix element $\Re_{\ell u}$ cannot be expressed explicitly in terms of "good" quantum numbers.[1, 43, 44] If the approximation of a symmetric top is assumed, Eq. (51) becomes†

$$S_J \simeq \frac{8\pi^3 \omega}{3hc} \frac{N}{p} \frac{\left| \Re_{ov'} \right|^2}{Q_R} \sum_{K=0}^{J} g_{JK} \exp\left[- \frac{E(J, K)}{kT} \right], \qquad (52)$$

where Q_R is the rotational partition function. With Eq. (52), we are assuming that most of the molecules are in the ground vibrational state, and that the induced emission term $\left[1-\exp(-hc\omega/kT)\right]$ is

---

* See Ref. 1, Eq. (7-125).

† See Ref. 1, Eq. (11-137).

approximated by unity at infrared frequencies.

For a "nearly symmetric top", the rotational energy is given by Eq. (34) (see Chapter I, Section B. 4),

$$E(J,K) = hc\left[J(J+1)\sqrt{BC} + (A-\sqrt{BC})K^2\right], \tag{34}$$

where the degeneracies are $g_{JK} = 2(2J+1)$ for $K \neq 0$ and $g_{JK} = 2J+1$ for $K = 0$.

Using Eq. (34), we may write

$$\sum_{K=0}^{J} g_{JK} \exp\left[-\frac{E(J,K)}{kT}\right] \simeq \{4J \exp\left[-\frac{hc\sqrt{BC}}{kT} J^2\right] \int_0^J \exp\left[-\frac{hc(A-\sqrt{BC})}{kT} K^2\right] dK\}, \tag{53}$$

where the summation has been replaced by an integral. Letting

$$\gamma = hc\sqrt{BC}/kT,$$

$$\beta = (A\sqrt{BC}-1), \tag{54}$$

and $$u' = 2\gamma J,$$

Eq. (53) becomes

$$\sum_{K=0}^{J} g_{JK} \exp\left[-\frac{E(J,K)}{kT}\right] \simeq \left\{\frac{2u'}{\gamma} \exp\left[-\frac{u'^2}{4\gamma}\right] \int_0^{u'/2\gamma} \exp\left[-\gamma\beta K^2\right] dK\right\} \tag{55}$$

or,*

$$\sum_{K=0}^{J} g_{JK} \exp\left[-\frac{E(J,K)}{kT}\right] \simeq \left\{u' \left(\frac{\pi}{\gamma^3 \beta}\right)^{\frac{1}{2}} \exp\left[-\frac{u'^2}{4\gamma}\right] \operatorname{erf}\left[\frac{u'}{2}\left(\frac{\beta}{\gamma}\right)^{\frac{1}{2}}\right]\right\}. \tag{56}$$

---

* Since $\operatorname{erf}(x) = \frac{2}{\sqrt{\pi}} \int_0^x \exp(-t)^2 dt.$

The rotational partition function can be approximated by*

$$Q_R \simeq \left(\frac{kT}{hc}\right)^{3/2}\left(\frac{\pi}{ABC}\right)^{1/2} = \left(\frac{\pi}{\sqrt[3]{\gamma(1+\beta)}}\right)^{1/2} . \tag{57}$$

Combining Eqs. (52), (56) and (57), the integrated intensity of the J^{th} line in the vibration-rotation band is given by

$$S_J \simeq \frac{1}{2}\, a\, u'\left(\frac{1+\beta}{\beta}\right)^{1/2} \exp\left[-\frac{u'^2}{4\gamma}\right] \operatorname{erf}\left[\frac{u'}{2}\left(\frac{\beta}{\gamma}\right)^{1/2}\right] \tag{58}$$

where

$$a \equiv a_{0v'} = \frac{8\pi^3 \omega_o}{3hc}\,\frac{N}{p}\,|\Re_{0v'}|^2 \tag{59}$$

refers to each branch of a vibration-rotation band consisting of P and R branches, and the wave number has been approximated by ω_o, the wave number at the band center. For a vibration-rotation band, the mean line spacing is

$$\delta^* = 2\sqrt{BC'} ; \tag{60}$$

it follows that

$$u' = 2\gamma J = \frac{hc\,|\omega-\omega_o|}{kT} . \tag{61}$$

From Eqs. (58), (60), and (61), the average spectral absorption coefficient, $\bar{P}_\omega$, equal to S_J divided by the mean line spacing, becomes

$$\bar{P}_\omega = \frac{a}{4\sqrt{BC}}\, u'\left(\frac{1+\beta}{\beta}\right)^{\frac{1}{2}} \exp\left[-\frac{u'^2}{4\gamma}\right] \operatorname{erf}\left[\frac{u'}{2}\left(\frac{\beta}{\gamma}\right)^{\frac{1}{2}}\right] . \tag{62}$$

---

* See Ref. 45, p. 208.

C. CALCULATIONS

The infrared absorption of water vapor at room temperature is due primarily to vibrational transitions from the ground state; as the temperature is raised, higher vibrational states become populated. In order to perform an accurate calculation for temperatures above 1000°K, hundreds of vibrational transitions must be taken into account and would necessitate using a computer.

For this reason, our calculations, at temperatures up to 1000°K, used the band centers and relative band intensities calculated for 300°K, given in Table 1* and the approximation, valid only for diatomic molecules, that

$$\sum_{v_1, v_2, v_3} a(v_1, v_2, v_3 \rightarrow v_1+\Delta v_1, v_2+\Delta v_2, v_3+\Delta v_3) \simeq \bar{a}(0, 0, 0 \rightarrow \Delta v_1, \Delta v_2, \Delta v_3). \tag{63}$$

In addition, the assumption was made that the integrated intensity variation with temperature is due primarily to the change of population of the ground state caused by the density variation; that is,

$$\bar{a}(T) = \left(\frac{T_o}{T}\right) \bar{a}(T_o). \tag{64}$$

This assumption was made even though the experiment (see Chapter III) showed the variation of the integrated intensities to be proportional to $T^{-0.99}$, $T^{-0.93}$ and $T^{-0.93}$ for the 1.38μ, 1.87μ and 2.7μ regions, respectively (see Fig. 34).

With these approximations, and using Eq. (62) and the integrated

---

* The calculations also neglected the band shift to lower frequencies with increasing temperature. This follows from the fact that the vibrational constants x_{ij} in Eq. (33) are negative.

intensities at 200°C given in Chapter III, the spectral absorption coefficients for water vapor have been calculated for all the experimental conditions. The results are shown in Figs. 23 to 33, along with the experimental results.

D. COMPARISON WITH EXPERIMENT

Reference to Figs. 23 to 33 indicates that the theoretical equations provide a crude fit to the data. The theoretical band contours are most obviously deficient in that they cannot account for the presence of the Q-branch in the perpendicular bands, and in failure to include the multiplicity of combination bands which contribute in a given spectral region.

REFERENCES

1. S. S. Penner, Quantitative Molecular Spectroscopy and Gas Emissivities, Addison-Wesley, Reading, Mass. (1959).

2. W. S. Benedict and E. K. Plyler, "Energy Transfer in Hot Gases", NBS Circular No. 523, p. 64 (1954).

3. J. T. Houghton and J. S. Seeley, Quart. J. Roy. Met. Soc. 86, 358 (1960).

4. C. C. Ferriso and C. B. Ludwig, General Dynamics-Astronautics, Tech. Rep. No. BBE 63-002 (1963).

5. J. H. Jaffe and W. S. Benedict, JQSRT 3, 87 (1963).

6. L. D. Gray, Ph. D. Thesis, California Institute of Technology, Pasadena, California (1963).

7. G. Bode, Ann. d. Phys. 30, 326 (1909).

8. E. K. Plyler, J. Opt. Soc. Am. 9, 545 (1924).

9. T. F. Collins, Phys. Rev. 26, 771 (1925).

10. E. Ganz, Ann. d. Physik 26, 331 (1936).

11. T. A. Curcio and C. C. Petty, J. Opt. Soc. Am. 41, 302 (1951).

12. E. K. Plyler and N. Acquista, J. Opt. Soc. Am. 44, 505 (1954).

13. N. E. Dorsey, Properties of Ordinary Water Substance, Reinhold Publishing Co., New York, N. Y. (1940).

14. T. F. Collins, Phys. Rev. 20, 486 (1922).

15. J. J. Fox and A. E. Martin, Proc. Roy. Soc. (London) 174, 234 (1940).

16. M. Van Thiel, E. D. Becker and G. C. Pimentel, J. Chem. Phys. 27, 95 (1957).

17. M. Van Thiel, E. D. Becker and G. C. Pimentel, J. Chem. Phys. 27, 486 (1957).

18. K. Buijs and G. R. Choppin, J. Chem. Phys. 39, 2035 (1963).

19. G. Némethy and H. A. Scheraga, J. Chem. Phys. 36, 3382 (1962).

20. H. Born and T. R. Oppenheimer, Ann. d. Phys. 84, 456 (1927).

21. H. Goldstein, Classical Mechanics, Addison-Wesley Publishing Co., Reading, Mass., Chapter 10 (1959).

22. H. Margenau and G. M. Murphy, The Mathematics of Physics and Chemistry, D. van Nostrand and Co., New York, N. Y., Chapters 9 and 10 (1943).

23. L. Pauling and E. B. Wilson, Jr., Introduction to Quantum Mechanics, McGraw Hill, New York (1935).

24. L. D. Landau and E. M. Lifshitz, Quantum Mechanics, Non-Relativistic Theory, Addison-Wesley, Reading, Mass. (1958).

25. G. Herzberg, Infrared and Raman Spectra of Polyatomic Molecules, D. van Nostrand and Co., New York (1945).

26. L. G. Bonner, Phys. Rev. 46, 458 (1934).

27. B. T. Darling and D. M. Dennison, Phys. Rev. 57, 128 (1940).

28. D. M. Dennison, Rev. Mod. Phys. 12, 175 (1940).

29. P. J. Wyatt, V. R. Stull and G. N. Plass, Aeronutronic Division of Ford Motor Co., Tech. Rep. No. SSD-TDR-62-127, Vol. II (1962).

30. E. K. Plyler and W. W. Sleator, Phys. Rev. 37, 1493 (1931).

31. D. H. Rank, K. D. Larsen and E. B. Bordner, J. Chem. Phys. 2, 464 (1934).

32. D. Bender, Phys. Rev. 47, 252 (1935).

33. H. H. Nielsen, Phys. Rev. 62, 422 (1942).

34. Handbook of Chemistry and Physics, 36th Edition, Chemical Rubber Publishing Co. (1954-55).

35. A. Guttman and S. S. Penner, J. Chem. Phys. 36, 98 (1962).

36. A. Guttman, JQSRT 2, 1 (1962).

37. O. C. Mohler, A Table of Solar Spectrum Wavelengths, 11984A to 25578A, U. of Michigan Press, Ann Arbor, p. 9 (1955).

38. D. E. Burch and D. A. Grynak, Aeronutronics Division of Ford Motor Co., Rep. No. U-1929 (1962).

39. M. Magat, J. phys. radium [7] 6, 179 (1935).

40. G. Tammann, Z. anorg. u. allgem. Chem. 235, 49 (1937).

41. F. S. Feates and D. J. G. Ives, J. Chem. Soc. 1956, 2798.

42. A. Thomson, Gruen Applied Science Labs., Inc., Pasadena, California, Tech. Note No. 5, Contract AF 04(645)-24(1957).

43. E. B. Wilson, Jr., J. C. Decius, and P. C. Cross, Molecular Vibration, McGraw-Hill, New York (1955).

44. P. C. Cross, R. M. Haines, and G. W. King, J. Chem. Phys. 12, 210 (1944).

45. S. S. Penner, Chemistry Problems in Jet Propulsion, Pergamon Press, London (1957).

APPENDIX A

Graphs Showing $\ell n(I_{\omega}^{o,a}/I_{\omega}^{a})$ as a Function of ω for Water Vapor Bands

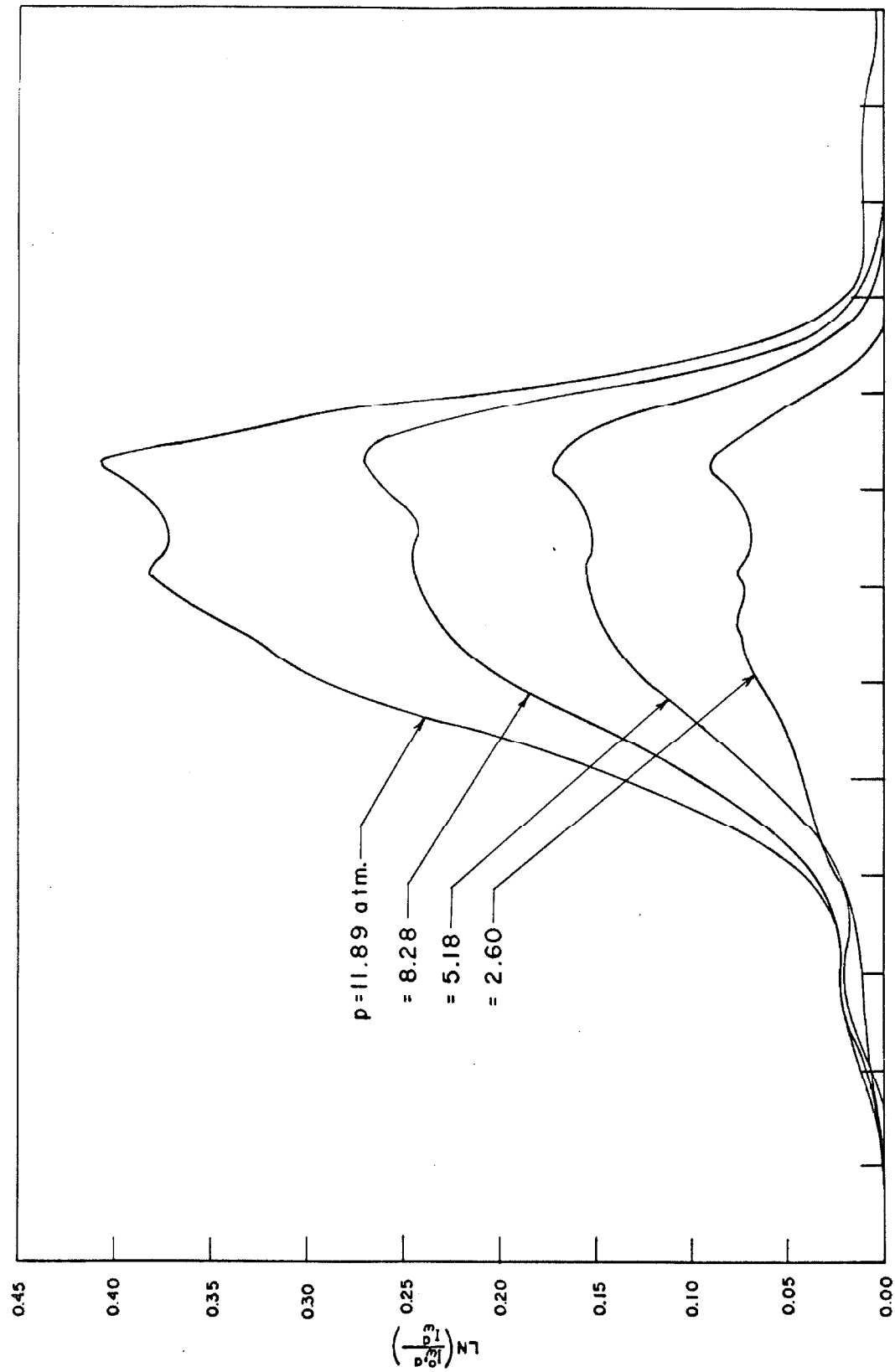

Fig. 42. The quantity $\ell n(I_{\omega}^{o,a}/I_{\omega}^{a,a})$ as a function of wave number for the 1.38μ region of water vapor at 200°C.

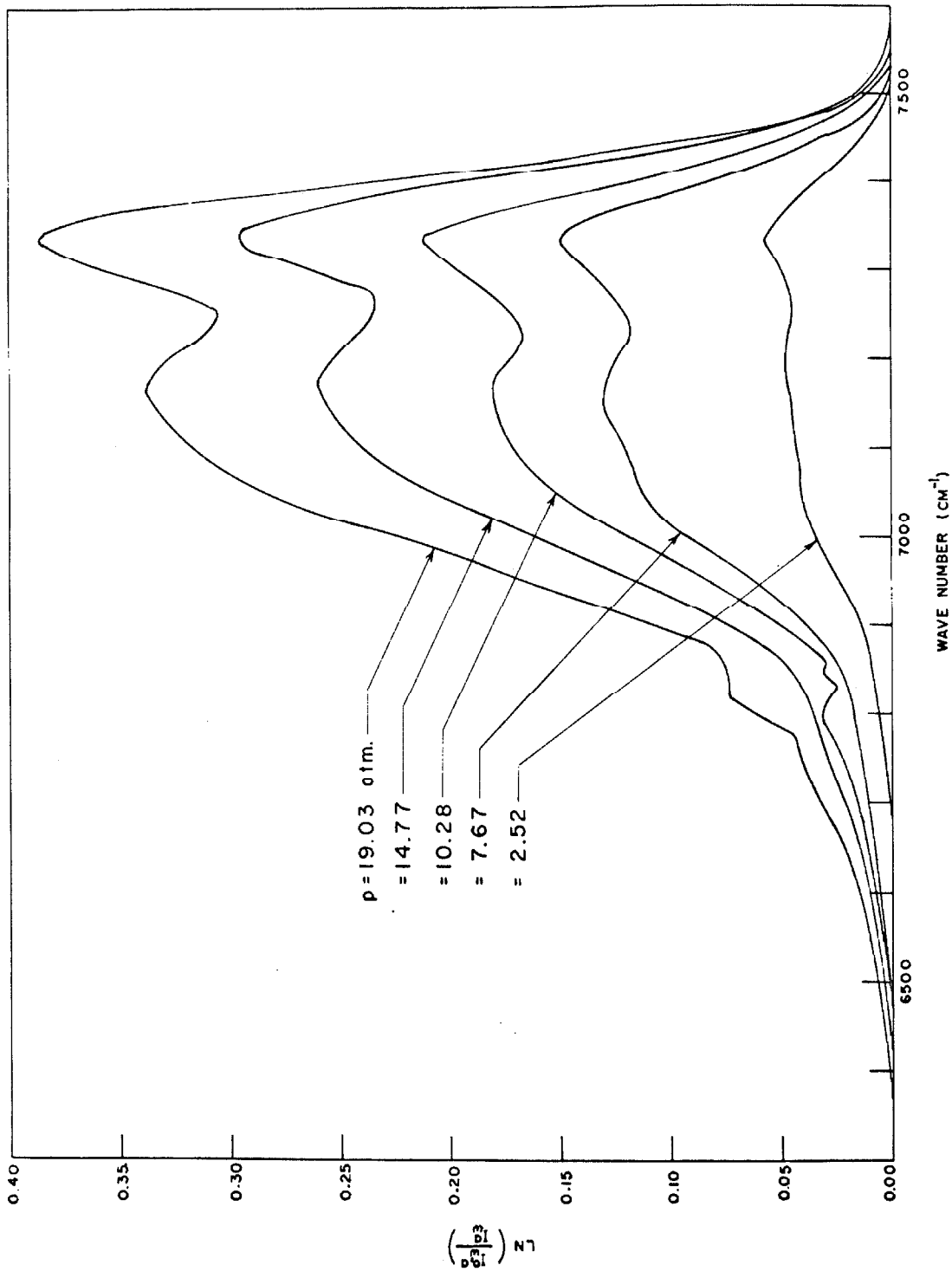

Fig. 43. The quantity $\ln(I_w^{o,a}/I_w^{a})$ as a function of wave number for the 1.38μ region of water vapor at 400°C.

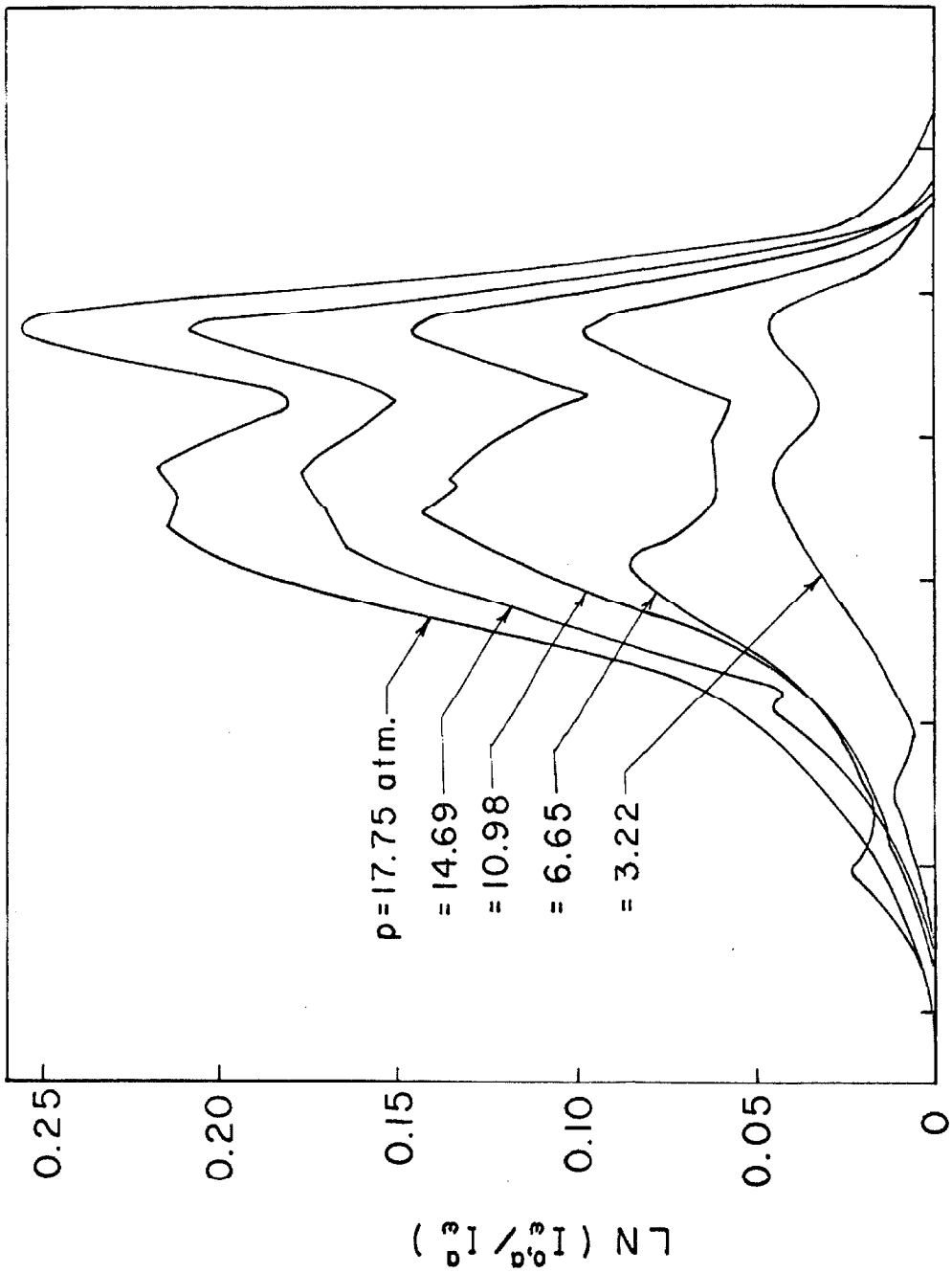

Fig. 44. The quantity $\ell n(I_w^{o,a}/I_w^a)$ as a function of wave number for the 1.38μ region of water vapor at 600°C.

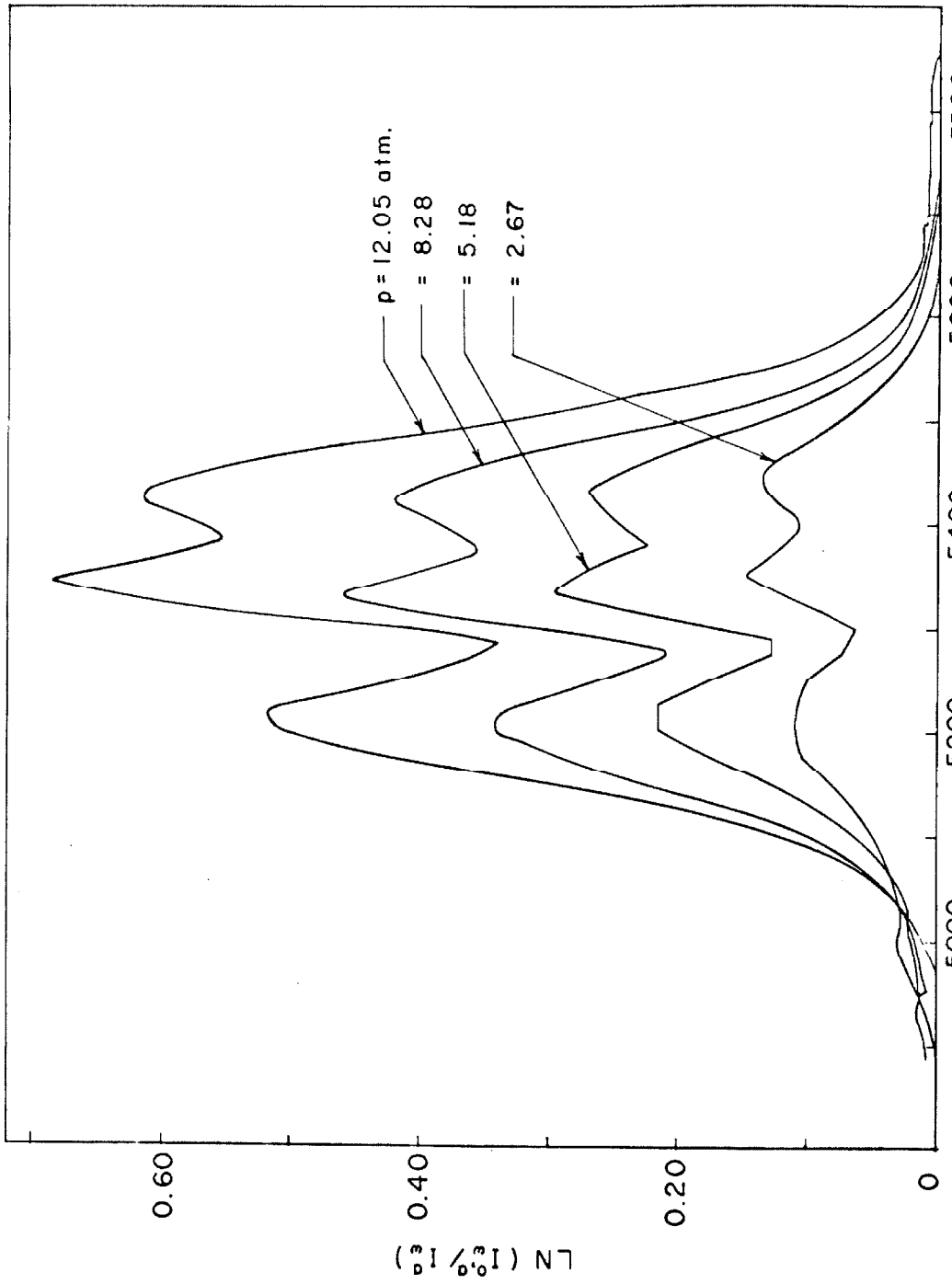

Fig. 45. The quantity $\ln(I_w^{o,a} / I_w^a)$ as a function of wave number for the 1.87μ region at 200°C.

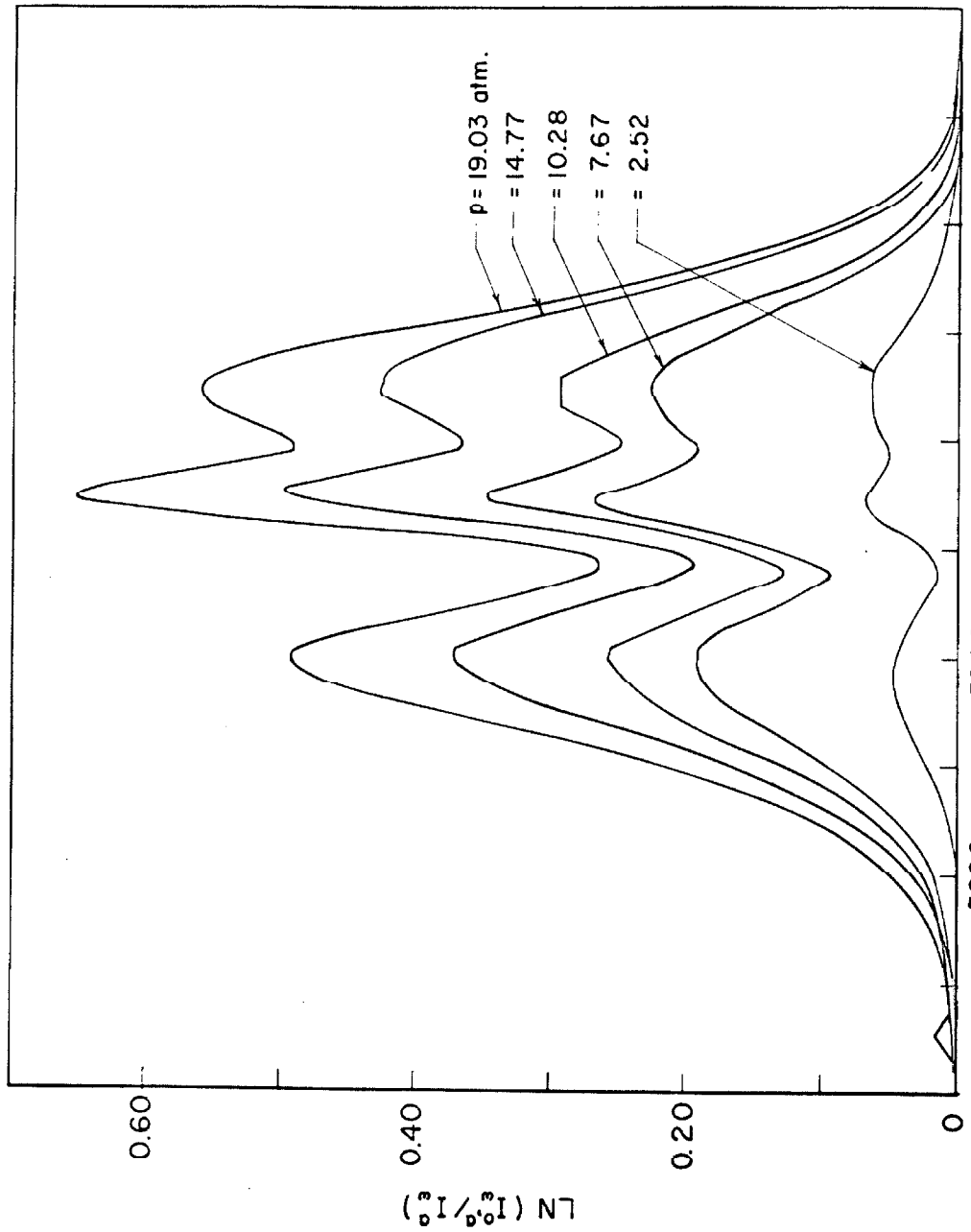

Fig. 46. The quantity $\ell n(I_w^{o,a}/I_w^{a})$ as a function of wave number for the 1.87μ reg on of water vapor at 400°C.

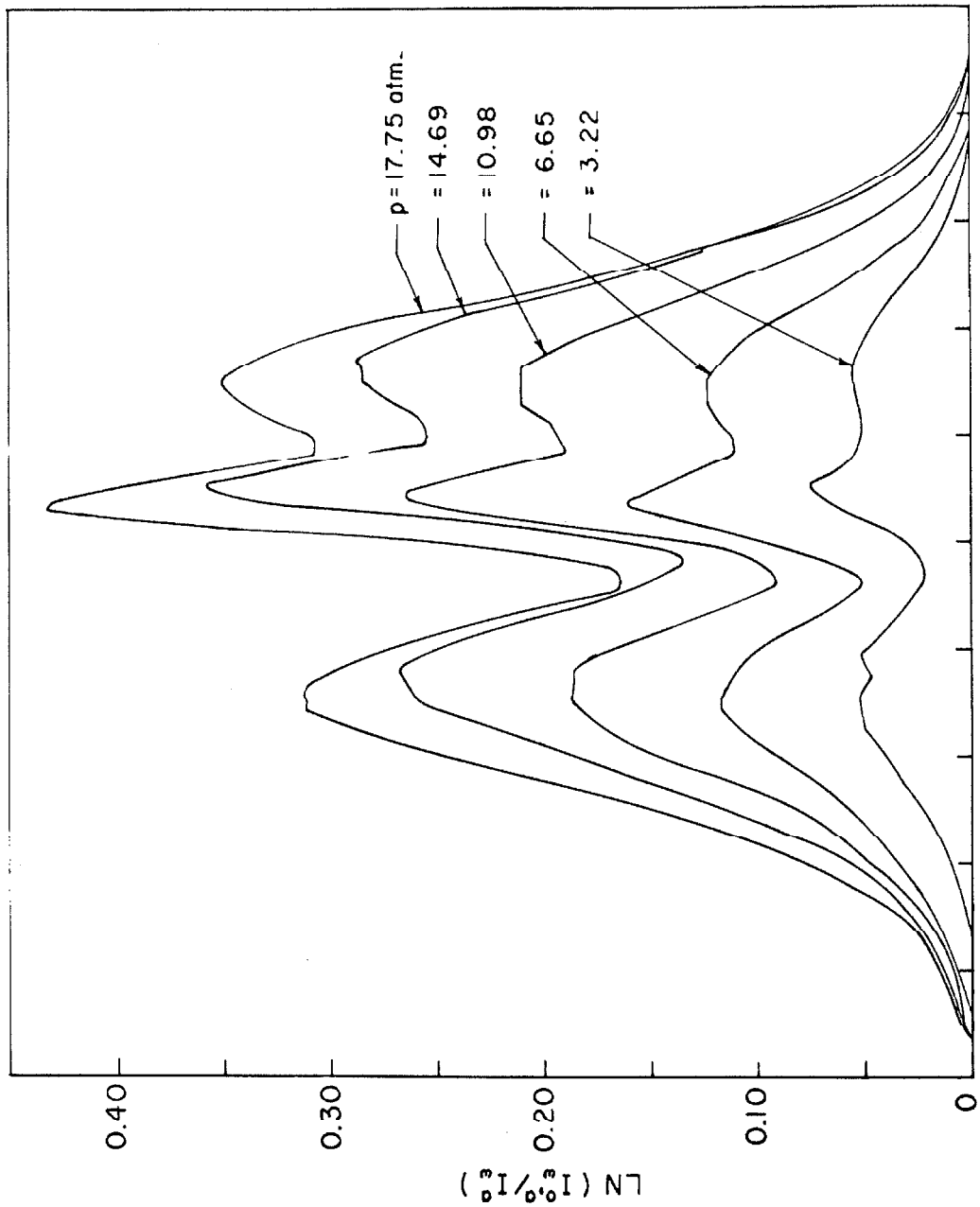

Fig. 47. The quantity $\ell n(I_{\omega}^{o,a}/I_{\omega}^{a})$ as a function of wave number for the 1.87μ region of water vapor at 600°C.

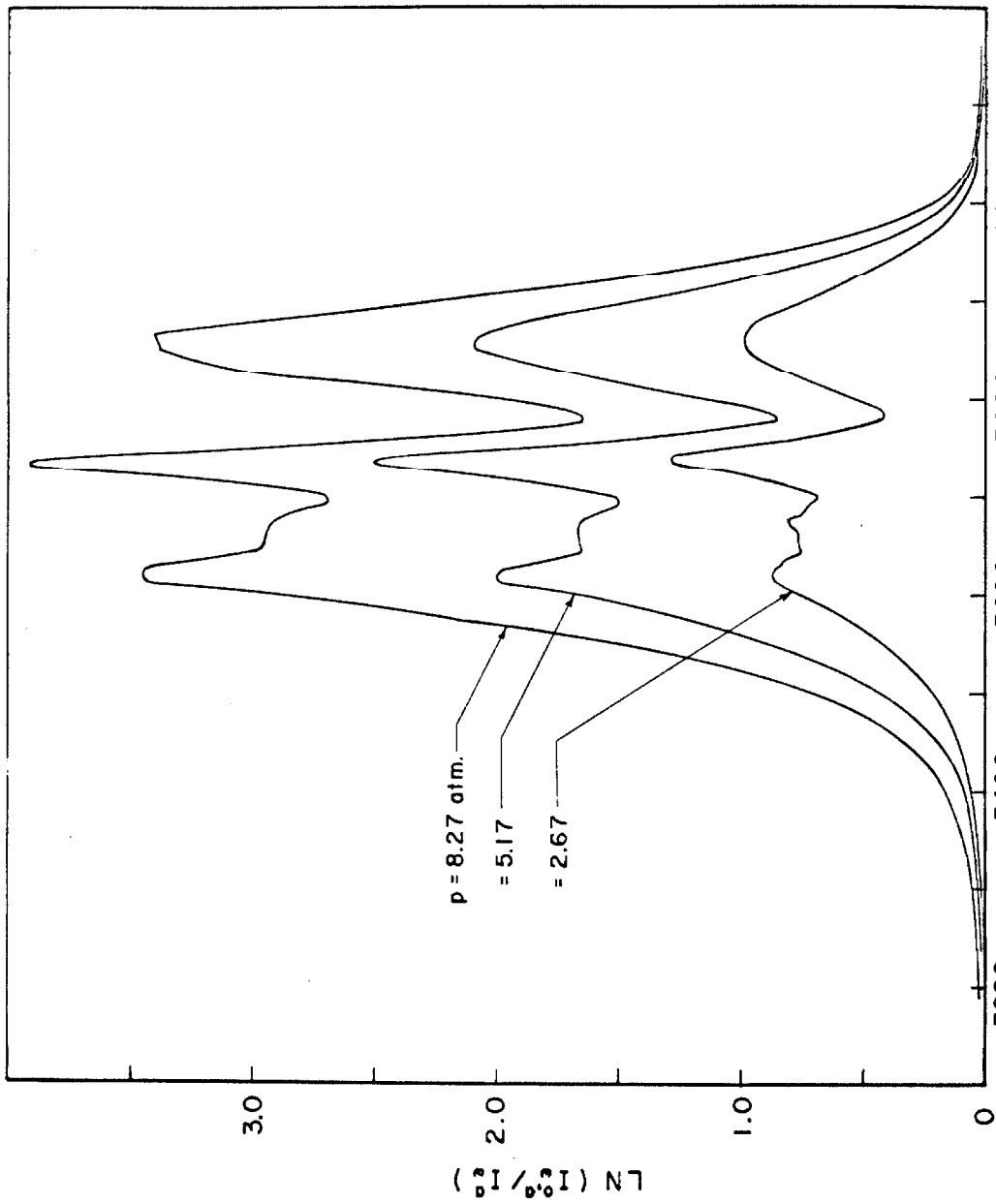

Fig. 48. The quantity $\ell n(I_{\omega}^{o,a}/I_{\omega}^{a})$ as a function of wave number for the 2.7μ region at 200°C.

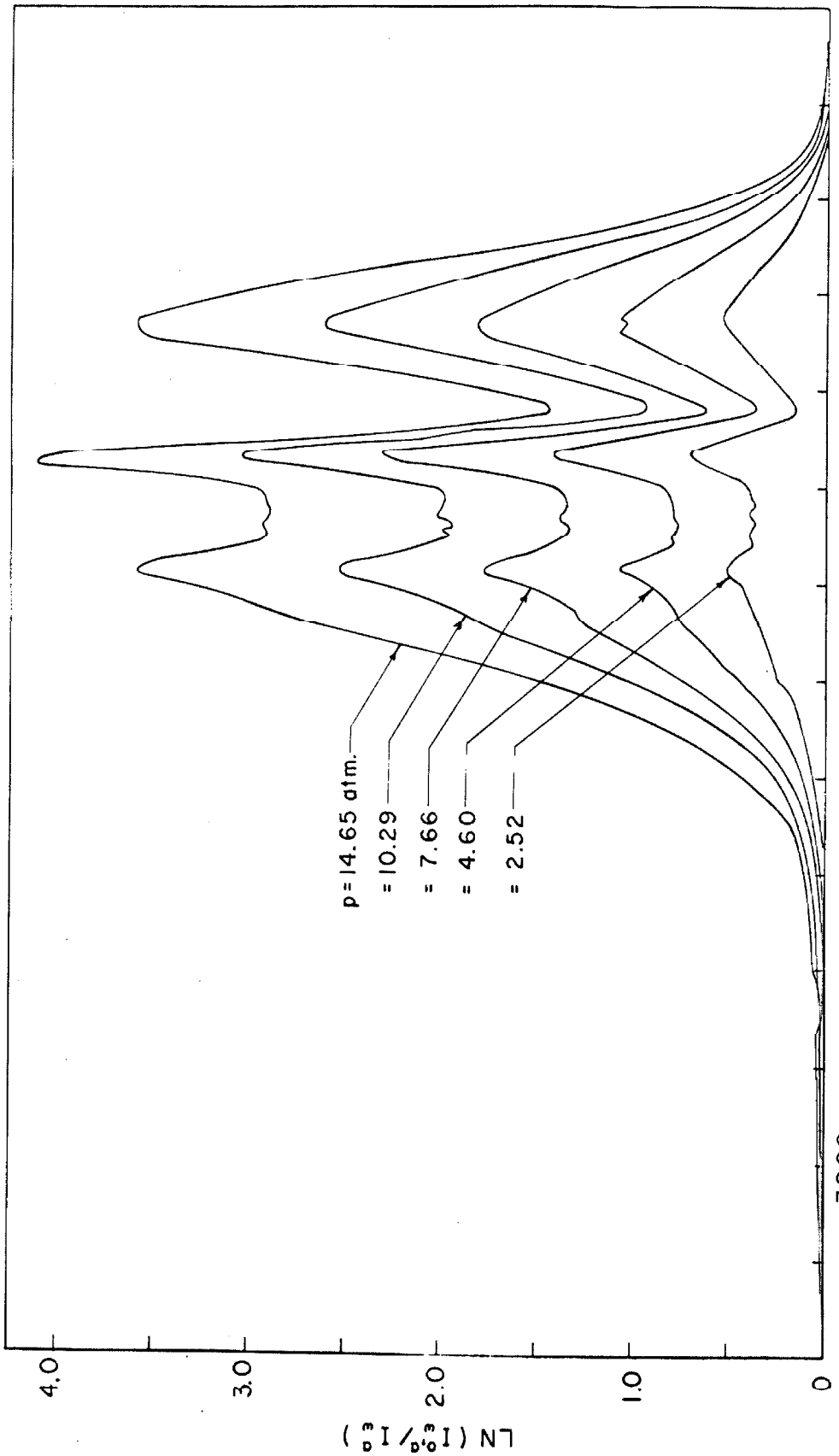

Fig. 49. The quantity $\ln(I_{\omega}^{o,a}/I_{\omega}^{a})$ as a function of wave number for the 2.7μ region of water vapor at 400°C.

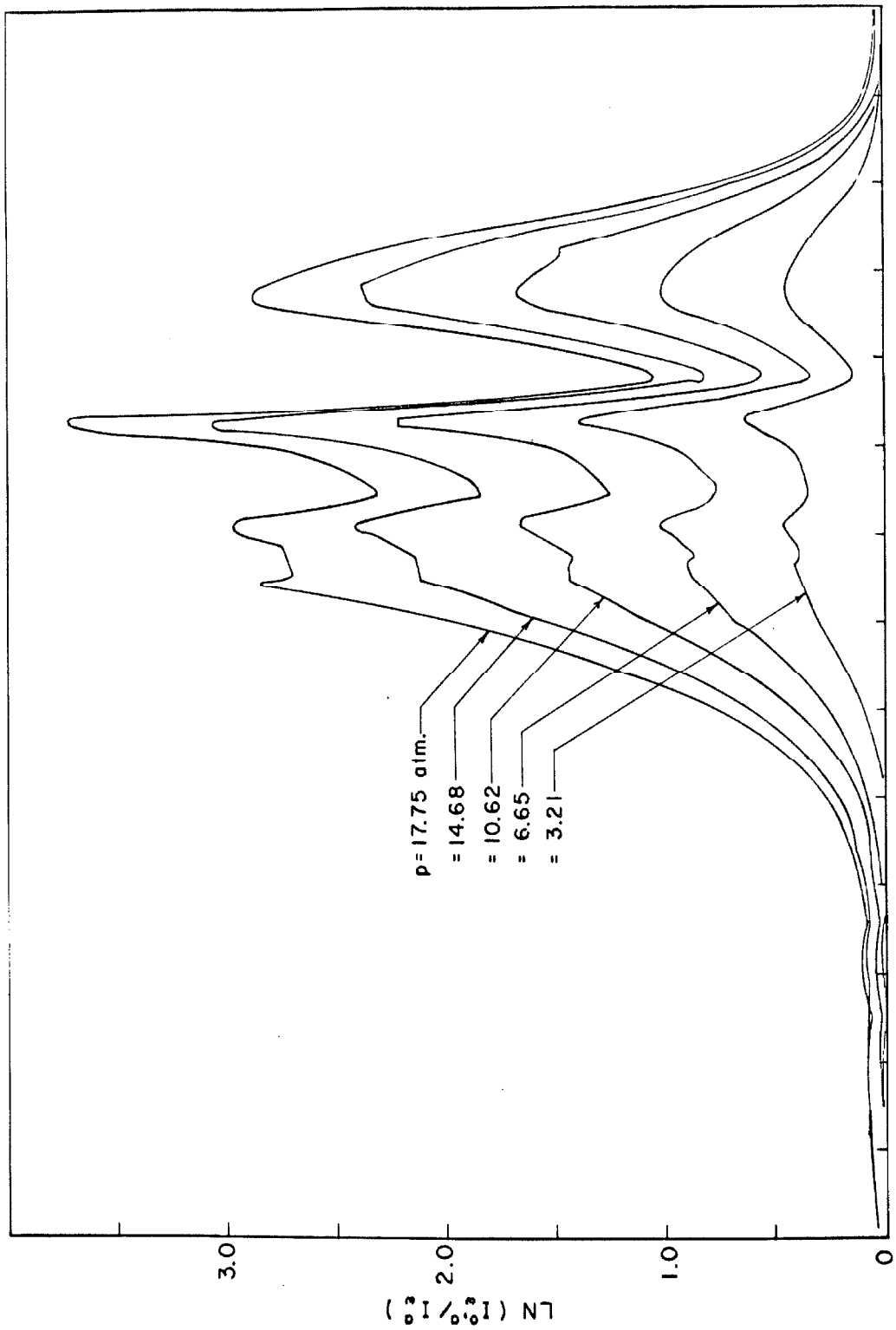

Fig. 50. The quantity $\ln(I_w^{o,a}/I_w^{a})$ as a function of wave number for the 2.7μ region at 600°C.

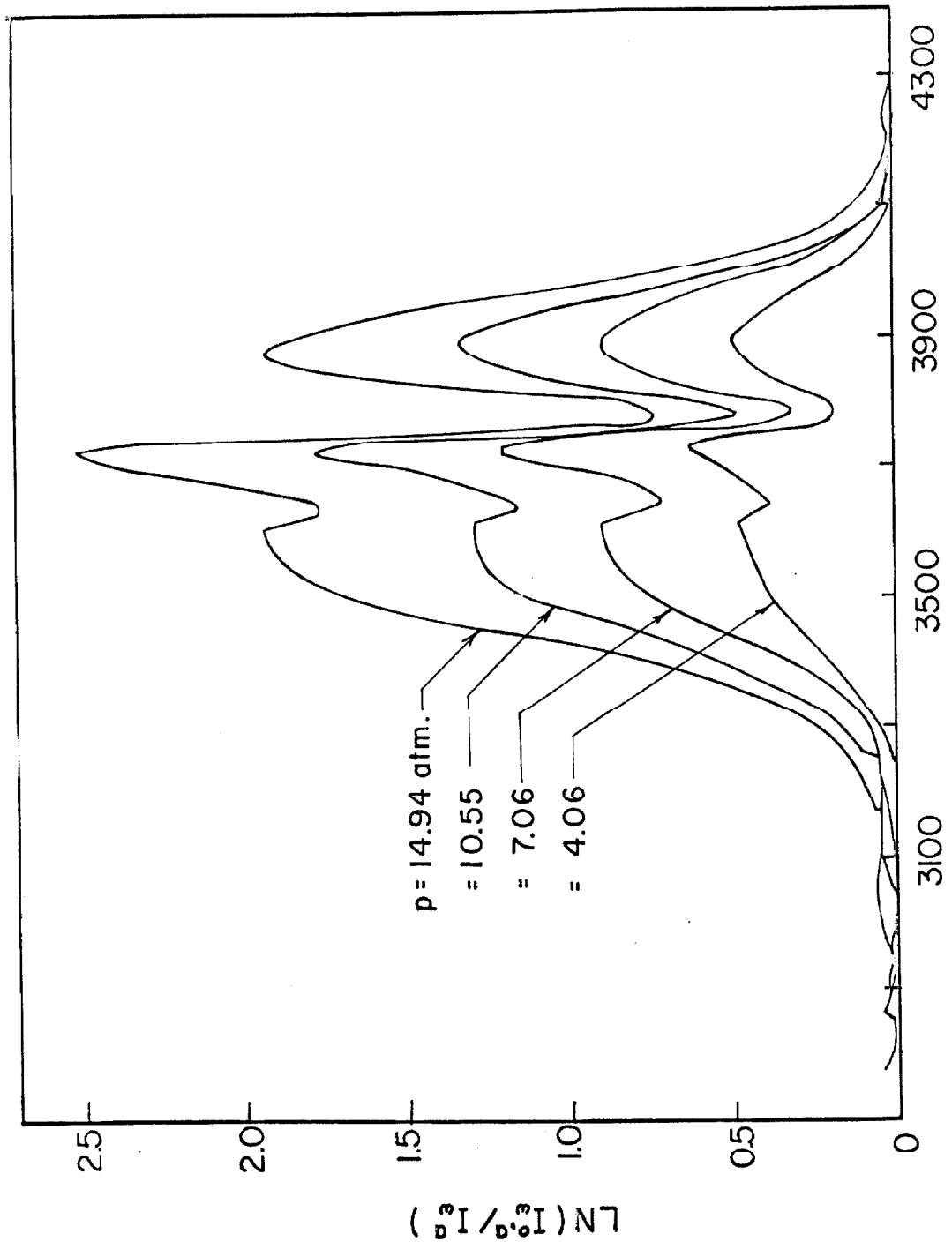

Fig. 51. The quantity $\ell n(I_{(\omega)}^{o,a}/I_{(\omega)}^{a})$ as a function of wave number for the 2.7μ region of water vapor at 1000^{o}K.

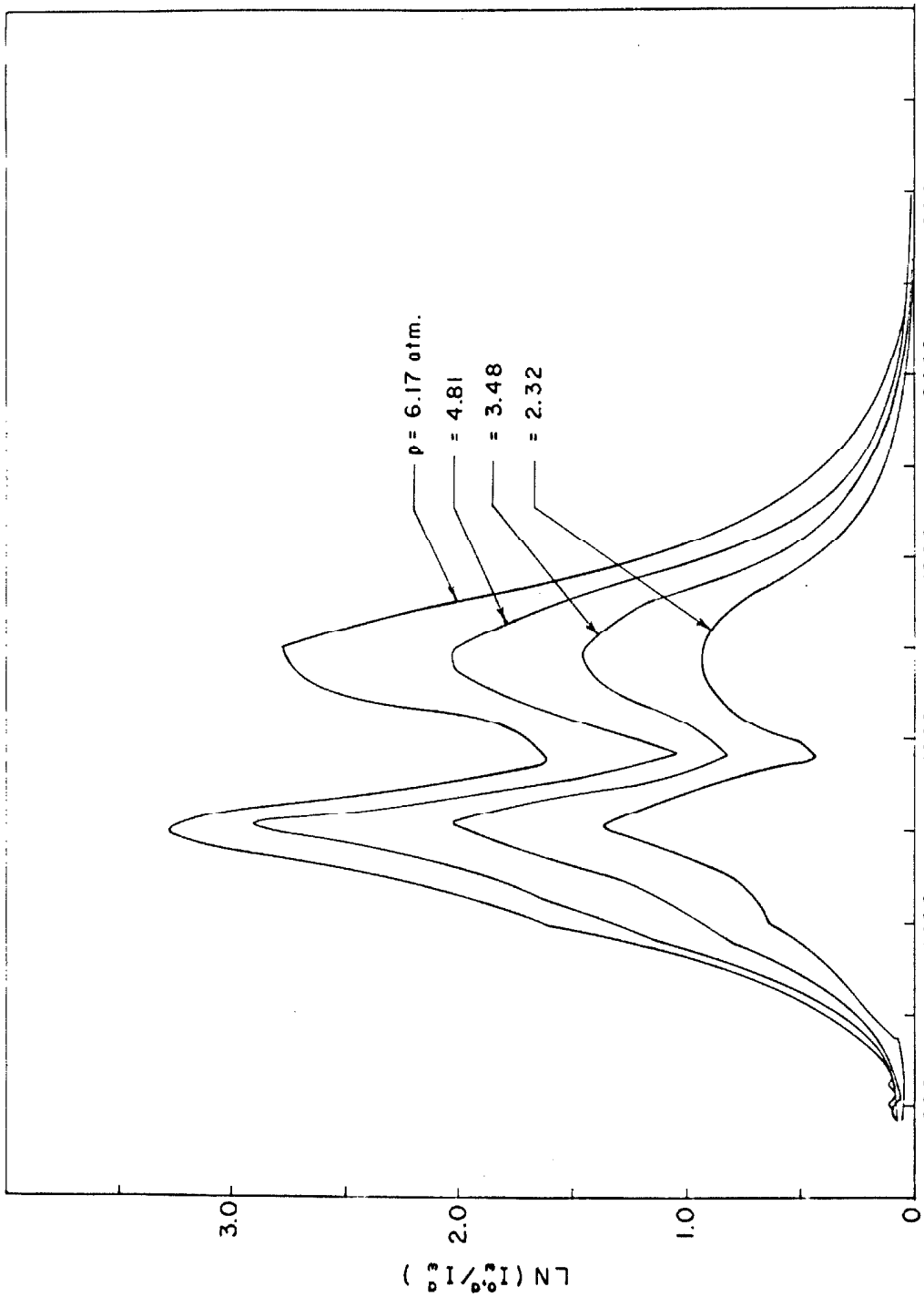

Fig. 52. The quantity $\ell n(I_{(i)}^{o,a}/I_{(i)}^{a})$ as a function of wave number for the 6.3μ region at 200°C.

APPENDIX B

Tables of the Experimental Values of

P_ω as a Function of ω for Water Vapor

1.38μ REGION

ω	P_ω(200°C)	P_ω(400°C)	P_ω(600°C)	ω	P_ω(200°C)	P_ω(400°C)	P_ω(600°C)	ω	P_ω(200°C)	P_ω(400°C)	P_ω(600°C)
6500		2.991×10^{-4}		6790		2.365×10^{-3}	1.956×10^{-3}	7080	1.704×10^{-2}	1.305×10^{-2}	9.919×10^{-3}
6505		3.091		6795		2.491	1.972	7085	1.776	1.317	9.934
6510		3.204		6800	3.207×10^{-4}	2.622	2.009	7090	1.847	1.328	9.949
6515		3.351		6805	3.739	2.752	2.046	7095	1.916	1.340	9.961
6520		3.499		6810	4.331	2.882	2.082	7100	1.952	1.352	9.969
6525		3.646		6815	4.990	3.012	2.117	7105	1.973	1.361	9.981
6530		3.794		6820	5.751	3.143	2.166	7110	2.004	1.370	9.998
6535		3.942		6825	6.512	3.209	2.228	7115	2.038	1.378	1.003×10^{-2}
6540		4.089		6830	7.273	3.230	2.291	7120	2.073	1.385	1.009
6545		4.237		6835	8.034	3.229	2.354	7125	2.108	1.393	1.014
6550		4.384		6840	8.795	3.217	2.417	7130	2.143	1.401	1.016
6555		4.539		6845	8.564	3.212	2.480	7135	2.178	1.408	1.019
6560		4.695		6850	7.955	3.209	2.613	7140	2.210	1.416	1.023
6565		4.851		6855	7.346	3.227	2.764	7145	2.241	1.424	1.025
6570		5.006		6860	6.737	3.250	2.906	7150	2.272	1.431	1.023
6575		5.162		6865	7.977	3.266	3.047	7155	2.303	1.442	1.020
6580		5.351		6870	9.408	3.289	3.162	7160	2.336	1.452	1.011
6585		5.572		6875	1.227×10^{-3}	3.494	3.277	7165	2.373	1.452	1.002
6590		5.809		6880	1.513	3.697	3.392	7170	2.410	1.450	9.975×10^{-3}
6595		6.052		6885	1.800	3.892	3.529	7175	2.447	1.444	9.922
6600		6.446		6890	1.988	4.094	3.754	7180	2.483	1.436	9.870
6605		6.846		6895	1.911	4.321	3.979	7185	2.519	1.429	9.817
6610		7.246		6900	1.834	4.554	4.203	7190	2.555	1.421	9.764
6615		7.646	1.341×10^{-4}	6905	1.757	4.801	4.423	7195	2.590	1.414	9.712
6620		8.046	1.948	6910	1.840	5.047	4.636	7200	2.624	1.407	9.604
6625		8.445	2.555	6915	2.089	5.293	4.846	7205	2.645	1.390	9.489
6630		8.845	3.179	6920	2.339	5.534	5.055	7210	2.664	1.365	9.342
6635		9.245	3.817	6925	2.588	5.770	5.244	7215	2.666	1.349	9.188
6640		9.644	4.191	6930	2.837	6.005	5.420	7220	2.668	1.344	9.036
6645		1.002×10^{-3}	4.488	6935	3.086	6.241	5.598	7225	2.667	1.339	8.885
6650		1.041	4.784	6940	3.356	6.477	5.778	7230	2.661	1.334	8.825
6655		1.079	5.081	6945	3.631	6.712	5.970	7235	2.664	1.327	8.807
6660		1.118	5.378	6950	3.906	6.917	6.167	7240	2.663	1.318	8.762
6665		1.156	5.674	6955	4.187	7.112	6.370	7245	2.661	1.309	8.689
6670		1.195	5.971	6960	4.632	7.299	6.574	7250	2.659	1.303	8.650
6675		1.233	6.306	6965	5.068	7.485	6.779	7255	2.655	1.297	8.697
6680		1.267	6.657	6970	5.461	7.674	6.984	7260	2.648	1.304	8.774
6685		1.304	7.054	6975	5.863	7.863	7.188	7265	2.644	1.315	8.803
6690		1.355	7.454	6980	6.293	8.051	7.391	7270	2.643	1.330	8.861
6695		1.406	7.855	6985	6.723	8.248	7.595	7275	2.642	1.348	8.943
6700		1.457	8.487	6990	7.153	8.534	7.798	7280	2.641	1.369	9.031
6705		1.507	9.463	6995	7.636	8.820	7.999	7285	2.641	1.397	9.205
6710		1.558	1.043×10^{-3}	7000	8.270	9.136	8.200	7290	2.666	1.425	9.440
6715		1.609	1.141	7005	8.898	9.452	8.397	7295	2.694	1.454	9.674
6720		1.660	1.227	7010	9.499	9.775	8.591	7300	2.722	1.482	9.908
6725		1.711	1.309	7015	1.010×10^{-2}	1.009×10^{-2}	8.679	7305	2.751	1.506	1.014×10^{-2}
6730		1.753	1.358	7020	1.070	1.042	8.766	7310	2.778	1.529	1.037
6735		1.779	1.408	7025	1.130	1.075	8.916	7315	2.804	1.552	1.061
6740		1.806	1.458	7030	1.187	1.099	9.068	7320	2.817	1.576	1.077
6745		1.832	1.507	7035	1.245	1.121	9.173	7325	2.803	1.598	1.096
6750		1.858	1.557	7040	1.303	1.146	9.274	7330	2.779	1.621	1.113
6755		1.885	1.615	7045	1.362	1.171	9.375	7335	2.729	1.635	1.131
6760		1.905	1.676	7050	1.408	1.194	9.476	7340	2.680	1.636	1.148
6765		1.926	1.734	7055	1.454	1.217	9.566	7345	2.630	1.636	1.165
6770		1.952	1.792	7060	1.500	1.240	9.653	7350	2.580	1.638	1.163
6775		1.990	1.828	7065	1.546	1.263	9.753	7355	2.529	1.632	1.153
6780		2.115	1.864	7070	1.592	1.281	9.858	7360	2.476	1.594	1.147
6785		2.240	1.900	7075	1.638	1.293	9.904	7365	2.358	1.554	1.145

1.38μ REGION (cont.)

ω	P_ω(200°C)	P_ω(400°C)	P_ω(600°C)
7370	2.239 x10^{-2}	1.494 x10^{-2}	1.146 x10^{-2}
7375	2.136	1.434	1.151
7380	2.034	1.381	1.130
7385	1.932	1.329	1.077
7390	1.830	1.255	1.026
7395	1.698	1.179	9.781 x10^{-3}
7400	1.558	1.103	9.291
7405	1.417	1.027	8.772
7410	1.277	9.520 x10^{-3}	8.253
7415	1.137	8.776	7.734
7420	9.971 x10^{-3}	7.976	7.211
7425	8.947	7.142	6.645
7430	8.225	6.308	6.078
7435	7.363	5.474	5.503
7440	6.349	4.778	4.928
7445	5.557	4.276	4.353
7450	5.098	3.808	3.778
7455	4.663	3.416	3.478
7460	4.283	3.023	3.240
7465	3.903	2.631	2.969
7470	3.523	2.228	2.686
7475	3.034	1.751	2.357
7480	2.352	1.280	2.002
7485	1.718	1.031	1.650
7490	1.589	7.820 x10^{-4}	1.301
7495	1.460	6.321	1.047
7500	1.332	4.990	9.940 x10^{-4}
7505	1.203	3.960	9.404
7510	1.074	3.326	8.868
7515	9.462	2.691	8.332
7520	8.176	2.057	7.796
7525	6.815	1.422	7.260
7530	5.455		
7535	5.378		

1.87μ REGION

ω	P_ω(200°C)	P_ω(400°C)	P_ω(600°C)
4850			1.251 x10^{-4}
4855			1.903
4860			2.555
4865			3.147
4870			3.583
4875			4.215
4880			4.902
4885			5.589
4890			6.208
4895			6.705
4900			7.202
4905			7.832
4910			8.070
4915			8.165
4920		2.251 x10^{-4}	8.222
4925		2.960	8.030
4930		3.624	7.837
4935		4.292	1.241 x10^{-3}
4940		5.062	1.342
4945		6.252	1.462
4950		7.243	1.578
4955		8.106	1.693
4960		8.968	1.807
4965		9.617	1.923
4970		1.014 x10^{-3}	2.116
4975		1.066	2.370
4980		1.112	2.628
4985		1.236	2.931
4990		1.486	3.196
4995		1.736	3.455
5000		1.987	3.727
5005		2.237	4.013
5010		2.476	4.300
5015		2.847	4.586
5020		3.042	4.881
5025		3.274	5.268
5030		3.586	5.626
5035		3.905	5.948
5040		4.221	6.269
5045	5.666 x10^{-4}	4.537	6.591
5050	7.450	4.899	6.964
5055	9.545	5.325	7.411
5060	1.378 x10^{-3}	5.747	7.866
5065	1.893	6.221	8.337
5070	2.408	6.679	8.805
5075	2.923	7.233	9.096
5080	3.948	7.743	9.515
5085	4.257	8.254	9.970
5090	5.052	8.778	1.043 x10^{-2}
5095	5.846	9.375	1.090
5100	6.640	9.968	1.137
5105	7.741	1.060 x10^{-2}	1.181
5110	8.951	1.125	1.218
5115	1.024 x10^{-2}	1.884	1.258
5120	1.153	1.247	1.297
5125	1.273	1.312	1.338
5130	1.415	1.398	1.380
5135	1.554 x10^{-2}	1.488 x10^{-2}	1.421 x10^{-2}
5140	1.690	1.565	1.459
5145	1.821	1.641	1.473
5150	1.967	1.718	1.487
5155	2.120	1.794	1.496
5160	2.273	1.874	1.502
5165	2.426	1.953	1.514
5170	2.590	2.002	1.511
5175	2.747	2.044	1.501
5180	2.912	2.088	1.491
5185	3.078	2.135	1.477
5190	3.249	2.162	1.458
5195	3.378	2.171	1.417
5200	3.479	2.179	1.382
5205	3.573	2.176	1.342
5210	3.578	2.135	1.286
5215	3.574	2.094	1.229
5220	3.508	2.054	1.173
5225	3.416	1.982	1.120
5230	3.340	1.907	1.072
5235	3.244	1.832	1.023
5240	3.095	1.756	9.742 x10^{-3}
5245	2.943	1.680	9.276
5250	2.790	1.587	8.967
5255	2.637	1.483	8.658
5260	2.571	1.379	8.469
5265	2.525	1.275	8.408
5270	2.479	1.261	8.229
5275	2.443	1.254	8.171
5280	2.388	1.224	8.497
5285	2.453	1.212	8.939
5290	2.620	1.201	9.521
5295	2.812	1.254	1.025 x10^{-2}
5300	3.035	1.316	1.110
5305	3.212	1.435	1.236
5310	3.335	1.587	1.356
5315	3.642	1.824	1.483
5320	3.991	2.050	1.629
5325	4.370	2.230	1.765
5330	4.494	2.412	1.870
5335	4.567	2.546	1.955
5340	4.686	2.672	1.966
5345	4.677	2.809	1.962
5350	4.489	2.832	1.947
5355	4.304	2.773	1.885
5360	4.138	2.700	1.837
5365	4.055	2.635	1.777
5370	3.992	2.545	1.718
5375	3.948	2.438	1.657
5380	3.909	2.339	1.587
5385	3.824	2.250	1.517
5390	3.872	2.148	1.482
5395	3.944	2.149	1.455
5400	4.017	2.159	1.464
5405	4.075	2.167	1.492
5410	4.151	2.203	1.515
5415	4.222	2.242	1.530

1.87μ REGION (cont.)

ω	P_ω(200°C)	P_ω(400°C)	P_ω(600°C)
5420	4.276×10^{-2}	2.290×10^{-2}	1.554×10^{-2}
5425	4.247	2.349	1.585
5430	4.198	2.407	1.612
5435	4.073	2.430	1.626
5440	3.962	2.447	1.642
5445	3.854	2.449	1.655
5450	3.743	2.424	1.658
5455	3.663	2.399	1.654
5460	3.512	2.380	1.655
5465	3.353	2.352	1.656
5470	3.194	2.328	1.636
5475	3.030	2.264	1.615
5480	2.866	2.186	1.582
5485	2.687	2.113	1.548
5490	2.506	2.041	1.516
5495	2.325	1.973	1.484
5500	2.138	1.891	1.426
5505	1.951	1.807	1.369
5510	1.781	1.713	1.312
5515	1.626	1.618	1.254
5520	1.473	1.519	1.194
5525	1.321	1.421	1.141
5530	1.169	1.328	1.088
5535	1.066	1.234	1.034
5540	9.710×10^{-3}	1.138	9.828×10^{-3}
5545	8.732	1.046	9.381
5550	7.753	9.711×10^{-3}	8.947
5555	6.775	9.127	8.516
5560	5.896	8.536	8.083
5565	5.420	7.917	7.645
5570	4.961	7.330	7.207
5575	4.502	6.711	6.756
5580	4.042	6.083	6.305
5585	3.583	5.555	5.855
5590	3.296	5.057	5.478
5595	3.103	4.583	5.074
5600	2.886	4.135	4.655
5605	2.669	3.668	4.234
5610	2.451	3.189	3.799
5615	2.234	2.709	3.392
5620	1.991	2.461	3.142
5625	1.754	2.258	2.897
5630	1.516	2.061	2.652
5635	1.279	1.862	2.407
5640	1.042	1.663	2.204
5645	8.957×10^{-4}	1.456	2.017
5650	8.902	1.254	1.817
5655	8.848	1.086	1.602
5660	8.793	8.962×10^{-4}	1.403
5665	8.738	8.307	1.253
5670	8.683	7.653	1.104
5675	8.626	6.998	1.042
5680		6.344	8.580×10^{-4}
5685		5.689	7.880
5690		5.037	7.139
5695		4.392	6.358
5700		3.746	5.578
5705		3.101	7.546

2.7 & 3.2μ REGION

ω	P_ω(200°C)	P_ω(400°C)	P_ω(600°C)	P_ω(1000°K)
2900				
2905				
2910				
2915			4.908×10^{-3}	
2920				
2925				
2930				
2935				2.513×10^{-4}
2940				1.316×10^{-3}
2945			4.840	1.818
2950				2.213
2955				1.932
2960		9.679×10^{-4}		1.652
2965				1.371
2970				1.090
2975				7.837×10^{-4}
2980			4.347	9.114
2985				1.174×10^{-3}
2990				1.437
2995				1.770
3000		8.660		2.130
3005				2.302
3010	6.632×10^{-4}			2.371
3015				2.441
3020			4.114	2.631
3025				2.871
3030				3.074
3035				3.221
3040		2.268		3.367
3045				3.513
3050				3.660
3055			3.558	3.802
3060				3.827
3065				3.851
3070				3.876
3075				3.901
3080		4.321		3.925
3085				3.945
3090			5.130	3.963
3095				3.985
3100	2.273×10^{-3}			4.005
3105				4.024
3110				4.085
3115				4.151
3120		1.663×10^{-3}		4.218
3125			5.708	4.284
3130				4.351
3135				4.677
3140				4.355
3145	4.057×10^{-4}			4.033
3150				3.710
3155				3.378
3160		7.873×10^{-4}	5.195	4.570
3165				4.294
3170				4.019
3175				3.912
3180			6.131	3.886
3185				

ω	P_ω(200°C)	P_ω(400°C)	P_ω(600°C)	P_ω(1000°K)
3190	1.265×10^{-3}			3.800×10^{-3}
3195				3.833
3200		2.534×10^{-3}	7.300×10^{-3}	3.807
3205				7.409
3210				8.795
3215				7.541
3220			8.378	7.073
3225				7.721
3230				8.451
3235	2.872			8.219
3240		4.069	9.797	8.392
3245				8.926
3250				9.245
3255				9.072
3260			1.042×10^{-2}	9.624
3265				1.081×10^{-2}
3270				1.201
3275				1.263
3280	3.733	7.120	1.242	1.244
3285				1.298
3290				1.414
3295				1.421
3300			1.438	1.585
3305				1.808
3310				2.033
3315				2.201
3320		9.189	1.701	2.365
3325	6.493			2.393
3330				2.393
3335				2.393
3340			2.117	2.393
3345		1.232×10^{-2}		2.408
3350	9.195			2.601
3355				2.857
3360			2.498	2.979
3365				3.101
3370		1.568		3.251
3375	1.269×10^{-2}			3.386
3380			3.062	3.506
3385				3.647
3390				3.817
3395		2.173		4.018
3400	1.612×10^{-2}		3.690	4.245
3405			3.857	4.472
3410			4.057	4.712
3415			4.252	4.891
3420		3.040	4.496	5.049
3425	2.414		4.740	5.307
3430			4.998	5.601
3435			5.281	5.928
3440			5.572	6.302
3445		4.555	5.869	6.607
3450	3.731	4.878	6.176	6.868
3455		5.198	6.491	7.193
3460		5.479	6.759	7.443
3465		5.686	7.017	7.693
3470		5.999	7.55[illegible]	7.84[illegible]
3475	4.960	6.348	7.5[illegible]	8.075

2.7 & 3.2μ REGION (cont.)

ω	P_ω(200°C)	P_ω(400°C)	P_ω(600°C)	P_ω(1000°K)	ω	P_ω(200°C)	P_ω(400°C)	P_ω(600°C)	P_ω(1000°K)	ω	P_ω(200°C)	P_ω(400°C)	P_ω(600°C)	P_ω(1000°K)
3480		6.721×10^{-2}	7.902×10^{-2}	9.487×10^{-2}	3765	1.975×10^{-1}	1.015×10^{-1}	6.196×10^{-2}	5.033×10^{-2}	4050	2.542×10^{-3}	7.352×10^{-3}	1.205×10^{-2}	1.595×10^{-2}
3485		7.199	8.248	8.941	3770	1.859	9.087×10^{-2}	5.70(	4.665	4055	2.08[illegible]	6.733	1.049	1.435
3490		7.696	8.593	9.378	3775	1.829	8.883	5.280	4.314	4060	1.52[illegible]	6.211	9.116×10^{-3}	1.265
3495		8.235	8.969	9.585	3780	1.788	8.540	5.087	4.180	4065	9.565×10^{-4}	5.433	8.207	1.095
3500	7.765×10^{-2}	8.873	9.332	9.781	3785	1.832	8.576	5.087	4.189	4070	6.555	4.578	7.358	1.004
3505		9.475	9.735	1.087×10^{-1}	3790	1.895	8.927	5.287	4.193	4075	4.844	3.871	6.548	9.669×10^{-3}
3510		1.003×10^{-1}	1.014×10^{-1}	1.090	3795	2.020	9.552	5.576	4.462	4080	3.133	3.442	5.707	8.978
3515		1.049	1.049	1.092	3800	2.169	1.020×10^{-1}	5.998	4.786	4085	1.422	2.984	5.174	8.079
3520		1.101	1.075	1.093	3805	2.356	1.100	6.462	5.151	4090		2.557	4.768	7.180
3525	1.164×10^{-1}	1.158	1.102	1.093	3810	2.556	1.205	6.980	5.611	4095		2.141	4.360	6.583
3530	1.241	1.217	1.141	1.093	3815	2.794	1.307	7.456	6.112	4100		1.742	3.970	6.158
3535	1.314	1.277	1.237	1.090	3820	3.004	1.392	7.943	6.620	4105		1.524	3.563	5.623
3540	1.435	1.338	1.308	1.087	3825	3.100	1.476	8.486	7.224	4110		1.306	3.228	5.003
3545	1.555	1.412	1.350	1.087	3830	3.224	1.554	9.012	7.768	4115		1.102	3.041	4.357
3550	1.694	1.471	1.309	1.087	3835	3.356	1.640	9.677	8.265	4120		9.521×10^{-4}	2.849	3.769
3555	1.808	1.524	1.289	1.087	3840	3.462	1.761	1.040×10^{-1}	8.917	4125		8.016	2.727	3.655
3560	1.946	1.618	1.289	1.087	3845	3.565	1.883	1.120	9.800	4130		7.054	2.591	3.541
3565	2.107	1.670	1.289	1.087	3850	3.538	1.997	1.198	1.044×10^{-1}	4135		6.527	2.445	3.427
3570	2.203	1.691	1.293	1.087	3855	3.528	2.089	1.271	1.096	4140		5.958	2.352	3.313
3575	2.352	1.724	1.306	1.091	3860	3.530	2.097	1.329	1.103	4145		5.258	2.289	3.199
3580	2.517	1.762	1.305	1.092	3865	3.540	2.110	1.361	1.104	4150		4.573	2.217	3.084
3585	2.656	1.809	1.316	1.093	3870	3.317	2.119	1.372	1.106	4155		3.883	2.122	2.970
3590	2.828	1.848	1.338	1.093	3875	3.197	2.085	1.371	1.107	4160		3.141	2.012	2.861
3595	3.032	1.908	1.366	1.094	3880	2.967	2.022	1.367	1.106	4165		2.397	1.848	2.736
3600	3.243	1.993	1.397	1.094	3885	2.758	1.949	1.360	1.089	4170		1.741	1.685	2.603
3605	3.465	2.043	1.414	1.095	3890	2.519	1.874	1.330	1.072	4175		1.228	1.563	2.493
3610	3.723	2.075	1.411	1.095	3895	2.309	1.790	1.295	1.054	4180		7.164×10^{-5}	1.541	2.436
3615	3.781	2.066	1.398	1.074	3900	2.109	1.711	1.276	1.032	4185		5.356	1.518	2.379
3620	3.785	2.049	1.355	1.045	3905	1.926	1.644	1.260	1.017	4190		4.269	1.492	2.322
3625	3.762	2.013	1.316	1.033	3910	1.817	1.574	1.233	1.005	4195		3.203	1.490	2.266
3630	3.624	1.918	1.248	1.028	3915	1.696	1.504	1.205	9.928×10^{-2}	4200				2.209
3635	3.538	1.842	1.173	1.048	3920	1.575	1.434	1.168	1.001×10^{-1}	4205				2.152
3640	3.384	1.771	1.118	1.066	3925	1.446	1.349	1.125	1.008	4210				2.085
3645	3.269	1.731	1.103	1.071	3930	1.307	1.263	1.077	9.785×10^{-2}	4215				1.971
3650	3.247	1.709	1.104	1.070	3935	1.168	1.171	1.021	9.095	4220				1.867
3655	3.225	1.715	1.116	1.070	3940	1.029	1.076	9.627×10^{-2}	8.587	4225				1.763
3660	3.203	1.718	1.128	1.090	3945	8.900×10^{-2}	9.828×10^{-2}	9.081	8.151	4230				1.733
3665	3.180	1.719	1.155	1.138	3950	7.753	8.878	8.551	7.794	4235				1.735
3670	3.141	1.708	1.180	1.190	3955	6.682	8.047	8.017	7.483	4240				1.738
3675	3.107	1.706	1.189	1.242	3960	5.808	7.340	7.481	7.121	4245				1.740
3680	3.089	1.715	1.205	1.277	3965	4.985	6.641	6.949	6.714	4250				1.742
3685	3.033	1.715	1.229	1.298	3970	4.246	5.989	6.428	6.309	4255				1.745
3690	2.968	1.713	1.253	1.316	3975	3.712	5.360	5.971	5.879	4260				1.747
3695	2.931	1.713	1.278	1.328	3980	3.257	4.865	5.515	5.474	4265				1.749
3700	2.957	1.747	1.334	1.379	3985	2.955	4.368	5.054	5.149	4270				1.741
3705	2.969	1.815	1.403	1.434	3990	2.500	3.883	4.586	4.813	4275				1.719
3710	3.094	1.930	1.513	1.453	3995	2.068	3.393	4.137	4.468	4280				1.697
3715	3.390	2.105	1.642	1.426	4000	1.634	2.992	3.704	4.122	4285				1.675
3720	3.656	2.225	1.747	1.414	4005	1.445	2.607	3.336	3.818	4290				1.653
3725	3.895	2.329	1.736	1.414	4010	1.177	2.281	3.029	3.511	4295				1.630
3730	4.052	2.275	1.734	1.402	4015	9.348×10^{-3}	1.987	2.719	3.181	4300				1.608
3735	3.875	2.184	1.552	1.337	4020	7.125	1.710	2.437	2.846	4305				1.586
3740	3.631	1.971	1.338	1.304	4025	5.722	1.474	2.162	2.588	4310				1.565
3745	3.200	1.730	1.133	1.088	4030	4.905	1.259	1.928	2.409	4315				1.541
3750	2.819	1.464	9.524×10^{-2}	8.993×10^{-2}	4035	4.089	1.098	1.693	2.209	4320				1.518
3755	2.491	1.284	8.198	7.990	4040	3.272	9.286×10^{-3}	1.518	1.976	4325				1.469
3760	2.252	1.125	7.108	6.579	4045	2.551	8.309	1.356	1.747	4330				1.383

2.7 & 3.2μ REGION (cont.)

ω	P_ω(200°C)	P_ω(400°C)	P_ω(600°C)	P_ω(1000°K)
4335				1.285×10^{-3}
4340				1.188
4345				1.088
4350				9.817×10^{-4}
4355				8.754
4360				7.692
4365				6.629
4370				5.567
4375				4.505
4380				3.442
4385				2.589
4390				1.918
4395				1.251

6.3μ REGION

ω	P_ω(200°C)	ω	P_ω(200°C)	ω	P_ω(200°C)	ω	P_ω(200°C)	ω	P_ω(200°C)	ω	P_ω(200°C)
1190	2.417×10^{-3}	1480	5.999×10^{-1}	1770	2.155×10^{-1}	2060	7.667×10^{-3}	2350	1.641×10^{-3}		
1195	3.692	1485	4.113	1775	1.982	2065	7.434	2355	1.668		
1200	5.788	1490	4.095	1780	1.824	2070	7.201	2360	1.696		
1205	7.117	1495	4.078	1785	1.724	2075	6.968	2365	1.724		
1210	8.435	1500	4.038	1790	1.623	2080	6.736	2370	1.751		
1215	8.921	1505	4.012	1795	1.541	2085	6.201	2375	1.779		
1220	8.731	1510	3.949	1800	1.457	2090	5.766	2380	1.806		
1225	6.798	1515	3.771	1805	1.373	2095	5.332	2385	1.834		
1230	3.560	1520	3.575	1810	1.295	2100	4.836	2390	1.862		
1235	2.581	1525	3.314	1815	1.219	2105	4.521	2395	1.889		
1240	4.478	1530	3.105	1820	1.178	2110	4.334	2400	1.917		
1245	8.281	1535	2.968	1825	1.145	2115	4.088	2405	1.944		
1250	1.435×10^{-2}	1540	2.817	1830	1.096	2120	3.872	2410	1.928		
1255	1.984	1545	2.643	1835	1.036	2125	3.656	2415	1.879		
1260	2.347	1550	2.502	1840	9.632×10^{-2}	2130	3.439	2420	1.827		
1265	2.519	1555	2.369	1845	8.860	2135	3.179	2425	1.774		
1270	2.862	1560	2.330	1850	8.139	2140	2.620	2430	1.721		
1275	3.145	1565	2.317	1855	7.524	2145	2.125	2435	1.668		
1280	3.432	1570	2.235	1860	7.148	2150	1.631	2440	1.617		
1285	3.707	1575	2.165	1865	6.836	2155	9.111×10^{-4}	2445	1.570		
1290	3.882	1580	2.095	1870	6.481	2160	1.916	2450	1.522		
1295	4.121	1585	1.782	1875	6.069	2165		2455	1.420		
1300	4.433	1590	2.268	1880	5.847	2170		2460	1.303		
1305	4.860	1595	2.311	1885	5.629	2175		2465	1.187		
1310	5.373	1600	2.335	1890	5.391	2180		2470	1.071		
1315	5.955	1605	2.306	1895	5.222	2185		2475	9.547×10^{-4}		
1320	6.547	1610	2.276	1900	5.005	2190	1.213×10^{-4}	2480	8.383		
1325	7.259	1615	2.307	1905	4.788	2195	3.454	2485	7.219		
1330	8.116	1620	2.469	1910	4.565	2200	5.695	2490	6.055		
1335	8.679	1625	2.610	1915	4.328	2205	7.797	2495	4.891		
1340	9.208	1630	2.743	1920	4.090	2210	8.549	2500	3.728		
1345	9.955	1635	2.902	1925	3.918	2215	8.592				
1350	1.072×10^{-1}	1640	3.083	1930	3.766	2220	8.635				
1355	1.133	1645	3.310	1935	3.615	2225	8.678				
1360	1.209	1650	3.341	1940	3.467	2230	8.642				
1365	1.285	1655	3.376	1945	3.286	2235	8.388				
1370	1.331	1660	3.459	1950	3.074	2240	8.398				
1375	1.434	1665	3.663	1955	2.862	2245	9.219				
1380	1.564	1670	3.676	1960	2.631	2250	1.004×10^{-3}				
1385	1.728	1675	3.684	1965	2.396	2255	1.086				
1390	1.891	1680	3.692	1970	2.181	2260	1.168				
1395	1.990	1685	3.702	1975	1.963	2265	1.250				
1400	2.113	1690	3.711	1980	1.766	2270	1.332				
1405	2.289	1695	3.740	1985	1.592	2275	1.414				
1410	2.415	1700	3.730	1990	1.439	2280	1.496				
1415	2.492	1705	3.687	1995	1.375	2285	1.578				
1420	2.563	1710	3.312	2000	1.318	2290	1.660				
1425	2.627	1715	3.170	2005	1.254	2295	1.742				
1430	2.636	1720	3.030	2010	1.187	2300	1.683				
1435	2.664	1725	2.994	2015	1.116	2305	1.630				
1440	2.734	1730	2.941	2020	1.041	2310	1.640				
1445	2.828	1735	2.874	2025	9.657×10^{-3}	2315	1.650				
1450	3.012	1740	2.803	2030	8.904	2320	1.660				
1455	3.188	1745	2.733	2035	8.118	2325	1.669				
1460	3.394	1750	2.619	2040	8.030	2330	1.679				
1465	3.584	1755	2.487	2045	8.102	2335	1.554				
1470	3.737	1760	2.359	2050	8.075	2340	1.528				
1475	3.881	1765	2.278	2055	7.900	2345	1.513				

APPENDIX C

Tables of the Experimental Values of

k_{ω}^{o} as a Function of ω for Liquid Water

ω	K_ω(27 °C)	K_ω(89 °C)	K_ω(159 °C)	K_ω(209°C)	ω	K_ω(27°C)	K_ω(89 °C)	K_ω(159 °C)	K_ω(209°C)	ω	K_ω(27°C)	K_ω(89 °C)	K_ω(159 °C)	K_ω(209 °C)
2180				218.2	2750	182.4	151.1	120.7	98.70	4040	86.22	86.89	102.0	102.2
2190				214.9	2760	194.0	160.6	127.6	104.2	4050	79.34	84.13	94.50	96.19
2200			226.5	198.3	2770	210.6	174.2	134.9	109.5	4060	74.47	81.36	87.14	92.75
2210			207.4	195.1	2780	227.3	186.1	142.9	115.0	4070	71.31	77.53	82.95	89.39
2220			202.5	197.2	2790	244.2	202.4	151.8	120.8	4080	68.50	73.84	79.26	85.35
2230			203.5	182.9	2800	262.9	219.4	161.2	126.3	4090	65.95	70.60	76.58	81.16
2240			183.7	168.4	2810	281.6	236.3	171.3	136.7	4100	63.39	68.26	74.09	76.99
2250		241.0	171.6	154.1	2820	301.3	253.4	182.9	143.8	4110	61.46	66.13	71.03	73.79
2260		229.6	167.3	152.0	2830	330.9	270.4	196.6	156.7	4120	59.58	64.36	67.54	70.60
2270		211.3	162.5	147.4	2840	360.4	287.5	218.4	167.6	4130	57.68	63.04	64.20	67.62
2280		204.6	158.9	138.0	2850	389.9	308.0	233.8	178.6	4140	55.69	61.57	61.82	65.06
2290		197.3	156.1	128.1	2860		330.9	250.6	199.5	4150	53.69	59.20	59.65	62.47
2300	261.6	198.1	146.8	123.4	2870		353.9	267.2	214.2	4160	51.76	56.45	57.35	59.87
2310	245.4	188.2	139.2	124.1	2880		380.1	284.1	229.0	4170	49.91	53.72	54.94	57.54
2320	237.0	175.4	133.6	121.4	2890		416.6	307.4	243.7	4180	48.05	51.43	52.62	54.82
2330	228.5	173.0	123.4	114.9	2900		453.6	343.9	261.0	4190	46.44	49.23	50.70	52.95
2340	221.4	164.4	119.9	105.2	2910			357.1	280.6	4200	44.90	47.38	48.96	50.99
2350	214.9	152.0	111.1	101.1	2920			382.1	299.9	4210	43.35	45.96	47.20	48.98
2360	207.8	150.8	108.1	97.00	2930			408.9	319.5	4220	41.77	44.52	45.43	47.07
2370	200.2	151.6	108.2	90.55	2940			435.6	343.9	4230	40.18	43.07	43.68	45.17
2380	192.5	142.9	106.5	83.87	2950			477.1	387.0	4240	38.73	41.63	42.03	43.66
2390	183.8	128.3	101.5	81.33	2960				396.9	4250	37.46	40.23	40.69	42.32
2400	175.5	122.6	96.36	76.04	2970				423.4	4260	36.20	38.84	39.36	40.93
2410	171.0	122.3	90.60	74.84	2980				450.6	4270	34.98	37.44	37.93	39.51
2420	166.5	120.2	86.44	73.79	2990				477.8	4280	33.73	36.17	36.36	38.12
2430	164.9	115.0	84.99	71.20	3000				512.1	4290	32.49	35.22	34.88	36.78
2440	163.5	109.3	83.66	66.94						4300	31.59	34.28	33.73	35.86
2450	151.3	105.0	80.96	64.88						4310	30.75	33.37	32.88	34.92
2460	137.4	102.0	78.06	64.66	3750	218.3	329.7	473.5	648.3	4320	29.91	32.45	32.01	33.96
2470	130.9	100.1	74.92	63.34	3760	196.2	299.8	425.6	567.0	4330	29.11	31.50	31.17	33.00
2480	127.5	96.30	71.87	58.56	3770	174.6	273.7	386.0	511.9	4340	28.29	30.54	30.33	32.05
2490	125.5	91.36	69.48	54.04	3780	162.6	247.3	343.9	459.4	4350	27.47	29.75	29.50	31.10
2500	124.5	88.66	68.46	53.38	3790	150.5	224.1	317.6	414.2	4360	26.71	28.98	28.73	30.29
2510	122.1	86.94	67.94	53.46	3800	142.2	211.5	294.5	374.1	4370	25.96	28.23	28.01	29.47
2520	118.2	85.08	67.84	53.75	3810	135.6	198.9	272.9	344.2	4380	25.21	27.50	27.28	28.64
2530	114.4	83.22	67.82	54.58	3820	129.0	186.4	256.3	318.6	4390	24.69	26.81	26.55	27.81
2540	113.4	82.34	67.72	55.16	3830	122.4	177.4	240.9	297.0	4400	24.20	26.13	25.80	27.01
2550	112.7	82.14	67.94	55.50	3840	118.4	170.9	228.2	280.1	4410	23.71	25.47	25.09	26.23
2560	111.8	82.52	69.27	55.85	3850	114.6	164.4	217.6	265.8	4420	23.16	24.76	24.48	25.62
2570	110.3	82.66	68.72	56.22	3860	112.7	157.9	208.3	251.3	4430	22.58	24.11	23.92	25.01
2580	109.8	83.62	72.84	56.78	3870	110.8	153.1	200.9	237.0	4440	22.01	23.56	23.42	24.40
2590	110.3	85.33	71.36	58.19	3880	108.9	145.0	194.6	226.0	4450	21.71	23.02	22.83	23.77
2600	110.4	87.86	72.85	59.53	3890	106.8	137.8	188.2	215.4	4460	21.40	22.57	22.19	23.16
2610	110.0	89.46	73.50	60.96	3900	105.2	135.2	182.0	201.5	4470	21.10	22.26	21.57	22.61
2620	109.4	90.95	74.10	62.78	3910	104.8	132.7	175.7	189.9	4480	20.86	21.98	21.17	22.26
2630	111.0	92.26	74.52	64.08	3920	104.8	130.2	169.4	181.2	4490	20.62	21.71	20.87	21.87
2640	113.4	93.91	75.74	64.69	3930	104.7	127.5	163.5	174.0	4500	20.38	21.46	20.55	21.48
2650	115.4	96.03	77.48	65.72	3940	104.4	124.7	157.8	166.8	4510	20.34	21.24	20.27	21.09
2660	119.2	98.68	80.05	67.52	3950	104.0	121.8	152.0	159.7	4520	20.27	21.03	20.00	20.70
2670	122.9	101.4	83.04	70.34	3960	103.1	118.8	146.2	152.6	4530	20.19	20.81	19.70	20.34
2680	127.0	105.0	87.20	73.19	3970	101.3	115.8	140.4	145.8	4540	20.24	20.56	19.50	20.15
2690	133.1	109.6	91.40	76.12	3980	99.81	111.8	134.9	139.4	4550	20.27	20.42	19.34	19.99
2700	139.3	114.3	95.75	78.86	3990	95.57	107.7	129.5	132.8	4560	20.31	20.41	19.26	19.74
2710	146.3	120.3	99.62	81.71	4000	93.80	103.5	124.1	126.4	4570	20.50	20.44	19.12	19.46
2720	153.8	127.7	103.3	85.64	4010	92.37	99.45	118.7	120.1	4580	20.69	20.45	18.96	19.18
2730	161.6	135.5	107.5	89.72	4020	92.68	95.32	113.7	114.1	4590	20.87	20.42	18.83	18.91
2740	172.0	143.5	114.0	93.53	4030	93.00	91.10	108.8		4600	21.03	20.38	18.73	18.73

ω	k_ω(27°C)	k_ω(89°C)	k_ω(159°C)	k_ω(209°C)	ω	k_ω(27°C)	k_ω(89°C)	k_ω(159°C)	k_ω(209°C)	ω	k_ω(27°C)	k_ω(89°C)	k_ω(159°C)	k_ω(209°C)
4610	21.13	20.43	18.63	18.53	5180	125.3	141.7	140.4	147.2	5750	6.653	5.626	4.228	4.381
4620	21.23	20.67	18.56	18.33	5190	120.4	141.0	148.5	154.4	5760	6.562	5.525	4.111	4.172
4630	21.50	20.92	18.57	18.31	5200	116.0	140.6	157.8	161.9	5770	6.472	5.443	3.990	3.921
4640	21.82	21.12	18.67	18.29	5210	111.3	140.9	161.3	169.5	5780	6.383	5.383	3.872	3.671
4650	22.14	21.25	18.77	18.28	5220	102.8	135.3	159.4	168.4	5790	6.293	5.320	3.762	3.436
4660	22.61	21.38	18.90	18.25	5230	97.62	123.1	159.2	166.5	5800	6.243	5.236	3.662	3.318
4670	23.16	21.53	19.02	18.25	5240	96.23	111.4	156.8	161.0	5810	6.209	5.146	3.604	3.219
4680	23.72	21.89	19.13	18.26	5250	90.58	101.6	135.5	146.0	5820	6.163	5.040	3.534	3.121
4690	24.35	22.24	19.24	18.34	5260	72.54	88.34	120.2	132.2	5830	6.118	4.965	3.460	3.040
4700	25.06	22.54	19.44	18.47	5270	62.55	77.06	105.3	118.2	5840	6.072	4.942	3.386	2.960
4710	25.76	22.90	19.65	18.58	5280	53.82	67.20	90.18	103.2	5850	6.027	4.919	3.325	2.879
4720	26.54	23.26	19.90	18.76	5290	44.83	53.63	70.45	86.83	5860	5.984	4.882	3.262	2.842
4730	27.63	23.73	20.20	18.98	5300	37.62	45.65	56.85	72.61	5870	5.974	4.852	3.193	2.823
4740	28.70	24.33	20.48	19.21	5310	29.97	39.39	48.44	61.53	5880	5.959	4.826	3.157	2.805
4750	29.76	25.04	20.79	19.41	5320	25.81	33.89	40.51	51.97	5890	5.943	4.799	3.120	2.778
4760	30.88	25.73	21.17	19.61	5330	22.46	28.82	35.55	44.14	5900	5.942	4.778	3.081	2.738
4770	31.93	26.48	21.60	19.78	5340	18.95	23.95	29.82	38.36	5910	5.947	4.759	3.043	2.698
4780	32.99	27.36	22.09	19.95	5350	16.79	21.58	25.75	33.09	5920	5.952	4.740	3.007	2.658
4790	34.23	28.24	22.64	20.36	5360	14.63	18.94	22.47	28.57	5930	5.971	4.713	2.968	2.607
4800	35.49	29.12	23.21	20.80	5370	13.52	17.18	19.50	26.38	5940	5.991	4.700	2.946	2.560
4810	36.73	30.05	23.72	21.28	5380	12.46	15.82	18.40	24.40	5950	5.992	4.685	2.930	2.514
4820	38.44	31.00	24.28	21.87	5390	11.56	14.52	17.15	22.06	5960	5.996	4.667	2.910	2.471
4830	40.40	32.03	25.01	22.49	5400	11.03	13.97	15.96	19.87	5970	6.001	4.694	2.890	2.428
4840	42.35	33.55	25.81	23.08	5410	10.49	13.38	14.84	18.09	5980	6.005	4.721	2.879	2.385
4850	44.39	35.01	26.74	23.67	5420	10.15	12.79	13.87	17.31	5990	6.009	4.747	2.873	2.352
4860	46.43	36.44	27.80	24.25	5430	9.833	12.20	13.40	16.58	6000	6.033	4.767	2.867	2.363
4870	48.48	38.02	28.84	24.81	5440	9.792	11.70	12.87	15.82	6010	6.113	4.793	2.889	2.384
4880	50.64	39.62	29.83	25.59	5450	9.825	11.46	12.37	15.04	6020	6.205	4.820	2.921	2.405
4890	52.97	41.26	30.99	26.49	5460	9.858	11.22	11.92	14.33	6030	6.295	4.845	2.951	2.415
4900	55.30	42.90	32.15	27.34	5470	9.876	11.00	11.52	13.81	6040	6.384	4.889	2.980	2.415
4910	57.63	44.56	33.35	28.18	5480	9.831	10.79	11.26	13.33	6050	6.473	4.938	3.005	2.415
4920	59.94	46.14	34.58	29.37	5490	9.785	10.60	10.94	12.84	6060	6.562	4.987	3.025	2.415
4930	62.14	47.75	36.16	30.62	5500	9.742	10.50	10.63	12.35	6070	6.651	5.029	3.045	2.422
4940	64.33	49.73	37.67	31.85	5510	9.712	10.42	10.32	11.90	6080	6.734	5.064	3.065	2.436
4950	66.51	52.16	39.36	33.07	5520	9.669	10.31	10.04	11.56	6090	6.796	5.098	3.085	2.452
4960	68.98	54.65	41.17	34.77	5530	9.621	10.21	9.775	11.20	6100	6.859	5.121	3.094	2.467
4970	71.61	57.21	43.45	36.59	5540	9.577	10.09	9.518	10.85	6110	6.923	5.151	3.103	2.488
4980	74.64	59.86	45.66	38.32	5550	9.533	9.940	9.261	10.51	6120	6.987	5.190	3.111	2.509
4990	78.12	62.65	47.96	40.04	5560	9.489	9.780	9.001	10.17	6130	7.050	5.228	3.125	2.530
5000	81.64	65.36	50.27	42.35	5570	9.419	9.634	8.748	9.826	6140	7.114	5.263	3.138	2.555
5010	78.79	68.24	53.07	45.04	5580	9.308	9.411	8.492	9.496	6150	7.217	5.302	3.142	2.581
5020	82.74	71.23	55.79	47.68	5590	9.191	9.187	8.236	9.161	6160	7.289	5.350	3.191	2.604
5030	86.65	75.33	58.58	50.30	5600	9.074	8.915	7.985	8.760	6170	7.351	5.396	3.241	2.626
5040	90.43	79.39	61.53	53.26	5610	8.966	8.601	7.736	8.360	6180	7.404	5.429	3.281	2.632
5050	94.90	83.46	65.14	56.89	5620	8.869	8.296	7.489	7.961	6190	7.454	5.487	3.317	2.632
5060	99.36	87.47	69.23	60.51	5630	8.694	8.030	7.202	7.571	6200	7.503	5.547	3.359	2.631
5070	103.8	91.56	73.29	63.93	5640	8.506	7.785	6.929	7.182	6210	7.553	5.607	3.412	2.631
5080	108.3	98.94	80.54	68.17	5650	8.319	7.539	6.644	6.810	6220	7.604	5.667	3.466	2.660
5090	111.1	103.4	89.34	74.32	5660	8.131	7.310	6.358	6.456	6230	7.756	5.733	3.518	2.705
5100	112.9	108.8	95.15	82.30	5670	7.944	7.082	6.071	6.101	6240	7.950	5.803	3.591	2.756
5110	114.7	114.1	100.8	90.67	5680	7.760	6.834	5.784	5.829	6250	8.108	5.879	3.659	2.810
5120	116.5	119.4	106.6	96.11	5690	7.607	6.589	5.518	5.630	6260	8.286	5.964	3.725	2.851
5130	118.2	124.7	112.5	101.5	5700	7.428	6.345	5.272	5.439	6270	8.463	6.099	3.792	2.890
5140	120.2	129.6	118.0	110.7	5710	7.249	6.118	5.027	5.232	6280	8.641	6.235	3.860	2.930
5150	122.3	134.3	123.5	120.5	5720	7.070	5.981	4.784	5.020	6290	8.819	6.371	3.928	2.969
5160	124.7	139.1	128.9	129.6	5730	6.891	5.845	4.579	4.808	6300	9.006	6.500	3.997	3.034
5170	127.2	142.7	134.6	138.7	5740	6.742	5.726	4.367	4.589	6310	9.223	6.648	4.082	3.108

ω	K_ω(27°C)	K_ω(89°C)	K_ω(159°C)	K_ω(209°C)	ω	K_ω(27°C)	K_ω(89°C)	K_ω(159°C)	K_ω(209°C)	ω	K_ω(27°C)	K_ω(89°C)	K_ω(159°C)	K_ω(209°C)
6320	9.423	6.800	4.192	3.183	6900	31.93	31.60	29.36	28.52	7480	2.356	2.095	1.324	2.679
6330	9.617	6.943	4.307	3.259	6910	31.65	31.98	30.11	29.5-	7490	2.274	1.971	1.193	2.479
6340	9.829	7.110	4.441	3.343	6920	31.39	32.36	30.93	30.57	7500	2.192	1.848	1.101	2.280
6350	10.41	7.253	4.576	3.427	6930	31.18	32.73	31.90	31.87	7510	2.110	1.726	1.009	2.080
6360	10.25	7.476	4.721	3.510	6940	31.00	33.14	32.85	33.19	7520	2.028	1.678		1.880
6370	10.46	7.657	4.871	3.595	6950	30.82	33.42	33.79	34.49	7530	1.947	1.623		1.771
6380	10.69	7.807	5.019	3.715	6960	30.64	33.55	34.70	35.77	7540	1.894	1.566		1.682
6390	11.00	7.965	5.167	3.840	6970	30.11	33.67	35.36	37.05	7550	1.858	1.517		1.614
6400	11.29	8.125	5.334	3.967	6980	29.32	33.71	35.97	38.33	7560	1.820	1.469		1.547
6410	11.58	8.267	5.489	4.100	6990	28.50	33.81	36.50	39.58	7570	1.781	1.420		1.479
6420	11.87	8.417	5.640	4.236	7000	27.73	33.95	37.02	40.33	7580	1.745	1.373		1.412
6430	12.16	8.679	5.792	4.373	7010	26.98	33.73	37.58	40.80	7590	1.708	1.327		1.314
6440	12.45	8.941	5.952	4.509	7020	26.20	33.23	37.81	41.01	7600	1.672	1.294		1.207
6450	12.74	9.203	6.123	4.645	7030	25.40	32.84	37.61	41.28					
6460	13.04	9.437	6.294	4.854	7040	24.60	32.52	37.03	41.56					
6470	13.52	9.681	6.471	5.091	7050	23.83	32.22	36.20	42.03					
6480	13.97	9.936	6.740	5.337	7060	22.85	30.79	35.24	41.80					
6490	14.40	10.19	7.005	5.582	7070	21.62	29.14	34.34	40.37					
6500	14.82	10.44	7.252	5.788	7080	20.39	27.67	33.38	39.04					
6510	15.23	10.77	7.493	5.977	7090	19.16	26.43	31.77	37.72					
6520	15.65	11.11	7.737	6.167	7100	17.93	25.18	29.28	36.13					
6530	16.06	11.44	7.986	6.357	7110	16.73	23.94	26.82	34.07					
6540	16.47	11.80	8.236	6.607	7120	15.62	22.71	24.60	32.01					
6550	16.98	12.16	8.468	6.905	7130	14.51	21.23	22.76	30.07					
6560	17.52	12.51	8.813	7.227	7140	13.40	19.13	20.88	28.16					
6570	18.05	12.86	9.175	7.547	7150	12.29	17.01	19.08	26.22					
6580	18.58	13.17	9.525	7.857	7160	11.17	15.06	17.26	24.12					
6590	19.12	13.56	9.875	8.181	7170	10.27	13.95	15.42	22.09					
6600	19.65	14.10	10.22	8.505	7180	9.371	12.87	14.09	20.09					
6610	20.18	14.64	10.60	8.829	7190	8.464	11.80	12.90	18.03					
6620	20.71	15.19	10.99	9.152	7200	7.488	10.71	11.71	16.02					
6630	21.25	15.71	11.39	9.653	7210	6.527	9.514	10.52	14.86					
6640	21.92	16.27	11.74	10.22	7220	6.346	8.795	9.218	13.79					
6650	22.59	16.89	12.32	10.81	7230	6.079	8.126	8.621	12.76					
6660	23.26	17.50	12.89	11.34	7240	5.811	7.457	8.146	11.65					
6670	23.92	18.09	13.44	11.86	7250	5.542	6.789	7.678	10.55					
6680	24.59	18.74	13.99	12.34	7260	5.312	6.125	7.104	9.836					
6690	25.25	19.44	14.54	12.82	7270	5.072	5.744	6.492	9.306					
6700	25.92	20.15	15.15	13.30	7280	4.815	5.503	5.995	8.746					
6710	26.58	20.86	15.78	13.78	7290	4.558	5.262	5.640	8.132					
6720	27.25	21.55	16.42	14.52	7300	4.301	5.022	5.324	7.517					
6730	27.88	22.23	17.08	15.28	7310	4.044	4.778	5.008	6.952					
6740	28.53	22.90	17.86	16.06	7320	3.806	4.520	4.689	6.656					
6750	29.18	23.58	18.62	16.84	7330	3.739	4.267	4.345	6.392					
6760	29.83	24.27	19.37	17.61	7340	3.657	4.018	4.141	6.151					
6770	30.36	24.95	20.12	18.36	7350	3.549	3.861	3.937	5.910					
6780	30.79	25.63	20.87	19.12	7360	3.448	3.705	3.729	5.665					
6790	31.14	26.30	21.59	19.87	7370	3.347	3.550	3.520	5.345					
6800	31.44	26.97	22.28	20.66	7380	3.246	3.394	3.294	5.018					
6810	31.74	27.60	22.98	21.44	7390	3.144	3.239	3.064	4.691					
6820	32.04	28.13	23.68	22.19	7400	3.043	3.083	2.835	4.365					
6830	31.93	28.62	24.38	22.95	7410	2.942	2.927	2.606	4.038					
6840	31.91	29.12	25.07	23.71	7420	2.841	2.769	2.376	3.803					
6850	31.90	29.62	25.77	24.47	7430	2.761	2.657	2.131	3.609					
6860	32.01	30.11	26.46	25.22	7440	2.686	2.557	1.943	3.436					
6870	32.06	30.48	27.15	25.97	7450	2.604	2.456	1.794	3.262					
6880	32.10	30.85	27.85	26.72	7460	2.520	2.343	1.640	3.076					
6890	32.07	31.22	28.61	27.52	7470	2.437	2.218	1.481	2.878					